New Generation Light Emitting Diodes: Fundamentals and Applications

Amit Yadav

Doctor of Philosophy

ASTON UNIVERSITY

March 2017

Aston University

New Generation Light Emitting Diodes: Fundamentals and Applications

Amit Yadav

Doctor of Philosophy

2017

Light emitting diodes (LEDs) have made tremendous progress in last 15 years and have reached to a point where they are reinventing and redefining artificial lighting. The efficiency and better control over light quality parameters have been the key attributes of LEDs that makes them better than the existing lighting solutions. Nevertheless, in their own realm they suffer from decrease in efficiency at higher currents, i.e. the "efficiency droop" phenomenon. Thus, a better understanding of the mechanisms leading to droop is of utmost importance. Moreover, the full potential in terms of light quality, i.e. colour rendering index (CRI) and correlated colour temperature (CCT) that can be offered by these devices can be further improved with existing or alternative schemes and device configurations.

In this thesis, a novel phosphor covered approach is investigated towards improving the CRI for indoor lighting applications. A monolithic di-chromatic LED emitting at blue and cyan wavelengths is used to pump a green-red phosphor mixture and a warm (CCT $\sim$ 3400 K) white light with a superior CRI of 98.6 is achieved. An alternate phosphor free solution to achieve warm white light emission is also studied. These monolithic di-chromatic QW devices emitting at blue and green wavelengths under electrical pumping demonstrated tuneable emission from cool (CCT $\sim$ 22000 k) to warm (CCT $\sim$ 5500 K) white light. A maximum CRI of 67, which is the highest value demonstrated for such devices till date to the best of my knowledge, is also achieved.

On the subject of efficiency of LEDs, temperature dependence of LEE and IQE of commercial InGaN/GaN based blue LED is studied in light of a step-wise processing procedure based on the ABC-model to determine these quantities. A decrease in both IQE and LEE with temperature is noted. On the other hand, efficiency decrease in the investigated AlGaInP based red LEDs under pulsed current shows a shift in the onset of efficiency decrease towards higher current values with decreasing pulse width with $< 1\%$ duty cycle. For sub-nanosecond pulses a linear relation between applied peak current and peak output power is obtained. These observations indicate device self-heating to be the major contributing factor for efficiency decrease in AlGaInP LEDs.

Keywords: *Internal quantum efficiency; Light extraction efficiency; Self-heating; Phosphor-free; high pulsed current; temperature dependence; CRI; CCT; Stealth dicing; sapphire dicing; ABC model; AlGaInP; monolithic LED*

To my Beloved Mother
Kamlesh Yadav

To my Daughter
Florence Yadav

To my Father
Krishan Kumar

To my Wife
Preeti Yadav

To my Brother
Atul Yadav

Acknowledgements

This thesis is a reflection of the journey that would not have been possible without the support and guidance, be it intellectual or emotional, offered to me at the time when most needed. First and foremost, with sincere gratitude and from the bottom of my heart I would like to thank my supervisor Prof. Edik U.Rafailov for offering me the opportunity to embark on this great inquest. His immense support, guidance and unwavering belief in me has been the driving force all along these past few years.

I would like to thank Dr. Ilya Tikov for his patience, knowledge and help from the experiments to inputs towards writing this thesis.

Special thanks to Dr. Sergey Karpov for the theoretical framework, described in chapter 5 and used in other chapters, developed during the course of the NEWLED project. Furthermore, I would like to thank Dr. Karpov for numerous scientific discussions, his inputs are a valuable lesson today and will be in future.

My heartiest thanks to Dr. Natalia Bazieva, Dr. Ksenia Federova, Dr. Karina Litvonova, Dr.Andrei Gorodetsky, Dr. Yuri Loika, Dr. Neil Gordon, Dr. Stanislov Kolpakov, and Mr. Andrew Abbot for all the discussions, guidance, support and help.

I would also like to thank all my friends at AIPT for all the laughs we shared during that lunch time and for all the support.

I would also like to acknowledge the support provided to by the European Union under the FP7 NEWLED project to pursue this thesis.

Finally, this thesis is a result of an earnest resolve and sacrifices of my mother; the belief of my father and brother; unwavering support and emotional balance of my wife and the eternal love of my daughter. It would like to thank my family with the knowledge that my deepest feeling to them cannot be expressed in words.

Table of contents

List of Abbreviations

InGaN	Indium Gallium Nitride
AlGaInP	Aluminium Gallium Indium Phosphide
GaN	Gallium Nitride
Al	Aluminium
CRI	Colour Rendering Index
MQW	Multiple Quantum Well
QW	Quantum Well
CCT	Correlated Colour Temperature
DBR	Distributed Bragg Reflector
AlGaN	Aluminium Gallium Nitride
Si	Silicon
LEE	Light Extraction Efficiency
IQE	Internal Quantum Efficiency
EQE	External Quantum Efficiency
GaAsP	Gallium Arsenic Phosphide
GaAs	Gallium Arsenide
VPE	Vapour Phase Epitaxy
GaP	Gallium Phosphide
Zn	Zinc
Ga	Gallium
In	Indium
MOCVD	Metal Organic Chemical Vapour Deposition
SSL	Solid-State Lighting
UV	Ultraviolet
NIR	Near Infra-red
InN	Indium Nitride
MIS	Metal-Insulator-Semiconductor
RCA	Radio Corporation of America
LD	Laser Diode

LEEBI	Low Energy Electron Beam Irradiation
DH	Double Heterostructure
SQW	single Quantum Well
CB	Conduction Band
VB	Valence Band
SRH	Shockley-Read-Hall
AR	Active Region
WPE	Wall-plug Efficiency
DADR	Density Activated Defect Recombination
EL	Electroluminescence
PL	Photoluminescence
EBL	Electron Blocking Layer
SPSL	Short-Period Superlattice
CIE	Commission International de I'Elairage
PW	Pulse Width
SD	Stealth Dicing
NA	Numerical Aperture
EM	Electro-Magnetic
TEM	Transmission Electron Microscope
PS	Phosphor Sheets
FWHM	Full Width Half Maximum
MBC	Monolithic Blue-Cyan
LER	Luminous Efficacy of Radiation
TDEL	Temperature Dependent Electroluminescence
FDTDF	Finite-Difference Time-Domain
T-IDEL	Temperature-Intensity Dependent Electroluminescence
ND	Neutral Density
RT	Room Temperature
FCA	Free-Carrier Absorption
CW	Continuous Wave
BW	Bandwidth

List of figures

List of tables

Chapter 1

Introduction

1.1 Light emitting diodes

Inorganic light emitting diodes (LEDs) are currently the most efficient light sources that are used for indoor and outdoor lighting applications. These devices are fundamentally monochrome light emitters based on two material systems, InGaN/GaN and AlGaInP. Emission across the whole visible spectrum from blue (based on InGaN) to red (based on AlGaInP) can be achieved depending upon the composition of indium (In) and aluminium (Al) in the respective alloy. The monochromatic (emission spectrum width of about 20-50 nm) nature of emission of LEDs has made targeted lighting efficient and versatile with better control on light parameters. On the other hand, to generate white light either a broad band source emitting across the visible spectral region or a combination of two or more monochromatic sources of appropriate wavelength is needed. Given the narrow emission width of the LEDs, white light emission is achieved using a few different approaches. The approaches of interest are (a) monolithic, (b) phosphor-converted LED (pc-LED). The ability of these sources to render true colours of an object is of critical importance for adequate and appropriate visual appearance. While a source with a colour rendering index (CRI) of 70-80 is suitable for outdoor applications, CRI around 90-95 is needed for indoor lighting, and much improvement in colour rendition is needed for more critical applications like art galleries, museums, hospitals, and exhibitions. The commercially available and simplest of the mentioned approaches is pc-LED involving a short wavelength blue/violet pump LED absorbed by a single or mix of phosphors for broad band emission creating white light due to colour mixing. Though maximum CRI of 99.1 [1] has been demonstrated using phosphors with emission band in red, green and blue spectral region, the issues due to the use of phosphor to achieve broadband emission reduces the overall efficiency of the source, which is further decreased with each added phosphor. The unavoidable Stoke's losses further reduces the efficiency along with inconsistent light quality due to different degradation times of each phosphor. Thus better solutions are needed to improve the efficiency of these sources by reducing the number of phosphors needed while maintaining acceptable CRI. Next, the monolithic approach is a phosphor

free one. A monolithic LED emits at more than one wavelength to generate white light. These polychromatic devices are based on InGaN/GaN material system. The first di-chromatic devices by Damilano et al. [2] in 2001 had MQW with different In composition thus emitting in blue and yellow spectral range with a maximum efficiency of 0.5% and correlated colour temperature (CCT) of $\sim$ 8000 K. Since then different approaches involving different shape and size nanostructures, QW light converter, dichroic filter, DBR resonant-cavity, nGaN/GaN/AlGaN dot-in-a-wire core–shell white LEDs on Si substrate, wafer bonding of blue and green QW LED [3] has been used to achieve efficient white light emission. All these approaches unlike the MQWs involves complex fabrication processes. To date, monolithic LEDs are far behind their counterparts, phosphor based white LEDs, in their efficiency, CRI and CCT. These parameters are limited due to degradation of material quality and increased polarization effects at higher In incorporation. Nevertheless, the approach is attractive due to promise of higher efficiency and better light quality that can be achieved with advancements in growth technology.

Apart from lighting, LEDs are used in automotive, indoor non-white lighting, signage, displays and many more applications. For the devices used in these applications, irrespective of the emission wavelength, internal quantum efficiency is one of the most critical parameter. The highly efficient InGaN/GaN devices emit in the blue spectral range. However, they suffer from the phenomenon of efficiency droop, i.e. reduction of efficiency with increasing current density. The physical processes leading to this droop are still under investigation. The Auger recombination, carrier leakage and carrier delocalistion along with device self-heating are different mechanisms that has been proposed. A similar decrease in efficiency as a function of current is also associated with AlGaInP based LEDs. In this case, due to different material properties, carrier leakage is considered to be the dominant mechanism leading to reduction of efficiency. Nonetheless, further experimental studies accompanied by theoretical estimations are needed to better understand the physical mechanisms for efficiency droop in blue LEDs and decrease of efficiency in red LEDs.

1.2 Organisation of thesis

In this thesis, first the white light sources using monolithic and pc-LED approach with improved light quality parameters within the realm of individual approach are demonstrated. Next, behaviour of efficiency as a function of current is investigated experimentally for InGaN/GaN (blue) and AlGaInP (red) LEDs under different operating conditions. This thesis is organised into 7 chapters which includes a brief introduction (chapter 1) and conclusion (chapter 7).

In chapter 2, a brief review on history of III-V LEDs, schemes for white light generation and efficiency droop mechanisms is presented.

In chapter 3, correlated colour temperature (CCT) and spectral behaviour of di-chromatic LEDs with blue-green quantum well (QW) under continuous wave current and pulsed pumping conditions is discussed. Highest colour rendering index (CRI) of 67 from these phosphor-free devices is demonstrated. Furthermore, the 'stealth dicing' of sapphire, a substrate used for the growth of InGaN/GaN based optical devices, using a femtosecond Ti:Sapphire laser (800 nm) is demonstrated.

A novel hybrid approach, comprising of dual wavelength LED and two phosphors to generate warm white light with CRI of 98.6 and tuneable colour characteristics is demonstrated in chapter 4.

In chapter 5, using a processing procedure based on the ABC-model, LEE and IQE of blue LEDs from experimental EQE is determined and their temperature dependence is discussed. It is shown that the model fits EQE (I) over 13 K - 400 K. Furthermore, temperature dependence of LEE is demonstrated and mechanisms involved are discussed.

The efficiency behaviour of AlGaInP LEDs under high current density 4.5 kA/cm^2 in the pulsed regime is presented in chapter 6. The efficiency reduction is attributed primarily to active region overheating, dominating over the electron overflow and the Auger recombination. Furthermore, a low LEE is recognised as the bottleneck for overall efficiency improvement

References

[1] T. Fukui, K. Kamon, J. Takeshita, H. Hayashi, T. Miyachi, Y. Uchida, S. Kurai, and T. Taguchi, "Superior Illuminant Characteristics of Color Rendering and Luminous Efficacy in Multilayered Phosphor Conversion White Light Sources Excited by Near-Ultraviolet Light-Emitting Diodes," *Jpn. J. Appl. Phys.*, vol. 48, no. 11, pp. 112101, 2009.

[2] B. Damilano, N. Grandjean, C. Pernot, and J. Massies, "Monolithic White Light Emitting Diodes Based on InGaN/GaN Multiple-Quantum Wells," *Jpn. J. Appl. Phys.*, vol. 40, no. Part 2, No. 9A/B, pp. L918–L920, 2001.

[3] Y. J. Lee, P. C. Lin, T. C. Lu, H. C. Kuo, and S. C. Wang, "Dichromatic InGaN-based white light emitting diodes by laser lift-off and wafer-bonding schemes," *Appl. Phys. Lett.*, vol. 90, no. 16, pp. 161115-1 – 161115-3, 2007.

Chapter 2

Background

2.1 Development of Light Emitting Diodes

Artificial lighting has been a hallmark of human evolution ever since wooden fire, wig lamps, wax candles to tungsten filament bulbs and lately fluorescent tubes. These light sources serve their purpose well with a wide range of applications in different areas: for example, sodium discharge lamps are used for street lighting because of their poor colour rendering and high efficiency, fluorescent lamps – for illuminating work place and incandescent bulbs – for lighting houses. These light sources are either based on "pyroluminescence", i.e. radiation from gas or vapour when excited by high temperature or "incandescence", which is emission of electromagnetic radiation when a material is heated to elevated temperatures.

Recently, solid state lighting (SSL) a new technology has entered the area of lighting. SSL relies upon light emitting diodes for generation of on-demand light of different colours. The colour selectivity is an important feature of LEDs since the direct electronic transitions based on the energy bandgap of the semiconductor material responsible for availability of discrete emission provides an unprecedented control on perceived emission. More importantly, white light for general illumination, due to the narrowband emission of LEDs, is achieved by exciting red, green and blue parts of the emission spectrum using different LEDs emitting each colour or by a broadband phosphor emitting in green red region pumped by a blue/UV LED. The discrete emission is possible due to two material systems InGaN and AlGaInP. A brief development history of these materials is presented in the subsequent subsections.

AlGaInP is a quaternary alloy of the III-phosphide material system. In the mole fraction configuration of $((Al_xGa_{1-x})_{0.5}In_{0.5}P)$ it is lattice matched to GaAs thus allowing for superior epitaxial growth. Emission tunability in the red-yellow spectral range is available with this alloy from $\sim$ 650 nm to $\sim$ 560 nm by varying the aluminium (Al) concentration (x) from 0% (i.e. InGaP) to 53% with associated direct bandgap energy difference of $\sim$ 1.9eV to $\sim$ 2.2 eV. Beyond 2.2 eV i.e $>$ 53% Al content the material becomes indirect due to crossover of Γ and X valleys leading to X valley having conduction band minimum at lower energy w.r.t Γ valley.

On the other hand $In_xGa_{1-x}N$ alloy belongs to III-Nitride material system. The workhorse of current day SSL, the highly efficient blue LED is based on InGaN. This material system can potentially cover the entire visible spectrum while keeping a direct bandgap all along for indium (In) composition of x = 0 with $\sim$ 3.5eV ($\sim$ 365 nm) energy bandgap of GaN to x = 1 (at least theoretically) emitting at $\sim$ 1.8 μm in near infra-red (NIR) with the energy bandgap of InN $\sim$ 0.7eV.

2.1.1 Brief history of AlGaInP LEDs

Electronic lighting was introduced in the early 20th century when H.J Round first observed emission of light from silicon carbide (SiC) on applying electrical power in 1907. This phenomenon is now known as "electroluminescence"(EL). He observed yellow, green, orange and blue emissions on application of voltage ranging from 10V to 110V (Figure 2.1) [1].

Fig. 2.1 Electroluminescence report by H.J. Round [1]

Losev, working on these SiC rectifying diodes, reported that emission mechanism for these devices is more 'similar to cold electronic discharge' and not incandescence [2, 3]. SiC has an indirect bandgap and thus the electrical to optical efficiency is very low, and the best SiC light-emitting diode (LED) with 0.03% of maximum efficiency was ever reported [4]. The introduction of III-V compound semiconductors

in the 1950's paved the way for the first gallium arsenide (GaAs) based p-n junction, epitaxially grown, infrared LEDs in 1962 [5–7]. In the same year, N. Holonyak demonstrated the first visible (red) gallium arsenic phosphide (GaAsP) LED. He engineered the bandgap of GaAs (1.424 eV), which is suitable for emission in the infra-red region at about 870 nm, to emit at wavelengths lower than 870 nm by incorporating phosphorus (P) by vapour phase epitaxy (VPE) [8]. In the following years, it was found that radiative efficiency of GaAsP diodes decreases rapidly due to direct – indirect transition of the bandgap with more than 44% phosphor content [9–11] and high density of dislocations due to large lattice mismatch between a GaAsP epilayer and a GaAs substrate [12].

In the 1960's, a few groups were investigating gallium phosphide (GaP) as well. First reports of GaP p-n junction LEDs came in 1963-1964 [13, 14]. Later, red and green GaP-based LEDs doped with isoelectronic impurities zinc (Zn) and oxygen (O), and nitrogen (N), respectively, were realized [15].

Another material under investigation for emission was aluminium gallium indium phosphide (AlGaInP). First reports of emission on this material system came in 1985 and 1986 by various groups in Japan [15]. Initially with GaInP (50% Ga and In) as the active region material with a lattice matched GaAs emission at 650 nm was achieved. Later, with development of MOCVD technology for growing double heterostructure and QW for Al containing materials emission at shorter than 650 nm was achieved. LEDs based on this material have undergone various structural improvements which includes MQW [16] and strained MQW active regions [17, 18], transparent p-type GaP window layer [19] and wafer bonding with transparent GaP substrate [20], and truncated inverted chip geometry by Krames et al [21] to make them more efficient. These LEDs have subsequently improved and is the only highly efficient material to emit in the red-yellow region of emission spectrum.

2.1.2 Brief history of InGaN/GaN LEDs

The first p-n homojunction GaN blue LED with 1% efficiency was reported by Akasaki et al. in 1992 [22]. The road to this first demonstration started with efforts to grow Gallium Nitride (GaN) in 1968 at Radio Corporation of America (RCA) by

Maruska. He chose sapphire due to its robust nature to grow GaN, and the first growth of single crystal GaN films was reported by him in 1969 [23]. These films without any intentional doping were n-type. Zn and magnesium (Mg) were used to achieve p-type doping. The first Mg-doped metal-insulator-semiconductor (MIS) diodes were developed by Pankove and his team in 1972 [15]. In these devices Mg as dopant was not exhibiting p-type conductivity, and the emission was related to impact ionization and tunnelling [15]. After much effort Akasaki and his team demonstrated p-type conductivity in GaN films by using Mg as p-type dopant, which led to blue p-n junction LED in 1992. Low energy electron beam irradiation (LEEBI) and post-growth annealing at high temperatures were reported as methods to activate Mg dopants in these films by Amano et al. and Nakamura et al. [24, 25].

Most blue and UV LEDs that we see today have active region of InGaN. Metal organic vapour phase epitaxy (MOCVD) was used to grow the first high-quality indium gallium nitride (InGaN) layer on GaN with sapphire as substrate in 1992 by Nakamura et al [26]. This technique is what is used currently to grow InGaN/GaN structures. This growth mechanism led to the first double heterostructure (DH) (p-GaN/n-InGaN/n-GaN) blue LED in 1993 [27]. Subsequently, single quantum well (SQW) and multiple quantum well (MQW) LEDs based on InGaN/GaN established this material system to be used as high brightness and high power blue LEDs. Lately, 60% of wall-plug efficiency (WPE) for blue LED fabricated using thin GaN technology at OSRAM was reported [28]. The performance of III-V visible LED with traditional light sources summarising their development since 1962 until the last decade has been reported by [29].

2.2 Post growth singulation technology for LEDs grown on Sapphire

To date most of the GaN LEDs are grown on a c-plane sapphire wafer. These LEDs needs to singulated after growth and fabrication process for encapsulation which projects a need to break sapphire along the streets between devices on the wafer. However, sapphire is the hardest material with Mohr's index of ~ 9, only

next to diamond. This makes sapphire dicing extremely challenging in terms of speed of production and yield i.e. working devices post singulaion process. Two basic techniques have been used to perform this task a) diamond sawing and b) laser dicing. While sawing with a diamond blade was the first technology to be used, it greatly reduces the wafer chip density primarily due to wide kerf width typically around 100μm - 200μm. Since, it is a mechanical and contact process it also produces a lot of heat, debris, and chipping. On the other hand laser dicing is a non-contact process based on interaction of matter and radiation [30]. Laser dicing can further be differentiated as (a) laser scribing and (b) stealth dicing.

Laser scribing is in principle an ablation process and is currently the workhorse technology for industrial scale LED/LD singulation. Nanosecond (ns) pulse lasers emitting in UV are traditionally used to scribe a line [31–34] either at the back of the wafer with 355 nm laser or with a 266 nm laser from top, i.e the side with devices, of the wafer. The back of the wafer is scribed with 355 nm ns laser or with a 266 nm ns laser from top, i.e. the side with devices, of the wafer. However, due to generation of heat a cooling system is required [35].

On the other hand, the "stealth dicing" is a technique, proposed by Hamamatsu Photonics K.K., Japan, where a tightly focused laser beam modifies the material inside the wafer. Pulse widths of ns and ps [36] has been shown to dice sapphire using stealth dicing. A periodic thermal modification of the material inside of a small volume inside the wafer by ns and ps pulses induces the needed damage due to thermal ablation. This technique is also limited due to low repetition rate of Q-switched lasers and a need for cooling system. On the other hand when performing stealth dicing with fs pulses the material modification is induced with high intensity pulses by spending only nano joules of energy [37]. The short duration of pulse greatly reduces the damage of the thin gold conductors induced by heat around the affected zone since the pulse duration is smaller than the time scale for ion-electron relaxation time [38]. This also gives additional benefits of high speed processing with modern day Ti-Sapphire lasers with repetition rate of $\sim$ 80 MHz [39] along with an eye safe environment for operating personnel operating the laser.

2.3 Theory

Semiconductors are materials which offer partial resistance to the flow of current or there electrical conductivity is between conductors and insulators. This conductivity profile can be modified with appropriate doping of the material. Addition of an acceptor impurity or the donor impurity atom to the otherwise intrinsic material make them p- or n-type materials respectively while keeping them electrically neutral. When such a p and n type semiconductors are combined a p-n junction is formed. At the junction, due to diffusion of holes and electron from p-type and n-type material respectively to the n- and p-type material, ionized acceptors and donors are left creating a region depleted of carrier i.e. depletion region with a built-in electric field preventing further diffusion. Such a device conducts when external field greater than the built-in field is applied in a forward bias configuration and will not conduct in a reverse bias configuration. For the point of view of LEDs, the optical process of emission and absorption which are confined to this region due to the availability of both holes and electrons are of interest. However, the probability of optical processes to occur depends on the type of bandgap of the semiconductor.

2.3.1 Energy bandgap

From atomic model theory we know that electrons can reside in one of the discrete energy levels around the nucleus. Quantum numbers, n, l, m, and s are used to properly define the energy level, orientation, magnetic moment and spin of the electron respectively. When atoms combine together to form a crystal their outermost shell splits and combine to form bands, called conduction and valence band, where each band has number of discrete energy levels closely placed within the band. In the conduction band (CB) the electrons can freely move around in the crystal and conduct current, and in the valence band (VB) the movement of electrons are restricted as a result of bonding among the atoms. The ability of conducting current in a semiconductor is attributed to electrons and holes. Holes are created only in the valence band due to absence of electrons from the quantum state,

and are the charge carriers in the valence band. Like electrical conduction, optical process also requires the two charge carriers, electron and holes, for generation of radiation from a semiconductor material

For optical purposes the orientation of bands in the k-space and energy difference between these two bands, i.e. the conduction band and valence band is of critical importance. Based on position of bands in the E k-space we can have a direct and indirect bandgap semiconductor.

A Direct bandgap semiconductor (Figure 2.2) is one for which the conduction band minimum and valence band maximum occurs at the same k-value and the momentum is conserved where, momentum ($\overrightarrow{p}$) is a vector given by

$$\overrightarrow{p} = \frac{h}{2\pi}\overrightarrow{k} \tag{2.1}$$

where, $\overrightarrow{k}$ is propagation vector of electron wave and is related to de-Broglie's wavelength λ_b, $\overrightarrow{k} = 2\pi/\lambda_b$

Whereas, when CB minimum and VB maximum does not occur for the same k-value in the E-k space for a semiconductor material it is known as indirect bandgap material (Figure 2.2).

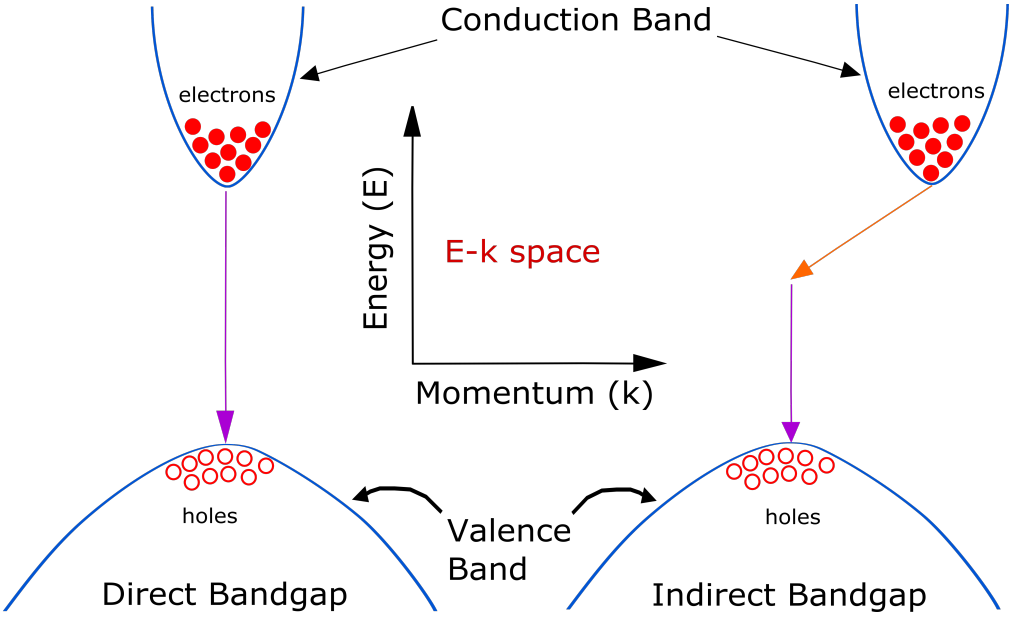

Fig. 2.2 Schematic for position of conduction band and valence band in E-k space for a direct and indirect band gap semiconductor.

2.3.2 Radiative and Non-radiative Recombination

Optoelectronic devices work on the principle of electron-hole recombination resulting in emission of photon. An electron occupying a quantum state in the CB will eventually lose its energy and combine with a hole in the VB. This transition of electron can be accompanied with or without emission of photon depending primarily on the bandgap of the semiconductor material.

Under non-equilibrium conditions, i.e. when electrons are excited from the VB to the CB by external source, optical or electric, creating electron-hole pairs with excess hole concentration in the VB and excess electron concentration in the CB, recombination of these charge carriers can be radiative or non-radiative.

2.3.2.1 Radiative recombination

When electrons and holes recombine with emission of a photon, the process is called radiative recombination. As recombination process is governed by principles of conservation of energy and momentum, such a direct transition is possible in direct bandgap semiconductors. In such semiconductors, mostly because of the same value of momentum vector k, for both the CB minima and the VB maxima, a momentum is conserved during the transition and since the transition is from the higher energy CB to the lower energy VB, emission of a photon (Figure 2.3(b)) of frequency, ν, proportional to the bandgap energy, conserves the energy.

$$E = h\nu \tag{2.2}$$

where,

E = energy gap

h = Planck's constant

ν = frequency of photon

2.3.2.2 Non-radiative recombination

When recombination of electron and hole is not accompanied by emission of a photon it is called non-radiative recombination. Such recombination is due to indirect

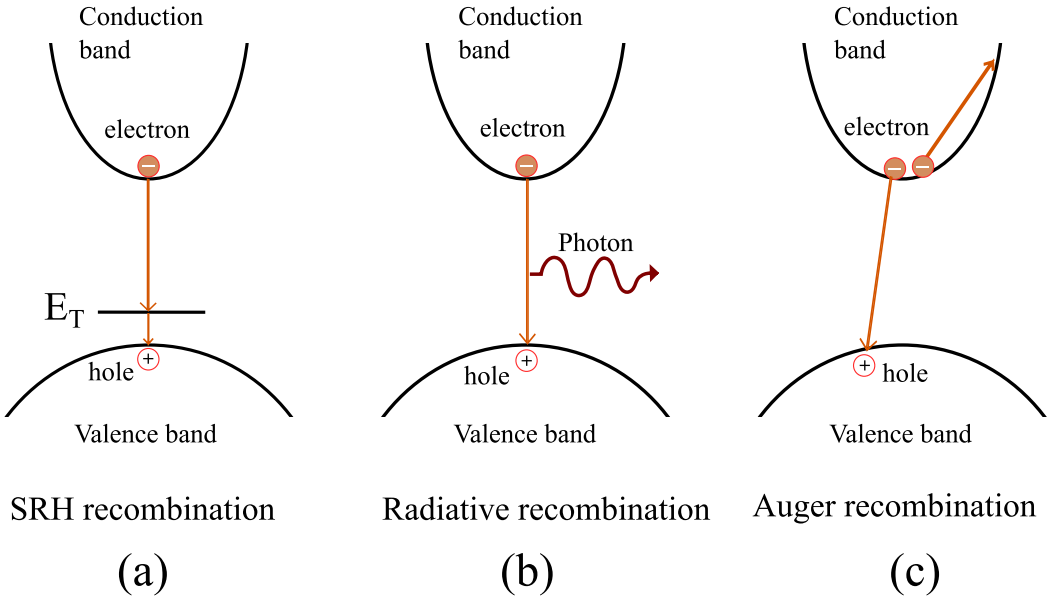

Fig. 2.3 Carrier recombination mechanisms (a) deep level (SRH) non-radiative recombination, (b) Radiative recombination and, (c) non-radiative Auger recombination.

transition of electron from the CB to the VB. This is the dominant process of recombination in indirect bandgap semiconductors. For this recombination, energy is dissipated in the form of lattice vibrations due to the difference in momentum of the CB and VB which is compensated by lattice vibrations known as phonons (Figure 2.4).

Spontaneous emission by radiative recombination is the preferred process for LEDs. However, non-radiative recombination can never be eliminated completely under practical circumstances. While non-radiative recombination is dominant over the other in indirect bandgap semiconductors, they are always competing with each other in direct bandgap semiconductors. The probability of recombination is determined by carrier radiative and non-radiative lifetime, τ_r and τ_{nr}, respectively, according to the equation

$$\tau_R^{-1} = \tau_r^{-1} + \tau_{nr}^{-1} \tag{2.3}$$

where, τ_R = Total Recombination lifetime

τ_r = Radiative recombination lifetime

$\tau_n r$ = Non-radiative recombination lifetime

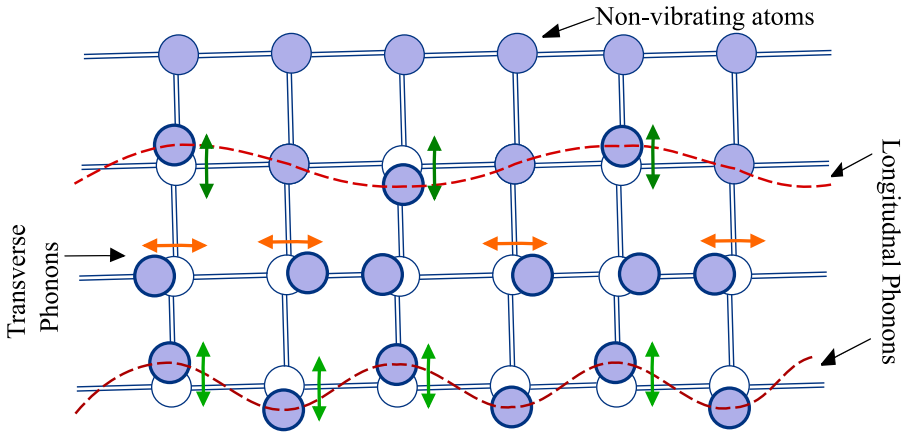

Fig. 2.4 Phonon vibrations in lattice.

For direct bandgap semiconductors $\tau_r \sim \tau_{nr}$ (approximately of same order), hence there is almost an equal probability of having both type of recombination. For radiative recombination to dominate the condition is, $\tau_r \ll \tau_{nr}$. To achieve this condition various physical mechanism that lead to non-radiative transitions, which are - a) Auger recombination, b) Deep level recombination and c) surface recombination needs to be reduced. For Auger recombination (Figure 2.3(c)), the energy released during the transition leads to either excitation of an electron higher up in the CB or pushing a hole deep into the VB. These newly excited carriers then thermalise to release this energy. The probability of Auger recombination is carrier concentration dependent according to the equation [15] -

$$R_{Aug} = Cn^3 \tag{2.4}$$

where, C = Auger coefficient.

This is considered as one of the main mechanism of efficiency droop in LEDs [40]. Deep level recombination or Shockley-Read-Hall (SRH) recombination occurs due to presence of energy levels within the forbidden gap. These energy levels occur due to the presence of defects, like interstitial defects, point defects, impurity atoms, or dislocations, in the semiconductor crystal. The energy structure of these defects is different from bulk crystal and lies within the forbidden gap. These intermediate energy levels act as efficient recombination centres by trapping the charge carriers

(Figure 2.3(a)). They are more efficient if they are close to the middle of the bandgap, so the position of these levels can greatly affect this recombination type.

Along with SRH, surface of semiconductor also contributes to non-radiative transitions due to the presence of dangling bonds can either create energy states in the forbidden gap or the re-arrangement of these bonds can substantially alter the electronic band structure at the surface. In both cases the conditions there are unwarranted energy states which acts as recombination centres and decreases τ_{nr} , thus promoting non-radiative recombination.

The SRH recombination rate and surface recombination probability depending on carrier concentration is illustrated mathematically as

$$R_{SRH} = An \tag{2.5}$$

where, A = SRH and surface recombination coefficient

2.4 Parameters to Access LED performance

2.4.1 Efficiency

Emission of photons due to recombination of electron and holes in LEDs occurs only in the active region (AR) of these devices. The AR of most modern day devices have double-heterostructure's (DH) and contains single or multiple quantum wells (QWs), embedded between the n- and p- doped layers (schematics are shown in chapters 3, 4 and 6) which confines the carriers due to their smaller bandgap thus greatly increasing the probability of interaction between the electrons and holes. The efficiency of this internal recombination process in the AR is termed as *Internal Quantum Efficiency* (IQE) and is a critical parameter to gauge the performance of the device.

IQE (η_{int}) is defined as the ratio of the number of photons generated in the AR in unit time to the number of electrons injected in the AR in unit time.

$$\eta_{int} = \frac{P_{int}/h\nu}{I/e} \tag{2.6}$$

where, P_{int} = Optical power generated inside the AR,

I = injection current,

e = charge of an electron,

h = Planck's constant

Since the optical power referred to in the above expression cannot be measured directly through experiments, it has to be estimated using indirect methods i.e. using theoretical models such as ABC-model (section 2.6). However, on the other hand optical power emitted in the free space from a LED is a measurable quantity along with the injected current. Thus, a total optical efficiency termed as *External Quantum Efficiency* (EQE) of a device can be determined.

EQE (η_{ex}) is defined as the ratio of the number of photons emitted in unit time to the number of electrons injected in unit time.

$$\eta_{ex} = \frac{P_{out}/h\nu}{I/e} \tag{2.7}$$

where, P_{out} = Optical power emitted to free space, and the rest of the parameters are as in (2.6)

In an ideal scenario, where all injected carriers reach the active region without any losses, no carrier is lost to non-radiative recombination and all photons generated in the active region are emitted to the free space, the IQE and EQE would be the same. However, in real devices even under the assumption of unit injection efficiency (η_{inj}), i.e. the fraction of injected carriers (electrons and holes) available in the AR for recombination; photon emitted in the AR will be lost before they could reach free space. This loss in extraction of photons to free space is due to several physical mechanisms. First and foremost, according to Snell's law, due to high refractive index of the semiconductor the critical angle for the emitted light to escape is quite small thus most of the generated light experiences the phenomenon of *total internal reflection*. Next, the emitted light and the totally internally reflected light can be absorbed at the metal contacts, by the substrate (depending on the absorption spectrum), confinement layers, and/or within the active region. The re-absorbed light, apart from the active region, is most likely to create a electron-hole which

will recombine non-radiatively thus reducing the light extraction. Such losses are accounted for under the *light extraction efficiency*(LEE) parameter.

LEE (η_{ext}) is defined as the ratio of number of photons emitted to free space per unit time to number of photons generated in AR per unit time.

$$\eta_{ext} = \frac{P_{out}/h\nu}{P_{int}/h\nu} = \frac{P_{out}}{P_{int}} \tag{2.8}$$

where, P_{out} = Optical power emitted to free space,
P_{int} = Optical power generated inside the AR

Another important parameter of performance is *wall plug efficiency or power efficiency* (WPE) and is defined as the ratio of the output optical power to input electrical power.

$$\eta_{WPE} = \frac{P_{out}}{I \times V} \tag{2.9}$$

where, P_{out} = Optical power emitted to free space,
I = Injected current,
V = Voltage drop across the forward biased LED at current I

2.4.2 Light Quality parameters

Photometry is study of response of human eye to light or perception of light. This restricts the wavelength range of interest to the visible spectrum (from 380 nm to 700 nm).

The basic photometric quantity is luminous intensity, measured in candelas (cd). Luminous intensity is defined as: "a monochromatic light source emitting an optical power of (1/683) watt at 555 nm into the solid angle of 1 steradians (sr) has a luminous intensity of 1 candela (cd)" [15].

Luminous flux (ϕ)is optical power as perceived by human eye, measured in lumen (lm). Illuminance is luminous flux per unit area, measured in lux. Luminance is related to surface area and is defined as "the ratio of the luminous intensity emitted in a certain direction (measured in cd) divided by the projected surface area in that direction (measured in m_2)" [15].

The Photometric quantities are estimated from the radiometric units using luminosity function or a photopic eye sensitivity function, V(λ) introduced by CIE in 1931 [15]. For example, luminous flux from radiant flux can be obtained as follows [41]:

$$\phi = 683.002 \frac{lum}{W} \int_{380nm}^{780nm} \phi_e(\lambda) V(\lambda) d\lambda \tag{2.10}$$

where, $\phi_e(\lambda)$ = radiant flux or optical power
$V(\lambda)$ = eye sensitivity function, and
683.002 is a pre-factor and the maximum luminous flux possible at the λ = 555 nm

V(λ) was later modified to accommodate for the initial underestimation of eye sensitivity in CIE 1931 V(λ) for blue-violet region . V(λ) function describes the human eye response within the wavelength range of 380 – 780 nm for any spectral power distribution.

Luminous efficacy: The above discussion paves the way for describing another type of efficiency for LEDs, known as *luminous efficacy*. It is measured in the units of lumen per watt and is described as the ratio of luminous flux (ϕ) to input electrical power (IV)

$$Luminous\ efficacy = \frac{\phi}{IV} \tag{2.11}$$

Another parameter, *luminous efficiency*, which is described as the ratio of luminous flux to radiant flux, is useful to gauge the perceptually useful light emission from the emitted spectral power distribution function S(λ). The perception of light is a subject of human vision. Human eyes have different cone cells broadly sensitive to red, green and blue region of the visible spectrum under ordinary or daytime light conditions. These cells allows for the colour distinction which is subjective because the sensation of colour from the same source vary with each individual. Towards this, the colorimetric response is quantified and standardised by CIE with colour matching functions $\bar{x}(\lambda), \bar{y}(\lambda), \bar{z}(\lambda)$ (fig. 2.6).

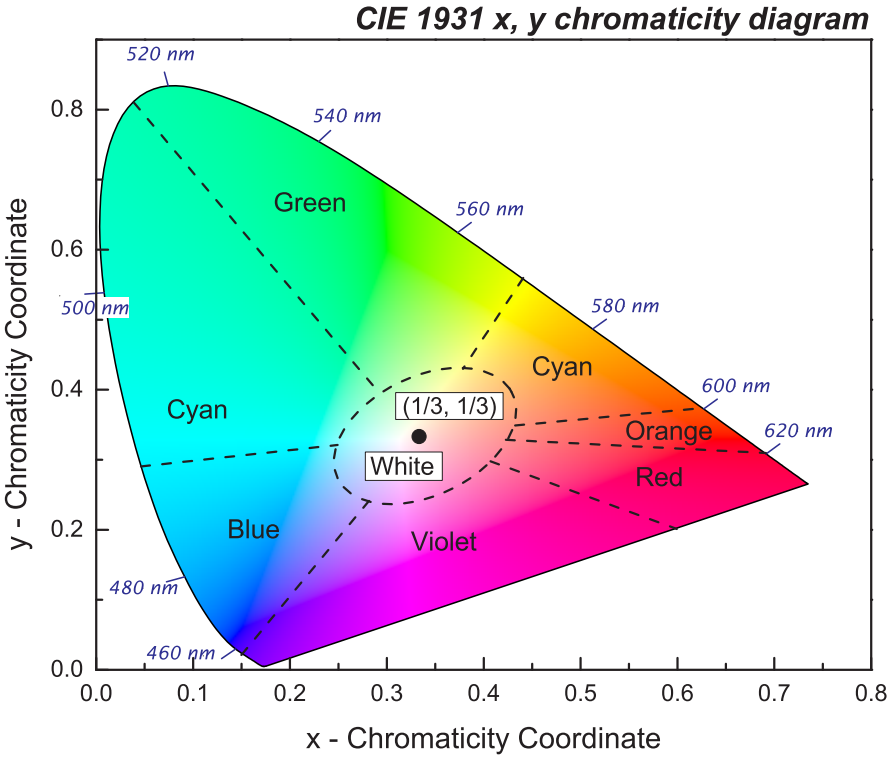

Fig. 2.5 CIE 1931 x,y chromaticity diagram. Wavelength (λ) on the boundary represented on the monochromatic colours. White colour is obtained at the centre of the diagram (adapted from [15]).

Colorimetry gives the qualitative and quantitative description of colour based on human perception. In 1931, to quantify colour perception, CIE described a colour diagram for a 2 degree observer, also known as chromaticity diagram (Figure 2.5). It is a two dimensional diagram with x and y coordinates depicting the colour of the light source. There is also a third z coordinate, which is removed after the normalization of tristimulus values (X,Y,Z), to obtain these x, y and z coordinates, for a standard 2D representation of the diagram. Together, these coordinates give a unique description of the chromaticity of the light source and are calculated as follows:

$$x = \frac{X}{X + Y + Z} \tag{2.12}$$

$$y = \frac{Y}{X + Y + Z} \tag{2.13}$$

$$z = \frac{Z}{X+Y+Z} = 1 - x - y \tag{2.14}$$

Where the tristimulus values X,Y and Z quantifies the stimulation response of the red, green and blue cone cells for a given spectrum. These values are obtained from inner product of the colour matching functions $\bar{x}(\lambda), \bar{y}(\lambda), \bar{z}(\lambda)$, and spectral power distribution function S(λ) as given below:

$$X = \int \bar{x}(\lambda) S(\lambda) d(\lambda) \tag{2.15}$$

$$Y = \int \bar{y}(\lambda) S(\lambda) d(\lambda) \tag{2.16}$$

$$Z = \int \bar{z}(\lambda) S(\lambda) d(\lambda) \tag{2.17}$$

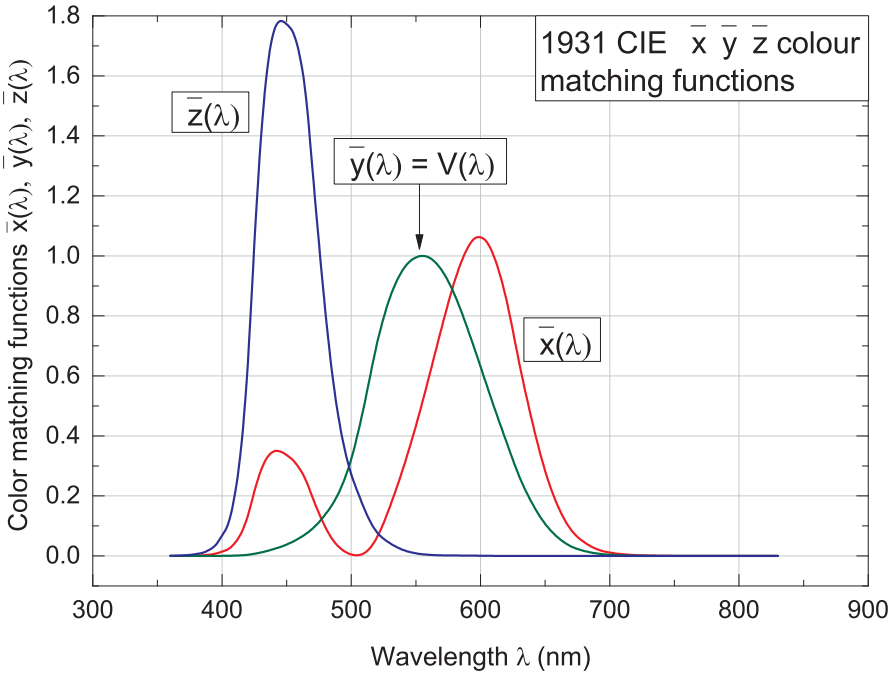

Fig. 2.6 Colour matching functions $\tilde{x}(\lambda)$,$\tilde{y}(\lambda)$,$\tilde{z}(\lambda)$ CIE 1931.

2.4.2.1 Correlated colour temperature (CCT)

Colour temperature may look like a strange parameter, however to quantify colour, a relationship between colour and temperature based on blackbody radiation is established. Planckian blackbody radiation spectrum, characterised by temperature of a black-body, is used as independent standard to quantify white light source with a single parameter of temperature (in kelvins). The intensity of the radiation from the blackbody is a function of wavelength and temperature, and was determined in 1900 by Max Planck [15] given by the relation

$$I(\lambda, T) = \frac{2hc^2}{\lambda^5} \frac{1}{e^{hc/\lambda k_B T} - 1} \tag{2.18}$$

According to Wein's law, at a given temperature the radiation spectrum of a black-body has a unique wavelength corresponding to its peak intensity as given by the relation

$$\lambda_{peak} = \frac{2880\ \mu m\ K}{T} \tag{2.19}$$

As the temperature of the blackbody increases the radiation pattern shifts from the infra-red to the visible spectrum. The chromaticity coordinates corresponding to radiation pattern at different temperatures can be calculated using the equations 2.12 - 2.14, which constitute Planckian locus, as shown in figure 2.7. A, B, C, E and D65 are the standard illuminants defined by CIE (1978) and are depicted in figure 2.7 along with their colour temperatures.

Correlated colour temperature or CCT is used for the light source that doesn't fall on the planckian locus. "Correlated colour temperature is the temperature of the Planckian radiator whose perceived colour most closely resembles that of a given stimulus at the same brightness and under specified viewing conditions [42]". On the uniform chromaticity diagram (CIE 1960) the chromaticity point with a similar CCT, given by the isothermal lines perpendicular to the planckian locus (as shown in figure 2.8), determines the colour or chromaticity of the light source under test.

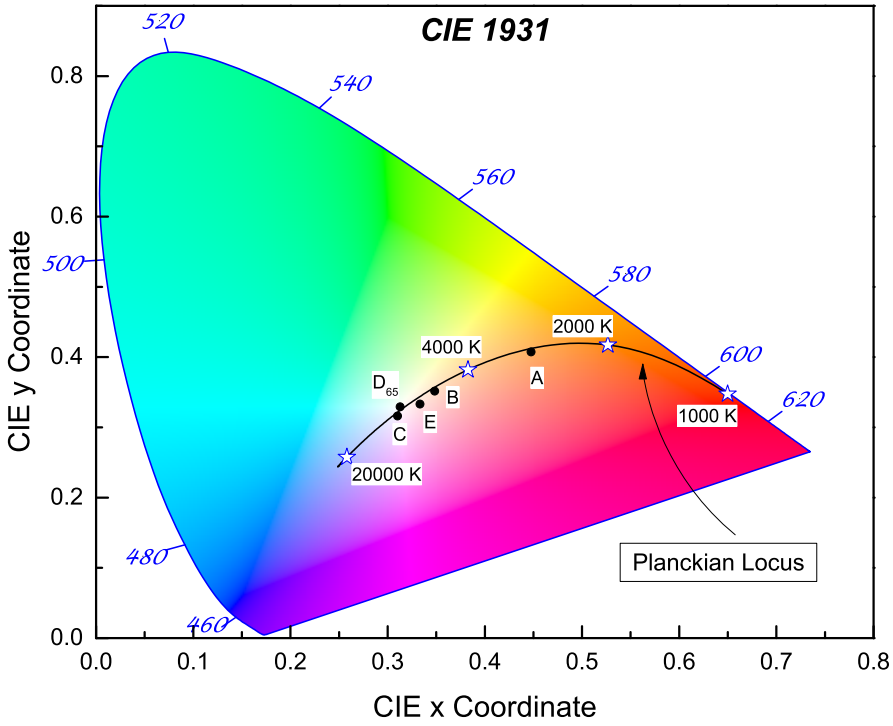

Fig. 2.7 CCT range on planckian locus and for CIE standard illuminant: A (incandescent source – 2856K), B (direct sunlight – 4870K), C (overcast source – 6770K), D65 (Daylight – 6500K) and E (equal energy illuminant point -0.3,0.3) (adapted from [15]).

2.4.2.2 Colour rendering index (CRI)

Colour rendering index (CRI) is an important parameter quantifying the capability of rendering colours of the object illuminated by a light source [43]. The maximum rating value of CRI has been defined as 100 for the planckian blackbody reference source that is assumed to have perfect colour rendering capabilities. CRI of a test white light source is determined by comparing it with colour rendering of a reference source. The reference source can be a planckian black body radiator with same colour temperature (if chromaticity coordinates of test source falls on the planckian locus) and CCT (if they fall off the planckian locus) or a standard reference illuminant can be used [43]. According to the CIE guide, general CRI (R_a) (calculated according to the relation 2.20) is determined using the special CRI_i (calculated according to the relation 2.21) of the 8 standard test colour samples . The 8 test samples are subset of the larger set of colour samples introduced by Prof.

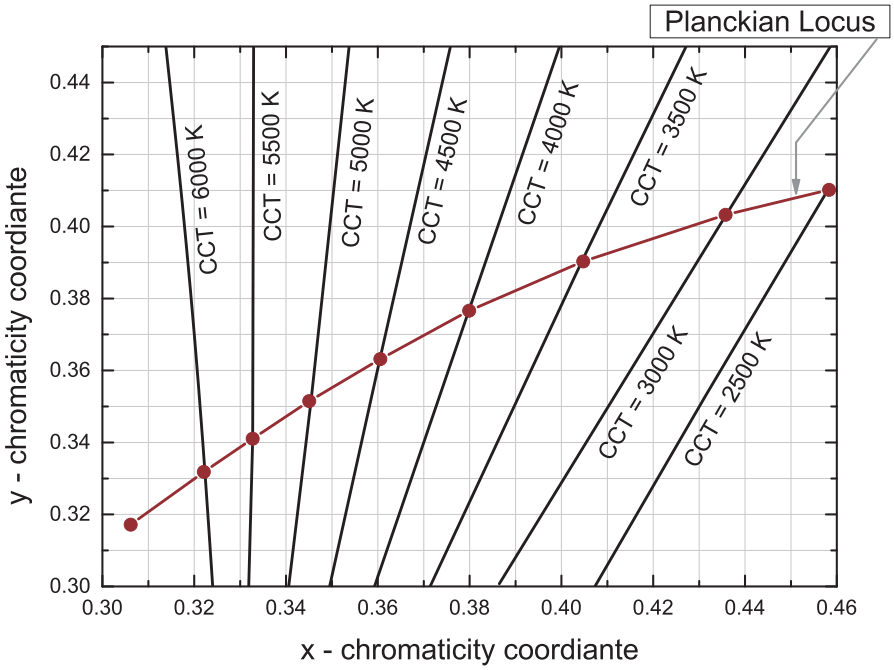

Fig. 2.8 Perpendicular lines of constant CCT in CIE (x, y) chromaticity diagram (adapted from [15]).

Albet H. Munsell in the *Munsell colour system*.

$$CRI = \frac{1}{8}\sum_{i=1}^{8} CRI_i \tag{2.20}$$

$$CRI_i = 100 - 4.6\Delta E_i^* \tag{2.21}$$

where, ΔE_i^* represents colour difference of a test sample when illuminated with a reference and a test source. The pre-factor 4.6 is for R_a of 60, for more information on calculation of CRI please refer to chapter 19 in [15] and the references within.

Apart from the eight samples, to further gauge the colour rendering ability of the test source, 6 more test samples can be used to supplement the initial assessment. The reflectivity of these samples are associated with particularly strong colours. These are known as special colour rendering indices and represented as R_9 to R_{14}.

2.4.3 Spectral properties of LED

The spectrum of LEDs, unlike lasers is not monochromatic and is also not broadband. A typical LED spectrum is in the range of 20-50 nm. To identify the emission wavelength of LEDs with single number four different descriptions are in common use. The most common is *Peak Wavelength*. It is the wavelength with maximum spectral power in the spectrum denoted as λ_P. Another description is known as *Centre Wavelength* ($\lambda_{1/2}$). It is described as the wavelength in the middle of the two connecting points at the spectral power = $(1/2)\lambda_P$. Next, *Centroid wavelength* (λ_c) which is the mean of all the wavelengths present in the spectrum provides a better description of single colour LEDs.

2.5 Efficiency Droop in III-Nitride LEDs

One of the key features of the LEDs is the promise of high energy efficiency leading to reduced energy consumption and hence contributing towards climate change. In this respect, when compared to existing light sources, LEDs have better energy efficiency. More radiant flux from the same LED can be obtained by operating them at higher driving currents. However, under such operating conditions the efficiency of these devices decreases exponentially. This variable dependence of efficiency on current is one of the crucial challenges to be addressed for LEDs to achieve their full potential and is well known as the phenomenon of *"Efficiency Droop"* [44]. It is the observed decrease in external quantum efficiency with increasing current density after attaining a peak value, as shown in figure 2.9. The peculiar shape of the EQE vs current dependence (see Fig. 2.9) is modelled using the ABC recombination model (see section 2.6), $R = An + Bn^2 + Cn^3$, where n represents the carrier concentration. The effect of coefficient A (representing SRH recombination) manifests as linear dependence at low current values before the radiative recombination term with coefficient B dominates at high currents. At very high currents the decrease in efficiency is attributed to the coefficient C of the cubic term. This gradual decrease in efficiency, after certain current density, is a serious issue with both InGaN and

AlGaInP LEDs; though most of the recent effort has been invested on GaN LEDs. It can be calculated using the expression :

$$EQE_{Droop} = \frac{EQE_{Peak} - EQE_I}{EQE_{Peak}} \tag{2.22}$$

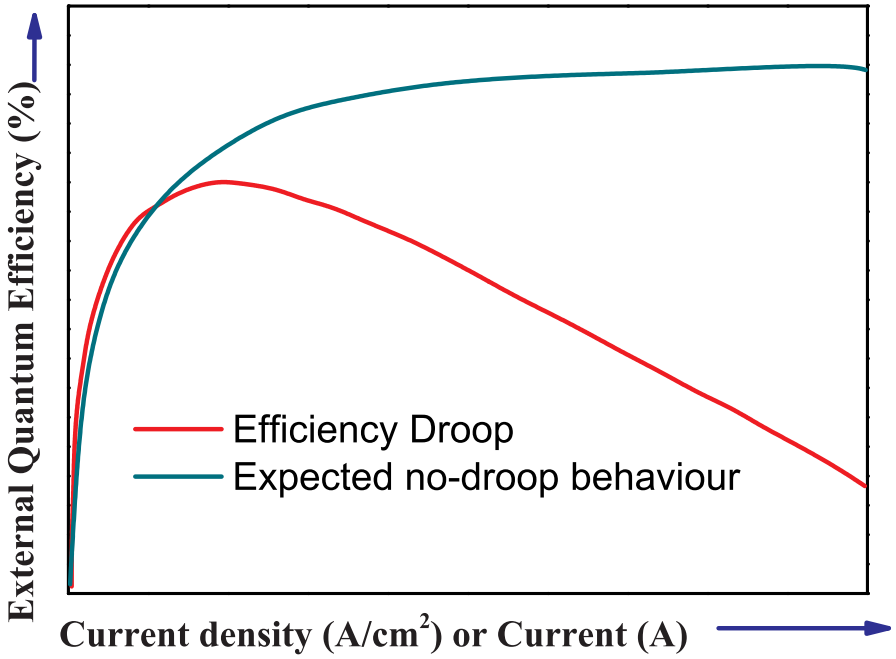

Fig. 2.9 Illustration of *Efficiency droop* in III-nitrides (not to scale).

Furthermore, the term efficiency droop is mostly used in reference to the GaN based LEDs. For AlGaInP the phenomenon is rather stated as decrease of efficiency and may or may not be referred as *droop*. In this text the term *droop* will be used to refer to efficiency decrease in GaN LEDs and will not be used in the context of AlGaInP LEDs.

The *Efficiency Droop* phenomenon in III-nitride LEDs has been observed under both photoluminescence and electroluminescence and is under intense investigation and debate in the research community. Several different physical processes has been proposed over last decade as the probable cause while a consensus on one or group of these processes has still not been achieved. A brief introduction about some of the proposed mechanisms is presented below.

2.5.1 Auger recombination

A three particle process, Auger recombination is the most debated mechanism concerning *droop* phenomenon for GaN LEDs. Direct Auger recombination is a non-radiative process in which when an electron and hole combines the energy is not released as a photon and is instead transferred to the third carrier, an electron or a hole, exciting it to another energy level i.e. higher in conduction band for electron and deeper or lower in the valence band for holes. It has a cubic dependence on carrier concentration and hence should contribute more towards the droop with increasing current. It is accounted by the coefficient C in the *ABC-model* (discussed in next section). The debate on the contribution of Auger recombination to efficiency droop is effectively centred around different experimental values reported for Auger coefficient (C). Shen et al. [45] reported values of the order of 10^{-30} cm^6 s^{-1} by performing resonant optical excitation on double heterostructure (DH) InGaN layer whereas values in the range of 10^{-27} cm^6 s^{-1} - 10^{-24} cm^6 s^{-1} reported by Ryu et al [46]. A number of experimental studies to extract the value of C using ABC model, neglecting carrier escape or leakage, has been performed on single and multiple QW and are reviewed by Piprek [44]. On the other hand much lower theoretical values for Auger coefficient of the order of 10^{-34} cm^6 s^{-1} [47] has been calculated. The low theoretical values (based on ABC model) are in contrast to the experimental values and are less likely to provide a good fit to the experimental data. Towards this, to account for the difference between the theoretical and experimental values additional Auger recombination mechanisms has been proposed. Phonon assisted indirect Auger recombination requiring a phonon for a third carrier to make a transition has been accounted along with direct Auger recombination by Kioupakis et al. [48] yielding Auger coefficient values in the range of 0.5×10^{-31} cm^6 s^{-1} - 2×10^{-31} cm^6 s^{-1}. However, this range is only enough to account for the lowest experimentally reported values of 1.8×10^{-31} cm^6 s^{-1} [49] and is not enough to account for most experimentally observed values in the range of $\sim 1.4\times10^{-30}$ cm^6 s^{-1} to 1×10^{-24} cm^6 s^{-1} [45, 46, 50–52]. On the other hand Delaney et al. calculated, from first principles using density functional and many-body-perturbation theory, values of Auger coefficient in the range of 1×10^{-34} cm^6 s^{-1} to 5×10^{-28} cm^6 s^{-1}.

They attributed this agreement of the values to the interband Auger recombination by accounting for another band above the conduction band for the wide band gap semiconductors thus estimating a coefficient of 2×10^{-30} cm^6 s^{-1} in complete agreement with Shen et al [45].

2.5.2 Carrier delocalisation

Most GaN devices are grown on sapphire substrate with a large lattice constant mismatch leading to a large number of defects, mainly point defects and threading dislocations, with a density of $\sim 10^9$ cm^{-2}. Despite that III-Nitride devices exhibit high IQE [53–57]. This has been explained by localisation of carrier in an in-plane local potential minimum before the carriers can reach and recombine at dislocations. Several mechanisms have been proposed for such localisation to be plausible and they are (a) fluctuations in width of QW [58–61], (b) In clustering [62, 63], (c) random alloy fluctuations [64, 65] and (d) hexagonal V-shaped pits or funnels caused by threading dislocations [66]. The first three mechanisms individually or collectively are responsible for localised potential minima whereas the V-pits around the threading dislocations is anti-localisation. It has been suggested that the very narrow QWs at the sides of the hexagonal pits create a high potential barrier around dislocation sites thus keeping them physically distant from these threading dislocations.

Thus it is reasonable to assume that local fluctuations in potential keeps the carriers and non-radiative recombination centres physically separated. Therefore when the active region is injected with low current densities these potential minimum are able to confine the carriers locally. However, at higher current densities these local minima gets overfilled with carriers and they start to escape i.e. gets delocalised only to be captured by dislocations and getting lost to non-radiative recombinations and thus lowering the efficiency [53–55, 67, 68]. These carrier can further lead to increased junction temperature due to heating caused by parasitic tunnelling current facilitated by threading dislocations [69]. This would only increase with increased carrier injection promoting acoustic phonon assisted tunnelling [69].

Haider at al. has in their studies proposed density activated defect recombination (DADR) as the possible mechanism for efficiency droop. They argued that the potential minima caused either by In composition fluctuations or QW width fluctuations shields the carriers from defects at low carrier density however at higher densities the carriers escape to rest of the QW thus recombining easily at defect recombination centres. They modelled the non-radiative loss due to carrier delocalisation and demonstrated a good fit with the experimental data for LEDs emitting at 410 nm and 530 nm.

More evidence towards delocalisation was presented by Wang et al. [55]. They studied the efficiency droop behaviour of two LEDs grown with different under layers (GaN and InGaN). Based on the PL studies they argued that the LED with InGaN underlayer had higher degree of localisation. For analysis the EQE(I) is analysed in three parts. They attributed higher peak IQE at lower current densities i.e.part (1) of EQE(I) and rapid drop at increased current densities i.e. part(2) of EQE(I), to carrier delocalisation. They further suggested that for current densities > 24 A cm^{-2} i.e. part (3) of EQE(I) efficiency droop is more likely to be caused by carrier leakage. Similar observation regarding carrier delocalisation has been made by Hammersley et al. [70] in their temperature dependent PL studies on InGaN QW LEDs.

On the other hand, contrary to all these observations Shubert et al. [71] based on recombination rate equation analysis of two InGaN LEDs with different dislocation densities, 5.3×10^8 and 5.7×10^9 cm^{-2} suggests carrier leakage at high current densities to be the dominant mechanism for efficiency droop. The experimental results presented in their paper clearly demonstrate higher peak efficiency and larger droop from low dislocation density LED.

Moreover, indium rich islands or In clustering due to segregation of InGaN is brought into doubt by Smeeton et al. [72]. They described that observation of such structures in TEM measurements [62] is due to the damage done by the electron beam rather than the compositional fluctuations. Galtery et al [73] later confirmed these observations with 3D atom probe measurements and describing observed indium distribution as random alloy distribution.

2.5.3 Electron Leakage

Electron leakage is the term used to account for all the injected electrons that escape the QWs in the active region and thus are not contributing towards photon emission irrespective of the physical mechanism responsible for loss of electrons to non-radiative recombination. These electrons then recombine in the p-GaN or p-type electrode. To restrict the leakage of carriers to p-side of the device AlGaN electron blocking layer (EBL) are implemented adjacent to p-GaN in the device structure. The idea is to create a high enough potential barrier for electrons to be reflected back towards the QWs. However, an emission beyond EBL in the p-doped region of the device has been observed [74, 75]. While this observation on one hand affirms the ineffectiveness of EBL on the other hand it also relates electron leakage directly to efficiency droop. The key observations made by the author relating droop and leakage are (i) spontaneous emission increases with current, (ii) lower peak EQE, (iii) onset of droop shifting to higher currents. The ineffectiveness of EBL has been mainly attributed to polarisation fields [76] for polar GaN LEDs grown on c-plane sapphire substrate. The positive sheet charge accumulated at the GaN barrier and AlGaN EBL interface, due to difference in the degree of spontaneous and piezoelectric polarisation between the two, attracts electrons. This skews the energy band diagram of EBL rather negatively thus reducing its effective height in terms of energy. One way to increase EBL barrier height would be to increase Al content of the AlGaN EBL layer, however, the achieved increase in barrier height would be ineffective due to a larger increment in the conduction band offset between GaN spacer and AlGaN EBL [77].

2.5.4 Other mechanisms

Among other mechanisms *poor hole injection* [78, 79] and *asymmetric carrier concentration and mobility* are considered as the cause of electron leakage [80]. Both these mechanisms have common root in not being able to achieve high hole concentration due to self-compensation of Mg dopant limiting the p-type doping of GaN. This results in lesser number of holes as compared to electrons obtained at

n-GaN with Si doping due to low ionization energy of $\sim$ 17 meV [81] compared to 170 meV ionization energy needed for Mg acceptors in GaN [82]. Along with this, EBL which is implemented to restrict electron escape poses a hindrance to hole movement due to valence band offset at the AlGaN and GaN spacer, thus leading to poor hole injection into the active region. This has been demonstrated to be a factor contributing to droop by implementation of a three terminal diode, where two anodes were used to improve hole injection [83]. On the other hand, the carrier concentration asymmetry due to difference in electron and hole concentrations, for the above mentioned reasons, along with lower hole mobility due to its higher effective mass have been together identified as mechanisms contributing to electron leakage and hence to droop [84].

2.6 ABC Model for efficiency analysis

One of the challenges in LED analysis is to determine IQE and LEE of the device which cannot be measured experientially. Therefore, these parameters need to be extracted from experimentally measurable quantities using theoretical models. In case of LEDs the most commonly and simple model to be used is recombination rate model or more famously known as ABC model. The simplicity of the model comes from the following underlying assumptions. First, the concentration of electrons and holes is equal. Second, all carriers undergo some sort of recombination within the active region and does not escape the AR. Finally, the recombination constants for SRH, radiative, and non-radiative i.e. A, B and C respectively are assumed to have negligible dependence on carrier concentration. Under steady state conditions the rate equation based on carrier concentration (n) is given as

$$R = An + Bn^2 + Cn^3 \tag{2.23}$$

$$R = \frac{I\ \eta_{inj}}{(q\ V_{AR})} \tag{2.24}$$

where, R is total recombination rate, I is injection current, q is elementary charge, V_{AR} is active region volume with high carrier concentration, B is radiative recombination constant, and η_{inj} is injection efficiency which is assumed to be 1. Subsequently IQE along with the output power (P_{out}), operation current (I), and EQE can be expressed in terms of n and the recombination constants and are give below along with η_{int} and η_{ex}.

$$\eta_{int} = \frac{Bn^2}{R} = \frac{Bn}{A + Bn + Cn^2} \tag{2.25}$$

$$\eta_{ex} = \eta_{int}\ \eta_{ext} = \frac{q\ P_{out}}{\hbar\nu\ I} \tag{2.26}$$

$$I = q\ V_{AR}\ (An + Bn^2 + Cn^3) \tag{2.27}$$

$$P_{out} = \hbar\nu\ \eta_{ext}\ V_{AR}\ Bn^2 \tag{2.28}$$

The popularity of the ABC model is driven by the understanding that a good fit with the experimental EQE variation with current or optical power and hence with IQE will provide more information and evidence of physical processes that can account for the non-thermal droop i.e. the phenomenon of efficiency droop. Towards this ABC model has been used to fit the experimental data with a good agreement. Using the model Shen et al [45] reported that Auger recombination is the likely reason behind for the high current efficiency droop. They performed PL studies on quasi-bulk InGaN layers with varying In content (9-15%), threading dislocation density and layer thickness. The ABC model is also in good agreement with the observations of Laubsch et al. [85] who reported phonon- or defect-assisted Auger recombination as the cause of droop citing previously reported [47] low values of Auger coefficient (C). In the ABC model, Auger recombination is the only reason included for the droop as the model accounts only for the recombinations occurring within the active region of the LED.

On the other hand, deviation of the model from experiment at high current densities after peak EQE is well known and hence the over-simplicity of the model has been criticised [52]. Towards this, to account for carrier leakage induced non-radiative recombination outside the active region that is separate from Auger recombination, a carrier leakage term has been proposed. Inclusion of such a term have shown improved agreement with experimental data at high current densities [44, 80, 86]. Though expansion of ABC model give a better fit in some cases the largely open question about the order of Auger coefficient and non-measurable carrier concentration under non-equilibrium conditions may not allow the model to clearly identify the basic physical mechanism responsible for droop.

2.7 White Light generation: monolithic and pc-LEDs

Human eyes have three types of cones that are most sensitive to specific wavelength range. Three primary wavelength or colour ranges are 420nm – 440nm, 530 – 540nm, and 600 – 630nm. Each of these ranges translates into blue, green and red colour regions, respectively. When mixed in an appropriate spectral ratio, other colours including white can be generated from these primary wavelengths.

The chromaticity coordinates for white light are located in the centre at the equal intensity point of the chromaticity diagram. Thus a number of optical spectra combinations can provide the needed white light emission. Towards this, LED based dichromatic, trichromatic and tetra-chromatic approaches with two, three and four emission peaks respectively can be exploited to generate white light. These approaches can be realised in more than one configuration. The most common and commercially available configuration is phosphor covered (pc-) LED. Most of these sources uses InGaN/GaN based blue LEDs to pump broadband yellow phosphor (YAG:Ce3+) and produce white light. These light sources have shown good values of CRI around 70-80, CCT in the range of 4000-8000 K [87] and luminous efficacy of 160 lm/W [88]. The lack of red component has been the primary reason for low CRI for this configuration. Thus a multi-phosphor approach is adopted where

pumping LED can be UV or blue but the photon recycling coating of phosphor is a mixture of two or three phosphors based on YAG (540-560 nm), Lutetium Aluminium Garnet (520-540 nm), Oxynitrides (500-650) and nitrides(615-660 nm) and LED with CRI $\sim$ 95 are made commercially available [89, 90]. Though high CRI sources can be realised using many phosphors it has some inherent issues. First, the well known Stoke's losses increase with addition of another phosphor thus affecting the overall efficiency of the source. Second, the angular uniformity of emission is dependent upon the scattering of light due to particle size and efficiency of phosphor is also a function of particle size. Thus use of multi-phosphor poses optimisation issue in achieving reasonable efficiency and uniformity of emission. Despite this, the advantages of broad emission spectrum and absorption strength, stable emission spectrum and efficiency at broad range of temperatures, along with saturation tolerance at stronger flux levels are driving the development and use of pc-LED.

The phosphor free approaches to white light generation are multichip and monolithic LEDs. A multichip source is a combination of three or more LEDs (thus tri- or tetra-chromatic) emitting at different wavelengths in the red, green and blue region of the spectrum. Although addition of more LEDs will improve the CRI the luminous efficacy of these sources is limited primarily due to "green gap"problem i.e. low EQE in the wavelength region of eye sensitivity curve. Furthermore, since the two different material system (as discussed before) are responsible for emission in high and low energy part of the spectrum they exhibit different optimal operating parameters leading to a requirement of complex circuitry for operation. Strong temperature dependence of AlGaInP LEDs also affects their operation at elevated temperature leading to non-optimal efficiency performance along with colour variation [91].

Since InGaN/GaN, in principle, can emit across the visible spectrum by varying the In composition, it has inspired researchers to develop single LED emitting at multiple wavelengths. This monolithic approach is also under development and investigation. In 2001, Damilano et al. proposed InGaN/GaN MQW monolithic white LEDs [92]. Since, then these LEDs are under development for improvement of

efficiency and colour parameters. Under this approach, following the basic principle of mixing different wavelengths (colours) in appropriate proportion (intensity), multiple InGaN quantum wells (QW) emitting at different wavelengths are used to achieve white light. MQWs are sandwiched between p and n type GaN layers and are intrinsic (or undoped) themselves. To achieve emission at short and long wavelengths indium (In) incorporation in the stacked QWs is varied and is predefined during the growth process. As no phosphor is used in this approach, the efficiency losses associated with phosphor are non-existent along with reduction of one process step (of phosphor deposition) in the LED fabrication. Though this approach follows the same principle as multichip approach of colour mixing the fundamental difference is that a single chip emits different wavelength against the assembly of several monochromatic chips using separate driver circuits and a feedback mechanism to maintain appropriate colour mixing. Also, as this approach uses a single material system the different ageing times in the multichip approach is addressed. Hence, monolithic LEDs show promising improvements and can be the way forward for SSL in the near future. Apart from QWs, nanopyramid GaN [93] and ZnO nanowires on GaN heterostructure's [94] are also under investigation . Other approaches like QW light converters [95] and distributed Bragg reflector (DBR) resonant- cavity have also been investigated [96].

References

[1] H. J. Round, "A note on carborundum," *Electr. World*, vol. 47, p. 309, 1907.

[2] O. Lossev, "CII. Luminous carborundum detector and detection effect and oscillations with crystals," *London, Edinburgh, Dublin Philos. Mag. J. Sci.*, vol. 6, no. 39, pp. 1024–1044, 1928.

[3] N. Zheludev, "Commentary. The life and times of the LED - a 100-year history," *Nat. Photonics*, vol. 1, no. April, pp. 189–192, 2007.

[4] J. A. Edmond, H.-S. Kong, and C. H. Carter, "Blue LEDs, UV photodiodes and high-temperature rectifiers in 6H-SiC," *Phys. B Condens. Matter*, vol. 185, no. 1-4, pp. 453–460, 1993.

[5] J. I. Pankove and M. J. Massoulie, "Injection luminescence from GaAs," *Bull. Am. Phys. Soc*, vol. 7, p. 88, 1962.

[6] R. N. Hall, G. E. Fenner, J. D. Kingsley, T. J. Soltys, and R. O. Carlson, "Coherent light emission from GaAs junctions," *Phys. Rev. Lett.*, vol. 9 (9), no. November, pp. 366–368, 1962.

[7] M. I. Nathan, W. P. Dumke, G. Burns, F. H. Dill, and G. Lasher, "Stimulated emission of radiation from GaAs p-n junctions," *Appl. Phys. Lett.*, vol. 1, no. 3, p. 62, 1962.

[8] N. Holonyak and S. F. Bevacqua, "Coherent (Visible) light emission from Ga(As(1-x)Px) junctions," *Appl. Phys. Lett.*, vol. 1, no. 4, p. 82, 1962.

[9] N. Holonyak, S. F. Bevacqua, C. V. Bielan, and S. J. Lubowski, "The "Direct-Indirect"transition in Ga(As(1-x)Px) p-n junctions," *Appl. Phys. Lett.*, vol. 3, no. 3, pp. 47 –49, 1963.

[10] N. Holonyak, C. Nuese, M. Sirkis, and G. Stillman, "Effect of donor impurities on the direct-indirect transition in Ga(As1 - xPx)," *Appl.Phys. Lett.*, vol. 8, no. 4, p. 83, 1966.

[11] M. H. Pilkuhn and H. Rupprecht, "Light Emission from GaAs(x)P(1-x) Diodes," *Trans. Metall. Soc. AIME*, vol. 230, no. 2, p. 282, 1964.

[12] C. M. Wolfe, C. J. Nuese, and N. Holonyak, "Growth and Dislocation Structure of Single-Crystal Ga(As(1-x)Px)," *J. Appl. Phys.*, vol. 36, no. 12, p.3760, 1965.

[13] J. Allen, M. Moncaster, and J. Starkiewicz, "Electroluminescent devices using carrier injection in gallium phosphide," *Solid. State. Electron.*, vol. 6, no. 2, pp. 95–102, 1963.

[14] H. Grimmeiss and H. Scholz, "Efficiency of recombination radiation in GaP," *Phys. Lett.*, vol. 8, no. 4, pp. 233–235, 1964.

[15] E. F. Schubert, *Light-Emitting Diodes*, 2nd ed. Cambridge: Cambridge University Press, 2006.

[16] K.-H. Huang and T.-P. Chen, "Light emitting diode structure," 1995. Available: https://www.google.com/patents/US5661742

[17] S. J. Chang and C. S. Chang, "650 nm AlGaInP/GaInP compressively strained multi-quantum well light emitting diodes," *Japanese J. Appl. Physics, Part 2 Lett.*, vol. 37, no. 6 A, pp. 653–655, 1998.

[18] S. J. Chang and C. S. Chang, "AlGaInP-GaInP compressively strained multiquantum-well light-emitting diodes for polymer fiber application," *IEEE Photonics Technol. Lett.*, vol. 10, no. 6, pp. 772–774, 1998.

[19] R. M. Fletcher, C. P. Kuo, T. D. Osentowski, K. H. Huang, M. G. Craford, and V. M. Robbins, "The growth and properties of high performance AlGalnP emitters using a lattice mismatched GaP window layer," *J. Electron. Mater.*, vol. 20, no. 12, pp. 1125–1130, 1991.

[20] F. A. Kish, F. M. Steranka, D. C. DeFevere, D. A. Vanderwater, K. G. Park, C. P. Kuo, T. D. Osentowski, M. J. Peanasky, J. G. Yu, R. M. Fletcher, D. A. Steigerwald, M. G. Craford, and V. M. Robbins, "Very high-efficiency semiconductor wafer-bonded transparent-substrate (AlxGa(1-x))0.5In0.5P/GaP light-emitting diodes," *Appl. Phys. Lett.*, vol. 64, no. 21, pp. 2839–2841, 1994.

[21] M. R. Krames, M. Ochiai-Holcomb, G. E. Hofler, C. Carter-Coman, E. I. Chen, I.-H. Tan, P. Grillot, N. F. Gardner, H. C. Chui, J.-W. Huang, S. A. Stockman, F. a. Kish, M. G. Craford, T. S. Tan, C. P. Kocot, M. Hueschen, J. Posselt, B. Loh, G. Sasser, and D. Collins, "High power truncated-inverted-pyramid (AlxGa(1-x))0.5In0.5P/GaP light-emitting diodes exhibiting >50% external quantum efficiency," *Appl. Phys. Lett.*, vol. 75, no. 2002, pp. 2365–2367, 1999.

[22] I. Akasaki, H. Amano, K. Itoh, N. Koide, and K. Manabe, "GaN-based UV/blue light emitting devices," in *GaAs Relat. Compd. Conf. Inst. Phys. Conf. Ser. No.129*, pp. 851 – 856, 1992.

[23] H. P. Maruska, "The Preparation and Properties of Vapor-Deposited Single-Crystal-Line GaN," *Appl. Phys. Lett.*, vol. 15, no. 10, p. 327, 1969.

[24] H. Amano, M. Kito, K. Hiramatsu, and I. Akasaki, "P-Type Conduction in Mg-Doped GaN Treated with Low-Energy Electron Beam Irradiation (LEEBI)," *Jpn. J. Appl. Phys.*, vol. 28, no. Part 2, No. 12, pp. L2112–L2114, 1989.

[25] N. Iwasa, S. Nakamura, and M. Senoh, "Method of manufacturing p-type compound semiconductor," 1994. Available: http://www.google.com/patents/US5306662

[26] S. Nakamura and T. Mukai, "High-quality InGaN films grown on GaN films," *Jap. J. Appl. Phys*, vol. 1457, 1992.

[27] S. Nakamura, M. Senoh, and T. Mukai, "P-GaN/N-InGaN/N-GaN Double-Heterostructure Blue-Light-Emitting Diodes," *Jpn. J. Appl. Phys.*, vol. 32, no. Part 2, No.1A/B, pp. L8–L11, 1993.

[28] J. Baur, F. Baumann, M. Peter, K. Engl, U. Zehnder, J. Off, V. Kuemmler, M. Kirsch, J. Strauss, R. Wirth, K. Streubel, and B. Hahn, "Status of high efficiency and high power ThinGaN®-LED development," *Phys. Status Solidi*, vol. 6, no. S2, pp. S905–S908, 2000.

[29] R. D. Dupuis and M. R. Krames, "History, Development, and Applications of High-Brightness Visible Light-Emitting Diodes," *J. Light. Technol.*, vol. 26, no. 9, pp. 1154–1171, 2008.

[30] M. Mendes, J. Fu, C. Porneala, X. Song, M. Hannon, and J. Sercel, "Lasers in the manufacturing of LEDs," in *Proc. SPIE 7584, Laser Appl. Microelectron. Optoelectron. Manuf. XV*, H. Niino, M. Meunier, B. Gu, and G. Hennig, Eds., p. 75840T, 2010.

[31] G. Y. Mak, E. Y. Lam, and H. W. Choi, "Precision laser micromachining of trenches in GaN on sapphire," *J. Vac. Sci. Technol. B Microelectron. Nanom. Struct.*, vol. 28, no. 2, p. 380, 2010.

[32] H. M. Lam, M. Hong, S. Yuan, and T. C. Chong, "Laser ablation of GaN/sapphire structure for LED," in *Proc. SPIE 4830, Third Int. Symp. Laser Precis. Microfabr.*, I. Miyamoto, K. F. Kobayashi, K. Sugioka, R. Poprawe, and H. Helvajian, Eds., p. 114, 2003.

[33] E. Illy, M. Knowles, E. Gu, and M. Dawson, "Impact of laser scribing for efficient device separation of LED components," *Appl. Surf. Sci.*, vol. 249, no. 1-4, pp. 354–361, 2005.

[34] A. Tamhankar and R. Patel, "Optimization of UV laser scribing process for light emitting diode sapphire wafers," *J. Laser Appl.*, vol. 23, no. 3, p. 032001, 2011.

[35] T. Nilsson, F. Wagner, R. Housh, and B. Richerzhagen, "Scribing of GaN wafer for white LED by water-jet-guided laser," in *Proc. SPIE 5366, Light. Diodes Res. Manuf. Appl. VIII*, S. A. Stockman, H. W. Yao, and E. F. Schubert, Eds., p. 200, 2004.

[36] Y. Zhang, H. Xie, H. Zheng, T. Wei, H. Yang, J. Li, X. Yi, X. Song, G. Wang, and J. Li, "Light extraction efficiency improvement by multiple laser stealth dicing in InGaN-based blue light-emitting diodes," *Opt. Express*, vol. 20, no. 6, p. 6808, 2012.

[37] S. Juodkazis and H. Misawa, "Laser processing of sapphire by strongly focused femtosecond pulses," *Appl. Phys. A*, vol. 93, no. 4, pp. 857–861, 2008.

[38] S. Juodkazis, K. Nishimura, S. Tanaka, H. Misawa, E. G. Gamaly, B. Luther-Davies, L. Hallo, P. Nicolai, and V. T. Tikhonchuk, "Laser-Induced Microexplosion Confined in the Bulk of a Sapphire Crystal: Evidence of Multimegabar Pressures," *Phys. Rev. Lett.*, vol. 96,no. 16, p. 166101, 2006.

[39] M. Squared, "Sprite XT." Available: http://www.m2lasers.com/lasers/all-lasers/sprite-xt.aspx

[40] J. Iveland, L. Martinelli, J. Peretti, J. S. Speck, C. Weisbuch, "Direct Measurement of Auger Electrons Emitted from a Semiconductor Light-Emitting Diode under Electrical Injection: Identification of the Dominant Mechanism for Efficiency Droop," *Phys. Rev. Lett.*, vol. 110, no. 17, pp. 177406, 2013

[41] L. Metrology, "Handbook of LED Metrology," *Instrum. Syst. GmbH*, 2000. Available: http://www.instrumentsystems.com/fileadmin/editors/downloads/Products/LED{_}Handbook{_}e.pdf

[42] Á. Borbély, Á. Sámson, and J. Schanda, "The concept of correlated colour temperature revisited," *Color Res. Appl.*, vol. 26, no. 6, pp. 450–457, 2001.

[43] CIE, "Publication number 13.3, Method of measuring and specifying colour rendering properties of light sources", 1995

[44] J. Piprek, "Efficiency droop in nitride-based light-emitting diodes," *Phys. Status Solidi Appl. Mater. Sci.*, vol. 207, no. 10, pp. 2217–2225, 2010.

[45] Y. C. Shen, G. O. Mueller, S. Watanabe, N. F. Gardner, A. Munkholm, and M. R. Krames, "Auger recombination in InGaN measured by photoluminescence," *Appl. Phys. Lett.*, vol. 91, no. 14, p. 141101, 2007.

[46] H.-Y. Ryu, H.-S. Kim, and J.-I. Shim, "Rate equation analysis of efficiency droop in InGaN light-emitting diodes," *Appl. Phys. Lett.*, vol. 95, no. 2009, p. 081114, 2009.

[47] J. Hader, J. V. Moloney, B. Pasenow, S. W. Koch, M. Sabathil, N. Linder, and S. Lutgen, "On the importance of radiative and Auger losses in GaN-based quantum wells," *Appl. Phys. Lett.*, vol. 92, no. 26, p. 261103, 2008.

[48] E. Kioupakis, P. Rinke, K. T. Delaney, and C. G. Van de Walle, "Indirect Auger recombination as a cause of efficiency droop in nitride light-emitting diodes," *Appl. Phys. Lett.*, vol. 98, no. 16, p. 161107, 2011.

[49] M. Brendel, A. Kruse, H. Jönen, L. Hoffmann, H. Bremers, U. Rossow, and A. Hangleiter, "Auger recombination in GaInN/GaN quantum well laser structures," *Appl. Phys. Lett.*, vol. 99, no. 3, p. 031106, 2011.

[50] M. Zhang, P. Bhattacharya, J. Singh, and J. Hinckley, "Direct measurement of auger recombination in In0.1Ga0.9N/GaN quantum wells and its impact on the efficiency of In0.1Ga0.9N/GaN multiple quantum well light emitting diodes," *Appl. Phys. Lett.*, vol. 95, no. 20, p. 201108, 2009.

[51] A. David and M. J. Grundmann, "Droop in InGaN light-emitting diodes: A differential carrier lifetime analysis," *Appl. Phys. Lett.*, vol. 96, no. 10, 2010.

[52] Q. Dai, Q. Shan, J. Cho, E. F. Schubert, M. H. Crawford, D. D. Koleske, M.-H. Kim, and Y. Park, "On the symmetry of efficiency-versus-carrier-concentration curves in GaInN/GaN light-emitting diodes and relation to droop-causing mechanisms," *Appl. Phys. Lett.*, vol. 98, no. 3, p. 033506, 2011.

[53] X. A. Cao, Y. Yang, and H. Guo, "On the origin of efficiency roll-off in InGaN-based light-emitting diodes," *J. Appl. Phys.*, vol. 104, no. 9, p. 093108, 2008.

[54] M. Shatalov, J. Yang, W. Sun, R. Kennedy, R. Gaska, K. Liu, M. Shur, and G. Tamulaitis, "Efficiency of light emission in high aluminum content AlGaN quantum wells," *J. Appl. Phys.*, vol. 105, no. 7, p. 073103, 2009.

[55] J. Wang, L. Wang, W. Zhao, Z. Hao, and Y. Luo, "Understanding efficiency droop effect in InGaN/GaN multiple-quantum-well blue light-emitting diodes with different degree of carrier localization," *Appl. Phys. Lett.*, vol. 97, no. 20, 2010.

[56] D. Watson-Parris, M. J. Godfrey, P. Dawson, R. A. Oliver, M. J. Galtrey, M. J. Kappers, and C. J. Humphreys, "Carrier localization mechanisms in InxGa1-xN/GaN quantum wells," *Phys. Rev. B - Condens. Matter Mater. Phys.*, vol. 83, no. 11, pp. 1–7, 2011.

[57] T. Sugahara, H. Sato, M. Hao, Y. Naoi, S. Kurai, S. Tottori, K. Yamashita, K. Nishino, L. T. Romano, and S. Sakai, "Direct Evidence that Dislocations are Non-Radiative Recombination Centers in GaN," *Jpn. J. Appl. Phys.*, vol. 37, no. 4, pp. L398–L400, 1998.

[58] N. Grandjean, B. Damilano, and J. Massies, "Group-III nitride quantum heterostructures grown by molecular beam epitaxy," *J. Phys. Condens. Matter*, vol. 13, no. 32, pp. 6945–6960, 2001.

[59] S. Dhar, U. Jahn, O. Brandt, P. Waltereit, and K. Ploog, "Effect of Exciton Localization on the Quantum Efficiency of GaN/(In,Ga)N Multiple Quantum Wells," *Phys. status solidi*, vol. 192, no. 1, pp. 85–90, 2002.

[60] D. M. Graham, A. Soltani-Vala, P. Dawson, M. J. Godfrey, T. M. Smeeton, J. S. Barnard, M. J. Kappers, C. J. Humphreys, and E. J. Thrush, "Optical and microstructural studies of InGaN/Gan single-quantum-well structures," *J. Appl. Phys.*, vol. 97, no. 10, p. 103508, 2005.

[61] J. Narayan, H. Wang, J. Ye, S. J. Hon, K. Fox, J. C. Chen, H. K. Choi, and J. C. C. Fan, "Effect of thickness variation in high-efficiency InGaN/GaN light-emitting diodes," *Appl. Phys. Lett.*, vol. 81, no. 5, pp. 841–843, 2002.

[62] D. Gerthsen, E. Hahn, B. Neubauer, A. Rosenauer, O. Schön, M. Heuken, and A. Rizzi, "Composition Fluctuations in InGaN Analyzed by Transmission Electron Microscopy," *Phys. status solidi*, vol. 177, no. 1, pp. 145–155, 2000.

[63] Y.-C. Cheng, E.-C. Lin, C.-M. Wu, C. C. Yang, J.-R. Yang, A. Rosenauer, K.-J. Ma, S.-C. Shi, L. C. Chen, C.-C. Pan, and J.-I. Chyi, "Nanostructures and carrier localization behaviors of green-luminescence InGaN/GaN quantum-well structures of various silicon-doping conditions," *Appl. Phys. Lett.*, vol. 84, no. 14, pp. 2506–2508, 2004.

[64] D.-P. Nguyen, N. Regnault, R. Ferreira, and G. Bastard, "Alloy effects in Ga(1-x)InxN/GaN heterostructures," *Solid State Commun.*, vol. 130, no. 11, pp. 751–754, 2004.

[65] L. Bellaiche, T. Mattila, L.-W. Wang, S.-H. Wei, and A. Zunger, "Resonant hole localization and anomalous optical bowing in InGaN alloys," *Appl. Phys. Lett.*, vol. 74, no. 13, pp. 1842–1844, 1999.

[66] A. Hangleiter, C. Netzel, D. Fuhrmann, F. Hitzel, L. Hoffmann, H. Bremers, U. Rossow, G. Ade, and P. Hinze, "Anti-localization suppresses non-radiative recombination in GaInN/GaN quantum wells," *Philos. Mag.*, vol. 87, no. 13, pp. 2041–2065, 2007.

[67] J. Hader, J. V. Moloney, and S. W. Koch, "Density-activated defect recombination as a possible explanation for the efficiency droop in GaN-based diodes," *Appl. Phys. Lett.*, vol. 96, no. 22, p. 221106, 2010.

[68] A. Kaneta, M. Funato, and Y. Kawakami, "Nanoscopic recombination processes in InGaN/GaN quantum wells emitting violet, blue, and green spectra," *Phys. Rev. B*, vol. 78, no. 12, p. 125317, 2008.

[69] B. Monemar and B. E. Sernelius, "Defect related issues in the “current roll-off” in InGaN based light emitting diodes," *Appl. Phys. Lett.*, vol. 91, no. 18, pp. 181 101–181 103, 2007.

[70] S. Hammersley, T. J. Badcock, D. Watson-Parris, M. J. Godfrey, P. Dawson, M. J. Kappers, and C. J. Humphreys, "Study of efficiency droop and carrier localisation in an InGaN/GaN quantum well structure," *Phys. status solidi*, vol. 8, no. 7-8, pp. 2194–2196, 2011.

[71] M. F. Schubert, S. Chhajed, J. K. Kim, E. F. Schubert, D. D. Koleske, M. H. Crawford, S. R. Lee, A. J. Fischer, G. Thaler, and M. A. Banas, "Effect of dislocation density on efficiency droop in GaInN/GaN light-emitting diodes," *Appl. Phys. Lett.*, vol. 91, no. 23, p. 231114, 2007.

[72] T. M. Smeeton, M. J. Kappers, J. S. Barnard, M. E. Vickers, and C. J. Humphreys, "Analysis of InGaN/GaN single quantum wells by X-ray scattering and transmission electron microscopy," *Phys. status solidi*, vol. 240, no. 2, pp. 297–300, 2003.

[73] M. J. Galtrey, R. A. Oliver, M. J. Kappers, C. J. Humphreys, D. J. Stokes, P. H. Clifton, and A. Cerezo, "Three-dimensional atom probe studies of an InxGa(1-x)N/GaN multiple quantum well structure: Assessment of possible indium clustering," *Appl. Phys. Lett.*, vol. 90, no. 6, p. 061903, 2007.

[74] K. J. Vampola, M. Iza, S. Keller, S. P. DenBaars, and S. Nakamura, "Measurement of electron overflow in 450 nm InGaN light-emitting diode structures," *Appl. Phys. Lett.*, vol. 94, no. 6, p. 061116, 2009.

[75] L.-B. Chang, M.-J. Lai, R.-M. Lin, and C.-H. Huang, "Effect of Electron Leakage on Efficiency Droop in Wide-Well InGaN-Based Light-Emitting Diodes," *Appl. Phys. Express*, vol. 4, no. 1, p. 012106, 2011.

[76] J. Piprek, R. Farrell, S. DenBaars, and S. Nakamura, "Effects of built-in polarization on InGaN-GaN vertical-cavity surface-emitting lasers," *IEEE Photonics Technol. Lett.*, vol. 18, no. 1, pp. 7–9, 2006.

[77] M.-H. Kim, M. F. Schubert, Q. Dai, J. K. Kim, E. F. Schubert, J. Piprek, and Y. Park, "Origin of efficiency droop in GaN-based light-emitting diodes," *Appl. Phys. Lett.*, vol. 91, no. 18, p. 183507, 2007.

[78] J. Xie, X. Ni, Q. Fan, R. Shimada, Ü. Özgür, and H. Morkoç, "On the efficiency droop in InGaN multiple quantum well blue light emitting diodes and its reduction with p-doped quantum well barriers," *Appl. Phys. Lett.*, vol. 93, no. 12, p. 121107, 2008.

[79] J. P. Liu, J.-H. Ryou, R. D. Dupuis, J. Han, G. D. Shen, and H. B. Wang, "Barrier effect on hole transport and carrier distribution in InGaN/GaN multiple quantum well visible light-emitting diodes," *Appl. Phys. Lett.*, vol. 93, no. 2, p. 021102, 2008.

[80] G. Verzellesi, D. Saguatti, M. Meneghini, F. Bertazzi, M. Goano, G. Meneghesso, and E. Zanoni, "Efficiency droop in InGaN/GaN blue light-emitting diodes: Physical mechanisms and remedies," *J. Appl. Phys.*, vol. 114, no. 7, p. 071101, 2013.

[81] W. Götz, N. M. Johnson, C. Chen, H. Liu, C. Kuo, and W. Imler, "Activation energies of Si donors in GaN," *Appl. Phys. Lett.*, vol. 68, no. 22, pp. 3144–3146, 1996.

[82] K. B. Nam, M. L. Nakarmi, J. Li, J. Y. Lin, and H. X. Jiang, "Mg acceptor level in AlN probed by deep ultraviolet photoluminescence," *Appl. Phys. Lett.*, vol. 83, no. 5, pp. 878–880, 2003.

[83] S. Hwang, W. Jin Ha, J. Kyu Kim, J. Xu, J. Cho, and E. Fred Schubert, "Promotion of hole injection enabled by GaInN/GaN light-emitting triodes and its effect on the efficiency droop," *Appl. Phys. Lett.*, vol. 99, no. 18, 2011.

[84] D. S. Meyaard, G.-B. Lin, Q. Shan, J. Cho, E. Fred Schubert, H. Shim, M.-H. Kim, and C. Sone, "Asymmetry of carrier transport leading to efficiency droop in GaInN based light-emitting diodes," *Appl. Phys. Lett.*, vol. 99, no. 25, p. 251115, 2011.

[85] A. Laubsch, M. Sabathil, W. Bergbauer, M. Strassburg, H. Lugauer, M. Peter, S. Lutgen, N. Linder, K. Streubel, J. Hader, J. V. Moloney, B. Pasenow, and S. W. Koch, "On the origin of IQE-'droop' in InGaN LEDs," *Phys. Status Solidi*, vol. 6, no. S2, pp. S913–S916, 2009.

[86] Q. Dai, Q. Shan, J. Wang, S. Chhajed, J. Cho, E. F. Schubert, M. H. Crawford, D. D. Koleske, M.-H. Kim, and Y. Park, "Carrier recombination mechanisms and efficiency droop in GaInN/GaN light-emitting diodes," *Appl. Phys. Lett.*, vol. 97, no. 13, p. 133507, 2010.

[87] M. Crawford, "LEDs for Solid-State Lighting: Performance Challenges and Recent Advances," *IEEE J. Sel. Top. Quantum Electron.*, vol. 15, no. 4, pp. 1028–1040, 2009.

[88] W. V. Lundin, A. E. Nikolaev, A. V. Sakharov, E. E. Zavarin, S. O. Usov, V. S. Sizov, A. L. Zakgeim, A. E. Chernyakov, and A. F. Tsatsulnikov, "High-efficiency InGaN/GaN/AlGaN light-emitting diodes with short-period InGaN/GaN superlattice for 530–560 nm range," *Tech. Phys. Lett.*, vol. 36, no. 11, pp. 1066–1068, 2010.

[89] S. Nizamoglu,T. Ozel, E. Sari, and H. V. Demir, "White light generation using CdSe/ZnS core–shell nanocrystals hybridized with InGaN/GaN light emitting diodes," *Nanotechnology*, vol. 18, no. 6, pp. 065709, 2007.

[90] S. J. Chang, L. W. Wu, Y. K. Su, C. H. Kuo, W. C. Lai, Y. P. Hsu, J. K. Sheu, J. F. Chen, and J. M. Tsai, "Si and Zn co-doped InGaN-GaN white light-emitting diodes," *IEEE Transactions on Electron Devices*, vol. 50, no. 2, pp. 519 – 521, 2003.

[91] S. Chhajed, Y. Xi, T. Gessmann, J.-Q. Xi, J. M. Shah, J. K. Kim, and E. F. Schubert, "Junction temperature in light-emitting diodes assessed by different methods," *Proc. SPIE 5739, Light-Emitting Diodes: Research, Manufacturing, and Applications IX*, vol. 5739, pp. 16–24, 2005.

[92] B. Damilano, N. Grandjean, C. Pernot, and J. Massies, "Monolithic White Light Emitting Diodes Based on InGaN/GaN Multiple-Quantum Wells," *Jpn. J. Appl. Phys.*, vol. 40, no. Part 2, No. 9A/B, pp. L918–L920, 2001.

[93] T. Kim, J. Kim, M. Yang, Y. Park, U.-I. Chung, Y. Ko, and Y. Cho, "Polychromatic white LED using GaN nano pyramid structure," in *Light-Emitting Diodes: Materials, Devices, and Applications for Solid State Lighting XVII*,

K. P. Streubel, H. Jeon, L.-W. Tu, and M. Strassburg, Eds., vol. 8641, no. 0001, pp. 86410E, 2013.

[94] J. R. Sadaf, M. Q. M. Israr, S. Kishwar, O. Nur, and M. Willander, "White Electroluminescence Using ZnO Nanotubes/GaN Heterostructure Light-Emitting Diode," *Nanoscale Res. Lett.*, vol. 5, no. 6, pp. 957–960, 2010.

[95] B. Damilano, N. Trad, J. Brault, P. Demolon, F. Natali, and J. Massies, "Color control in monolithic white light emitting diodes using a (Ga,In)N/GaN multiple quantum well light converter," *Phys. Status Solidi*, vol. 209, no. 3, pp. 014005, 2009.

[96] C. Yu, H. Lirong, and Z. Shanshan, "Monolithic white LED based on AlxGa(1-x)N/InyGa(1-y)N DBR resonant-cavity," *J. Semicond.*, vol. 30, no. 1, pp. 014005, 2009.

Chapter 3

Monolithic di-chromatic InGaN/GaN WHITE LED: CCT tuneability and CRI

I. E. Titkov, **A. Yadav**, V. L. Zerova, M. Zulonas, A. F. Tsatsulnikov, et. al, "Internal quantum efficiency and tunable colour temperature in monolithic white InGaN/GaN LED," Proc. SPIE 8986, Gallium Nitride Materials and Devices IX, 89862A, 2014.

A. Yadav, I. E. Titkov, A. V. Sakharov, W. V. Lundin, A. Nikolaev, et. al, "High colour rendering dichromatic monolithic light emitting diode with tuneable colour temperature," in CLEO-Europe, Munich, OSA, 2015.

A.Yadav, S. A. Kolpakov, N. T. Gordon, H. Kbashi, E. U. Rafailov, and K. Zhou, "Stealth dicing of sapphire with NIR femto-second laser," Applied Physics A, vol. 123, no. 5, pp. 369, 2017.

In this chapter, di-chromatic white LEDs with blue-green QW under CW and pulsed pumping are presented. CCT and spectral behaviour under different pumping conditions is discussed. Highest CRI of 67 from these devices with no optical pumping and without explicit red spectral band is demonstrated. Furthermore, singulation of LED from the wafer after fabrication is also demonstrated with fs pulses due to multi-photon absorption.

3.1 Preface

In this chapter the di-chromatic monolithic LEDs grown on c-plane sapphire substrate for white light emission are discussed. It is divided into two parts. In the first part (section 3.2 onwards) the CRI, CCT and spectral behaviour of these devices are presented. The second part (section 3.6 onwards) details the *stealth dicing* technique where femtosecond laser pulses are used to dice sapphire substrate for faster and efficient singulation of LEDs from the wafer. Each part is complete on its own with an introduction, experiment, results and conclusion sections.

3.2 Phosphor free monolithic white LEDs

White LED's based on InGaN are used in many applications from backlighting to mobile displays and general illumination [1–3]. The requirements on characteristic and quality of white light emission differ with application. While phosphor covered blue LEDs with improved colour rendering index (CRI) and luminous efficacy are replacing traditional light sources[3] at offices, museum and similar application areas, high CRI is irrelevant for indicator and signage. For outdoor street lighting, industrial use and parking spaces sources with CRI $\geq$ 60 and CT $\leq$ 8000 K are considered adequate[3–5]. Hence white light source with tunable CRI and CCT are desirable. Towards this, a multichip approach with vertical or lateral combination of blue, green and red LEDs can be used for white light generation. However, this approach requires complex fabrication procedures, driving circuits, and device design; thereby affecting reliability and increasing production cost [2]. White light emission has also been achieved with CdSe/ZnS nanocrystals and by doping of InGaN quantum wells (QWs) with Si and Zn [6, 7]. These approaches along with the shortcomings of the multichip approach have an additional disadvantage of non-tunability. Meanwhile, the theoretical possibility of emission from $\sim$ 0.7 eV to $\sim$ 3.5 eV by indium (In) variation in InGaN QWs, is also being explored [8–11]. This all semiconductor monolithic approach holds potential of efficient colour tunable sources with high CRI.

Monolithic approaches involving nanostructure engineering have been explored previously for white light emission. A dual wavelength, 5000 K to 20000K colour tunable, multifacet QW LED was demonstrated by Funato et al. in 2008 [12]. Nguyen et al. have reported colour tunability and CRI values more than 90 for "dot in a wire" core shell LEDs on silicon [13]. Nevertheless, this approach requires a complex growth and fabrication process with precise control over wire diameter and dot size, which is not ideal for mass production. Also, luminous efficacy of these devices is still far from phosphor covered LEDs [13]. Li et al. demonstrated dual wavelength MQW LED with 46% indium (In) content for red emission peak at 2.12 eV thus achieving emission colour from red to yellow to white with CRI of 85.6 [14]. However, large lattice mismatch between higher In incorporated InGaN red QW on GaN substrate results in issues related to charge separation and increased defect density [15]. A simpler fabrication approach of vertically stacked QWs emitting at two distinct wavelengths has been reported. Active regions of such devices can consist of either (i) longer wavelength emitting passive QWs pumped by active blue QW [16] or (ii) all electrically pumped active QWs [8, 11, 17]. The first approach is similar to phosphor covered LEDs and the total emission spectrum is dependent on passive QWs in active region. Also, since the passive QWs are designed to operate on the green gap spectral range they being less efficient than phosphor for that range and their sensitivity to active QW emission wavelength is a disadvantage[18]. The best CRI for such devices reported is 41[16]. White light emission from all electrically pumped QWs with CCT $\sim$ 6000K has been reported previously[19].

In this chapter all electrically pumped phosphor free, colour tuneable monolithic white LED is presented. The device is designed for dichromatic emission at 450 nm and 550 nm. The emission wavelengths are chosen so that the line joining the corresponding x-y coordinates on CIE 1931 chromaticity diagram passes through the white region. The x-y tristimulus coordinates of standard D65 illuminant are demonstrated with these devices at current densities of 6.21 A/cm^2. It is also shown that CRI of over 60 can be demonstrated with these devices and CCT of emission in such LEDs can be easily tuned by modulation of pumping current.

3.2.1 Device structure and Experiment

The di-chromatic monolithic blue-green LED (Z091228b) studied in this work was fabricated by Ioffe institute (St. Petersburg, Russia) to achieve white light emission by exploiting complimentary wavelengths/colours. The layer specifications for the structures is given in Table 3.1. Figure 3.1 depicts the schematic of the device studied in this work. The QW LEDs were grown on c-plane sapphire substrate by metal organic chemical vapour deposition (MOCVD). Next a n-type GaN layer with 5e18 cm^3 Si doping concentration is deposited on sapphire after an i-GaN buffer layer. To improve carrier injection into the multiple quantum wells a graded short period superlattice (SPSL) of 24 nm thickness with 1nm alternate repetitions of InGaN and GaN is grown on top of n-GaN. The indium concentration is increased with each repetition. The SPSL is grown using the conversion method and is detailed in [20].

Table 3.1 Specification of di-chromatic monolithic White LED (Z091228b) with blue-green active regions.

No	Layer	Z091228b
1	p-GaN	180 nm
2	p-$Al_{0.15}Ga_{0.85}N$	18 nm
3	i-GaN	8nm
4	InGaN	3 nm active QW -2 (green)
5	i-GaN	8 nm
6	InGaN	3 nm active QW -1 (blue)
7	i-GaN	8 nm
8	InGaN	3 nm active QW -1 (blue)
9	i-GaN	12 nm
10	InGaN/GaN SL	24 nm (1+1) $\times$ 12 periods
11	n-GaN/Al_2O_3	n $\sim$ 5e18

This is followed by an i-GaN spacer of 12 nm before the blue and green QW's were grown. Afterwards two blue QW's and one green QW is grown in that order with an i-GaN barrier of 8 nm between each QW. A 18 nm p-$Al_{0.15}Ga_{0.85}N$ electron blocking layer (EBL) was then grown on top of green QW after the 8 nm i-GaN barrier. Finally a top p-GaN layer is grown on which the Ni/Ti/Au top p-contact is deposited during fabrication.

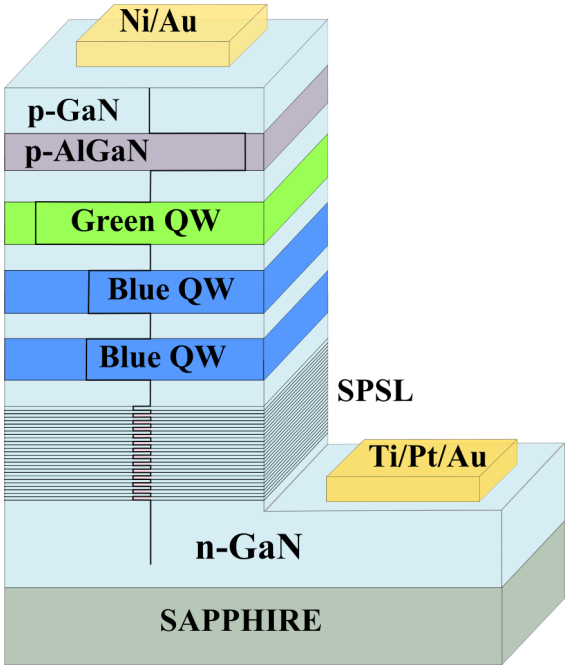

Fig. 3.1 Schematic of the layer structure and conduction band diagram for monolithic di-chromatic white LED

The structures were then fabricated and processed in 1310 × 1310 μm^2 (MK-24) packages [21]. This was done by Scientific-Technological Centre of Microelectronics and Submicrometer Heterostructures, Russian Academy of Science.

The optical characteristics of the monolithic di-chromatic LED are studied under both continuous wave (CW) and pulsed regime (PR). 'Keithley 2400' is used as a CW source for currents up to 1A while pulses of width from 100 ns to 100μs with a duty cycle of 1%-95% were generated using 'Agilent 8114A' pulse generator. To accurately estimate the efficiency, radiant flux and colour characteristics all measurements at room temperature (RT) are done in an integrating sphere. A fraction of scattered light from the sphere was coupled, using a calibrated fibre, to 'CDS-700' spectrometer from Labsphere. 'LightMtrx' software was used to derive all electrical and optical parameters from the spectrometer. The flexibility of adjusting the exposure time of the spectrometer, between 1 ms to 5000 ms, allowed to measure wide range of radiant flux from 1 nW to 100 mW.To obtain green/blue integrated intensity ratio, we measured blue and green part of the emission spectra separately by adjusting the digital apertures.

3.2.2 Results

In this section electrical and optical characteristics of the investigated di-chromatic monolithic white LEDs are presented.

3.2.2.1 Current-Voltage characteristics

First the current-voltage (I-V) characteristics, as shown in fig. 3.2, of the diode are investigated to establish the electrical quality of the LED. The experimental (I-V) data is fitted with Shockley's diode equation accounting for parasitic resistance by including a shunt and series resistance. From the fitting procedure a high shunt resistance of 170 MOhms is obtained indicating low leakage current at low pumping levels. A 25 Ohms of series resistance indicates usual concentration of free carriers in the cladding layers (both p and n type). The ideality factor obtained from the fitting is, $\eta = 4.3$, quite high, and is attributed to i-GaN barrier layers between the QW [22, 23].

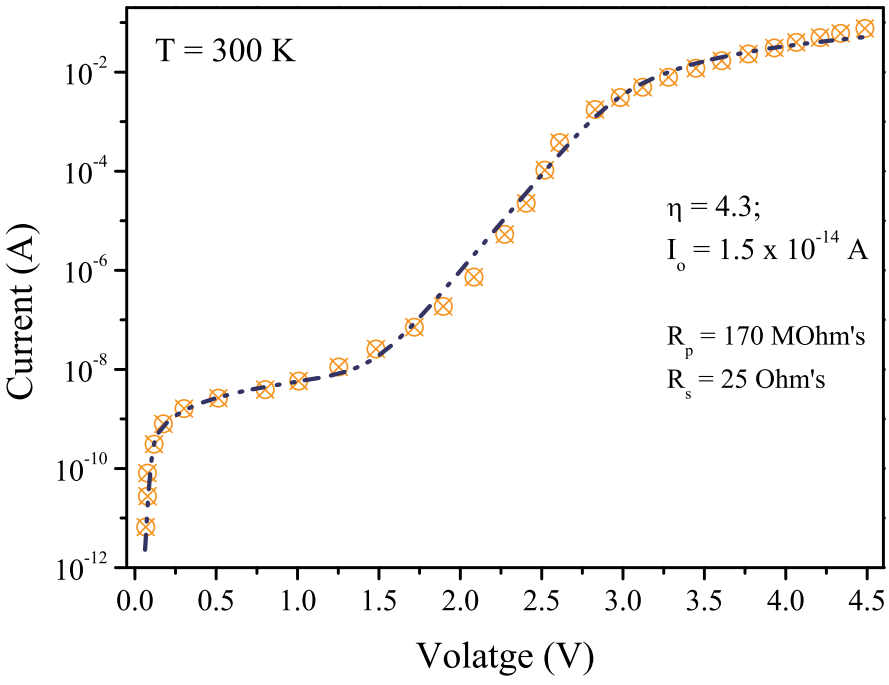

Fig. 3.2 Current-voltage characteristics of the monolithic blue-green LED under forward biased condition. The experimental data is fitted with Shockley's equation modified to account for parasitic resistance.

3.2.2.2 CRI and Spectral analysis

The electroluminescence (EL) behaviour of monolithic white LEDs is studied at room temperature in continuous wave (CW) regime. Figure 3.3 shows EL spectra for these devices with increasing currents up to 500 mA. Two distinct peaks in fig. 3.3 indicate that both shallow and deep In concentration QWs are operating in their respective blue and green spectral regions. From figure 3.3a it is seen that at lower currents less than 80 mA the green peak dominates the emission spectrum with blue emission getting stronger with increasing carrier concentration. This is attributed to non-uniform distribution of injected holes, primarily due to their lower mobility and higher effective mass holes will radiatively recombine in the QW closer to the p-side. However with further increase in current, more holes travel through the barrier layer and are available for recombination in blue QW's.

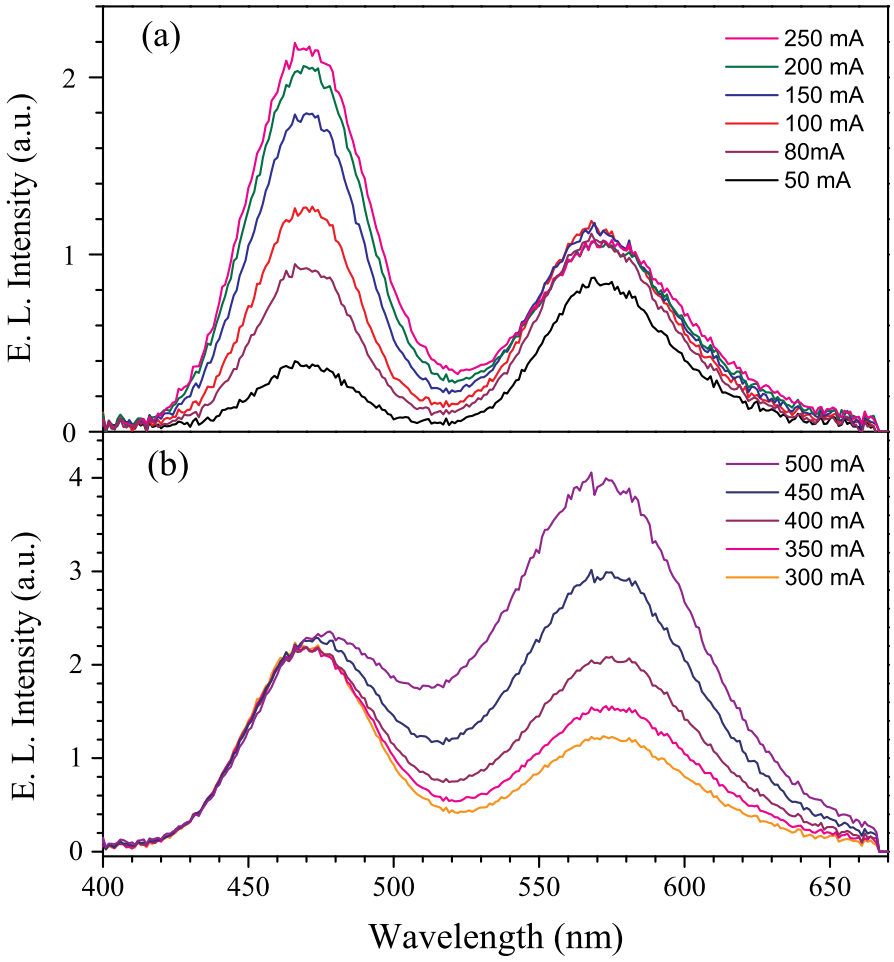

Fig. 3.3 Electroluminescence (EL) spectra of monolithic white LED pumped under CW current of (a) 50-250 mA, (b) 300-500 mA.

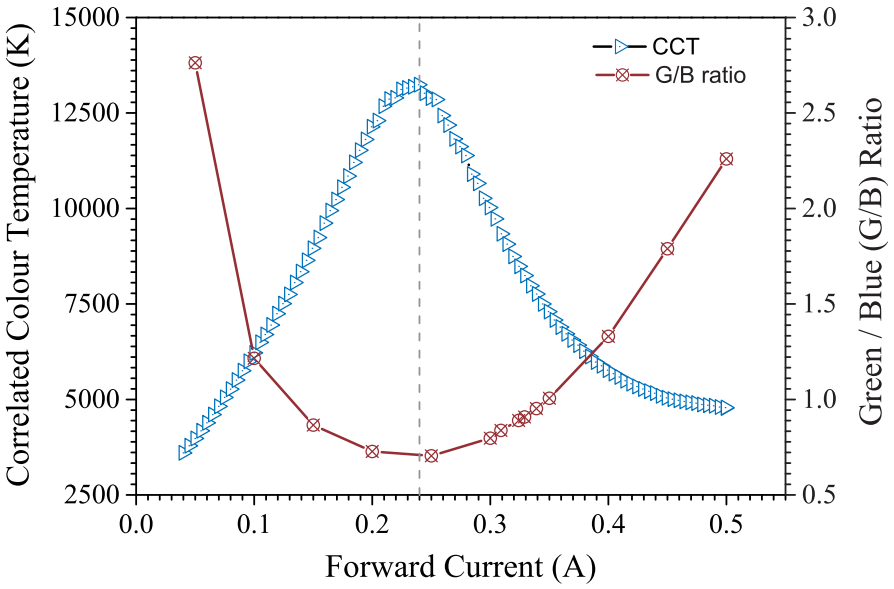

Fig. 3.4 Green/Blue (G/B) ratio and corresponding CCT tuning with variation of CW current.

On further increasing the current up to 100 mA the emission from the green QW is clamped and the radiative recombination in the blue QW is enhanced. For very high CW current injection i.e. $>$ 300 mA, increased radiative recombination in green QW and saturated blue emission peak is observed (see fig 3.3b). This is understood to be caused by the carrier redistribution due to band-filling of blue QW leading to electron overflow thus making more carriers, i.e. electrons, available for recombination in the green QW.

The tuning of CCT and G/B ratio with varying current is shown in figure 3.4. The dashed red line associates the highest CCT obtained from this device to the minima of green/blue (G/B) integrated intensity ratio. This indicates the dominance of blue peak in this region of operation. For injection current between 100 mA and 350 mA, G/B ratio is $<$ 1 and blue peak dominates resulting in cool white emission. For other regions, increase in green intensity results in tuning of emission towards warmer colour temperature.

Commission International de I'Elairage (CIE 1931) chromaticity coordinates with associated CCT at different currents are shown in figure 3.5. The coordinates (0.4172, 0.4375) at 40 mA moves to (0.2686, 0.2716) at 240 mA and CCT increase from 3600K to 13240K (fig. 3.5(a)). With further increase in current a movement

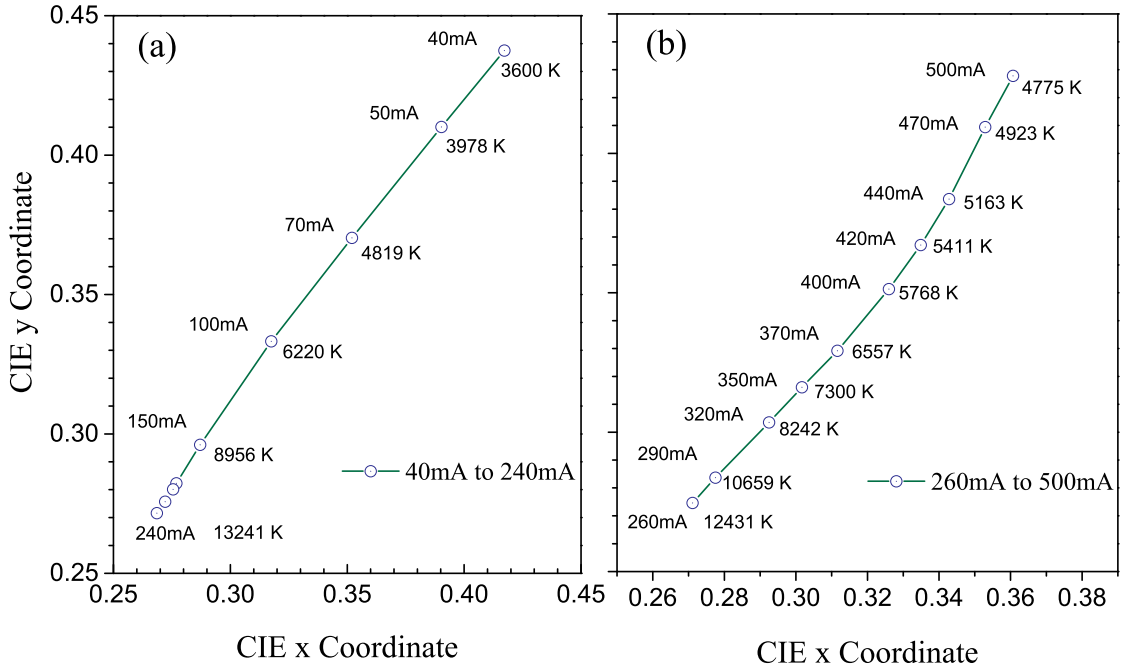

Fig. 3.5 CIE Chromaticity coordinates and corresponding CCT at various injection currents (a) I from 40 mA to 240 mA, and (b) I from 260 mA to 500 mA.

towards warmer CCT values can be seen with 4775 K at (0.3607, 0.4278) for 500 mA (fig. 3.5(b)). This distinctly depicts an excellent warm to cool white CCT tunable simple monolithic LED. The CRI for device under test is under 40 for less than 70 mA however, with increasing carrier density the spectral broadening of the green peak is asymmetric and spectral emission contribution at longer wavelengths (fig. 3.3b) $>$ 600 nm improves the visible spectral region coverage thus improving the CRI values to $>$ 60 with a maximum of 67.3 at 335mA ever reported for such devices (fig. 3.6a).

Though further increase in current broadens the green peak, a blue shift of 4 nm in peak wavelength is observed for the current is increased to 500 mA from 400 mA. Also this broadening is asymmetric with increased spectral emission at shorter wavelengths. This shift can be attributed to band-filling and screening of quantum cascade stark effect at higher currents. A red shift of 7nm in peak wavelength for blue emission is also observed for current $>$ 300 mA up to 500 mA which otherwise remains constant at 469 nm which is generally indicative of increase in junction temperature. The decrease in CRI for current $>$ 350 mA (fig. 3.6a) can be explained by the change in the green/blue (G/B) spectral power density ratio and shift in

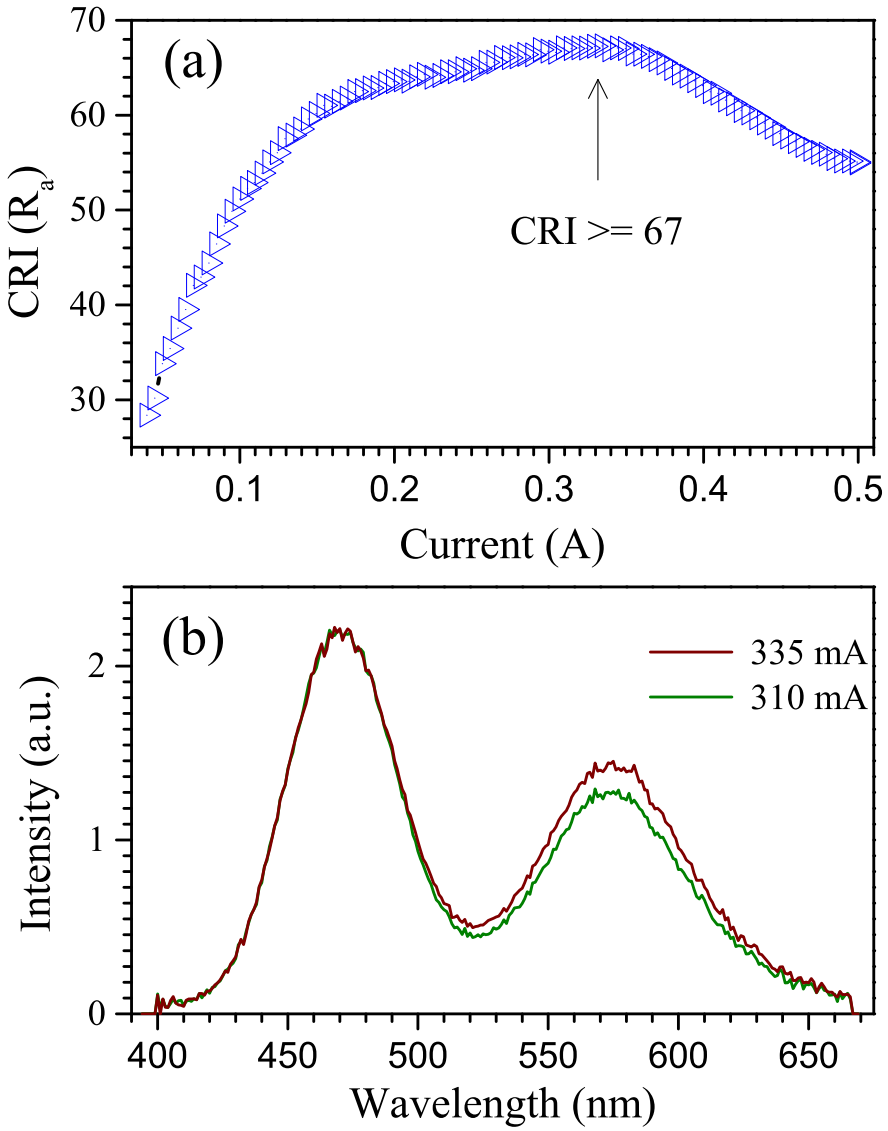

Fig. 3.6 (a) Evolution of CRI with increasing current, and (b) EL Spectrum at current values with CRI 67 with a maximum of 67.3 at 335 mA.

the peak emission wavelength for both blue and green QW's. This indicates that apart from broadened spectra, CRI in such devices is sensitive to G/B ratio, since maximum CRI is obtained for G/B ratio between 0.84 and 1 (six closely spaced green stars in figure 3.4). Spectrum of this region is shown in figure 3.6b.

3.2.2.3 CCT tuneability

From the point of view of practical applications, the current dependence of the LED colour characteristics is an undesirable factor, as additional current control

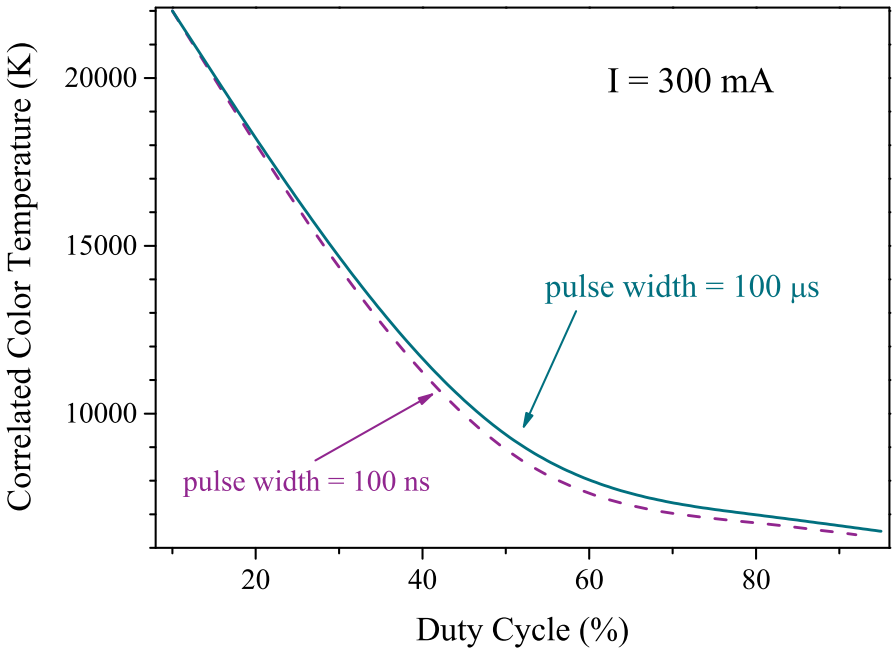

Fig. 3.7 CCT vs. Duty Cycle of the white LED measured in the integration sphere at 100 ns and 100 µs pulse durations.

is required for their stabilization. On the other hand, this effect opens additional opportunity for controlling the colour parameters of monolithic LEDs by the current variation. To achieve such control, pulsed pumping with different amplitude and durations is suitable.

In this section, with another LED chip taken from the same wafer, dependence of CCT on pulse width and duty cycle is presented. For this the device is pumped with pulses of width 100 ns to 100 μs with duty cycle in the range of 1% to 95% for currents up to 2 A with a maximum luminous flux of 2.26 lm. All measurements were taken at room temperature with an integration sphere.

Overheated regime

Under pulse regime of operation for duty cycle $>$ 1% device self heating is not completely avoided and is referred to as overheated mode of operation here. Figure 3.7 shows the dependence of CCT on duty cycle and pulse width. It can be clearly seen that negligible correlation exists between pulse width and CCT. On the other hand CCT is strongly affected by the change in duty cycle and decreases from 22000 K to ∼5500 K with change in duty cycle from 10% to 95%. The evolution of

emission spectra with changing duty cycle at 2 A is shown in figure 3.8 (b). It is also found that luminous flux of these devices shows negligible dependence on pulse duration in the range of 0.1 μs to 10 μs for various duty cycle (see fig. 3.8 (a))

Non-overheated regime

To mitigate the effects of self-heating on the optical properties of LED at high currents pulses up to 2 A with duty cycle of 1% and pulse width in the range

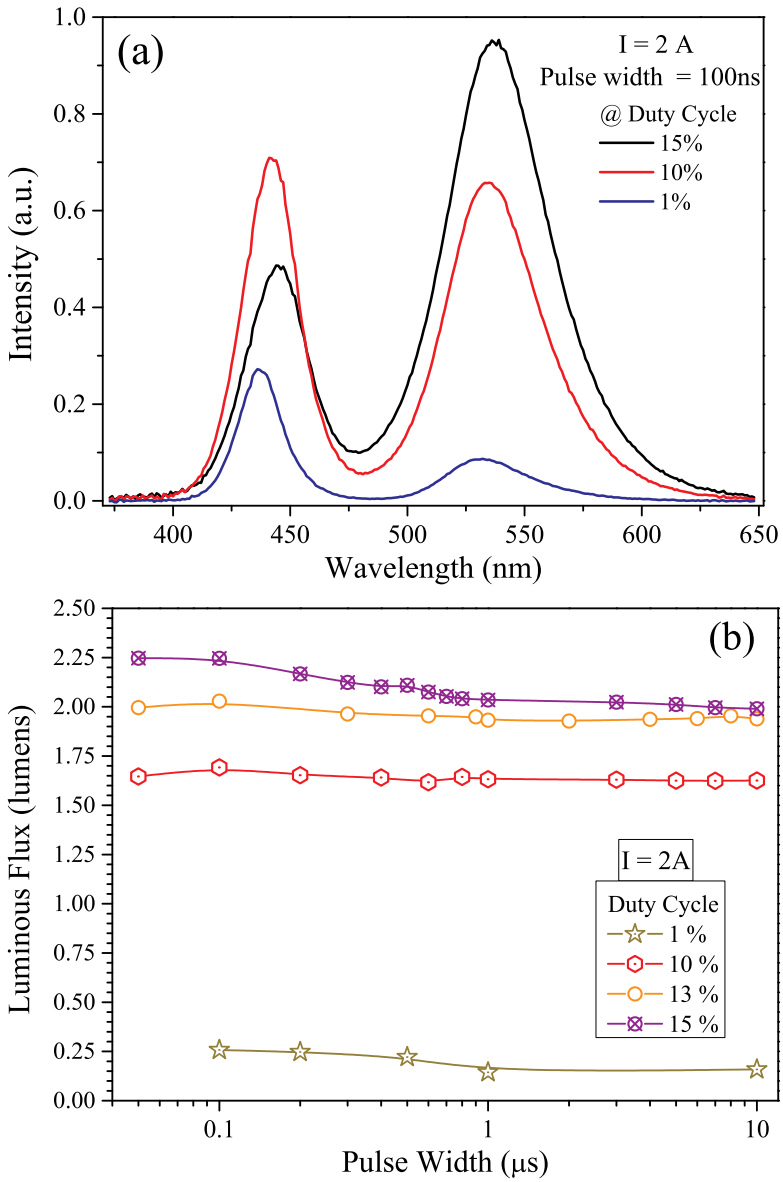

Fig. 3.8 (a) Emission spectrum under 100 ns pulses of 2 A amplitude for 15%, 10% and 1% duty cycle. (b) Almost constant luminous flux at various pulse width for constant duty cycle is demonstrated for 1%, 10%, 13% and 15% duty cycles for I = 2A.

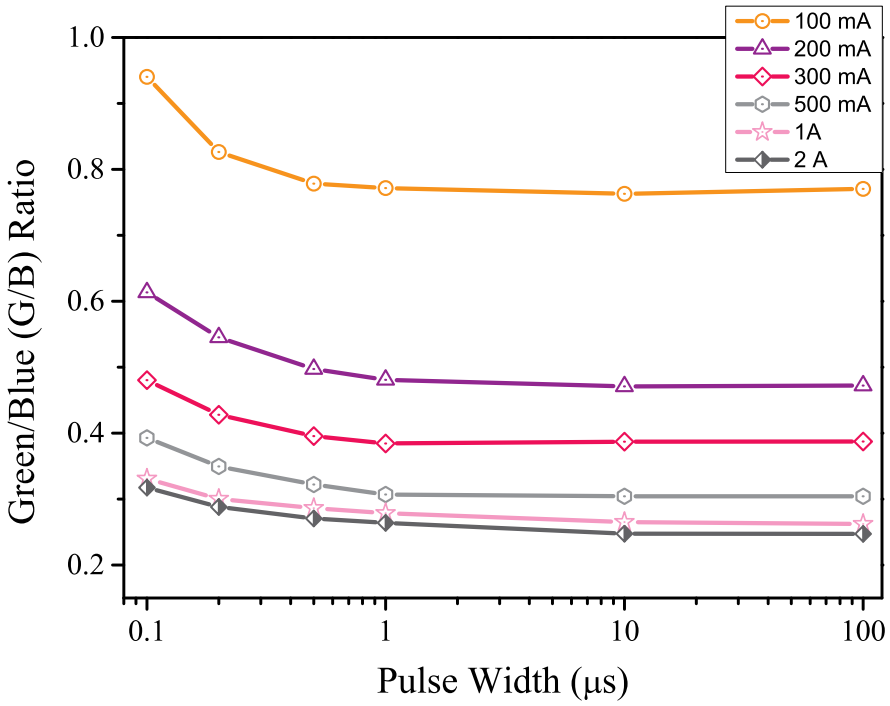

Fig. 3.9 Green/Blue bands ratio vs. pulse width measured at different currents and 1% Duty cycle. The figure demonstrates colour mixing tuneability for non-overheated mode.

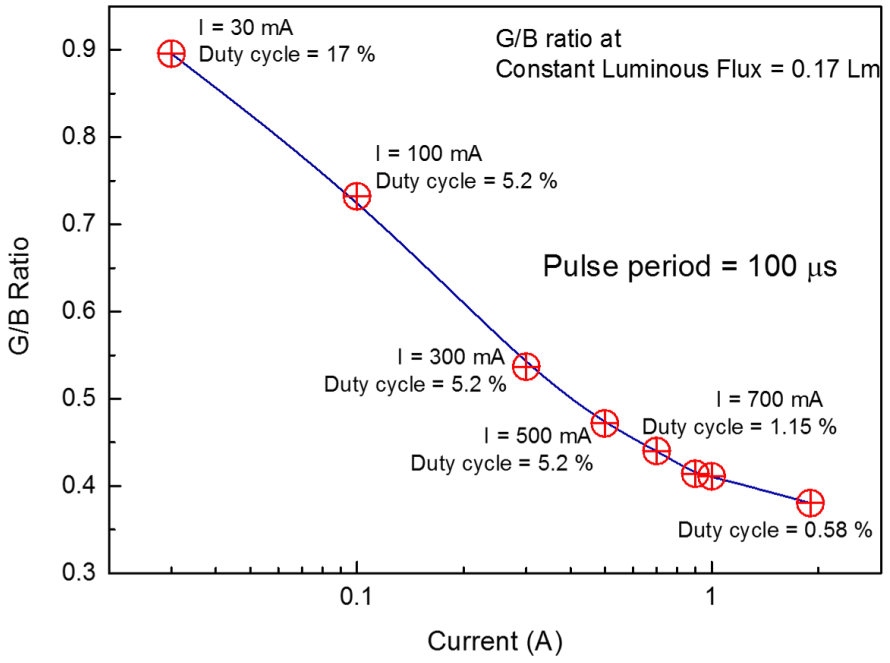

Fig. 3.10 Dependence of intensities of the green blue emission on current at pulsed excitation while keeping a constant luminous flux 0.14 Lm.

of 100 ns to 100 μs are applied. Since CCT tuneability is dependent on colour mixing of the emission bands and hence the spectral content and their strength

green-blue (G/B) integrated intensity ratio is studied over range of above mentioned pulsed durations and duty cycle. As shown in figure 3.9, it is found that the G/B ratio can be kept almost constant at a given current over a wide range of pulse widths allowing us to maintain the CCT while dimming the LED. On the other hand it can also be inferred (see fig. 3.9) that G/B ratio (and hence the CCT) can also be tuned in the range of 0.8 to 0.2 by modulating the input current and pulse width. Thus it is possible to keep the input electrical power constant and by simultaneously increasing the current from 100 mA to 2 A and decreasing the pulse width while tuning the G/B ratio (and hence CCT). Furthermore, it is also demonstrated, as shown in figure 3.10, that a constant luminous flux output of 0.17 lm is maintained by modulating current and duty cycle at a constant 100 μs period of separation between the pulse. This effect leads to change of colour coordinates of the emission in wide enough range. Different spectral behaviour from the first chip can be explained by its high sensitivity to the GaN barrier thickness [18].

3.2.3 Discussion and Summary

In this chapter, a di-chromatic monolithic white LED based on InGaN/GaN MQW is demonstrated. The MQW active region consists of vertically stacked two blue QW's emitting at $\sim$ 450 nm and one green QW emitting $\sim$ 550 nm. A CRI of 67 is achieved, which is the highest value demonstrated till date to the best of the knowledge of the author for such devices i.e. phosphor free, monolithic di-chromatic MQW LED emitting in blue and green spectral region.

It is shown that these phosphor-free devices can be tuned, by CW current modulation, to emit from cool white ($\sim$ 13000 K) to warm white ($\sim$ 2700 K) light. Considering the sensitivity of emission spectrum on current and hence the CCT which is likely to give non-consistent colour temperatures due to thermal effects pulse current regime is investigated on another LED from the same wafer. Using pulse current CCT is found to be tuneable about 3 times from $\sim$ 6000 K to $\sim$ 20000 K by modulating duty cycle only at a constant current of 300 mA and almost independent of pulse duration.

Furthermore, it is demonstrated that almost constant luminous flux can be maintained at a constant current and duty cycle even with pulses differing in duration by three orders of magnitude form 0.1 μs to 100 μs. It is also shown that G/B emission ratio (hence CCT), at duty cycles of 1% to avoid device self-heating, can be tuned about three times by varying current and pulse width. This degree of control over CCT tuneability by modulating current and pulse parameters allowed to obtain a constant luminous flux and varying G/B ratio (hence CCT) by modulating pulse current amplitude and duty cycle (or PW) with constant period of 100 μs between simultaneous pulses.

Finally, to improve the CRI even further and to restrict the CCT in the warmer region of white light emission a red phosphor with absorption spectrum in the blue region can be implemented or augmenting them with AlGaInP red LEDs will also allow to achieve much warmer emission without compromising too much on CCT tuneability. Also, further improvements in output lumen's and efficiency are needed to fully realise the potential of these devices. While much of such improvement is expected come from improved growth process with increasing In composition in the QW. It has also been suggested that along with advancement in QW growth and fabrication careful modulation of electrical behaviour of the QW confinement layers can improve the emission spectrum [18].

3.3 Stealth dicing of sapphire substrate

Sapphire is the substrate material used for industrial production of InGaN/GaN LEDs including white LEDs for illumination. These LEDs are in high demand due to their superior efficiency and long lifetime and hence methods to improve yield and production time at any stage of production process will be very cost effective. One such area is device singulation for packaging after fabrication. However, sapphire is one of the hardest material and thus difficult to break. Towards this laser based technologies has been exploited to improve yield, and throughput. The currently employed laser dicing is a thermal process and is better known as laser ablation. Laser ablation has mostly been achieved using UV lasers. UV lasers with nano-second or pico-second pulses have been used primarily due to absorption of around 25% at 300 nm and increasing with decreasing wavelength to about 60% at 200 nm. In this wavelength range 2- or 3- photon absorption process helps in achieving the thermal threshold for material phase transformation.

Another technique called “Stealth dicing”(SD) has been used to singulate LEDs. Unlike scribing by laser ablation, SD is done with lasers for which the test material has high transmission. A tightly focused laser beam with the help of a high numerical aperture (NA) lens is focused in the interior of the material to induce damage and generate cracks. Several such sequences of damage along different depths will make it easy to separate the devices. Since most of the SD on sapphire has been done using ns pulses the process becomes thermal in nature [24]. However, the same technique can also make use of femtosecond pulses probably reducing the thermal component. When these pulse are focused inside the material they exert an electric field with peak values more than the atomic bonding energy (10^9V/m) [24] and since the short pulse duration is tightly focused all energy is delivered to a designated area thus opening up the possibility of multi-photon absorption. Also, pulse width being shorter that electron-photon coupling relaxation time restricts heat spreading.

Sapphire is nearly transparent in near infra-red (IR) region of the EM spectrum. Femtosecond pulses with nJ of energy have been shown to cause phase modification on sapphire due to plasma formation at the focal spot of the focused pulse creating

pressures of $\sim$ 10 TPa [25, 26]. However, using fs pulses of energy in the range of $\sim$ 10-30 μJ optical damage inside the material due to coulomb explosion induced by multi-photon absorption, i.e. by rupturing the atomic bonding of the crystal can be induced. Here, 800nm, 140 fs pulses are used to induce damage in 350 μm polished sapphire wafer.

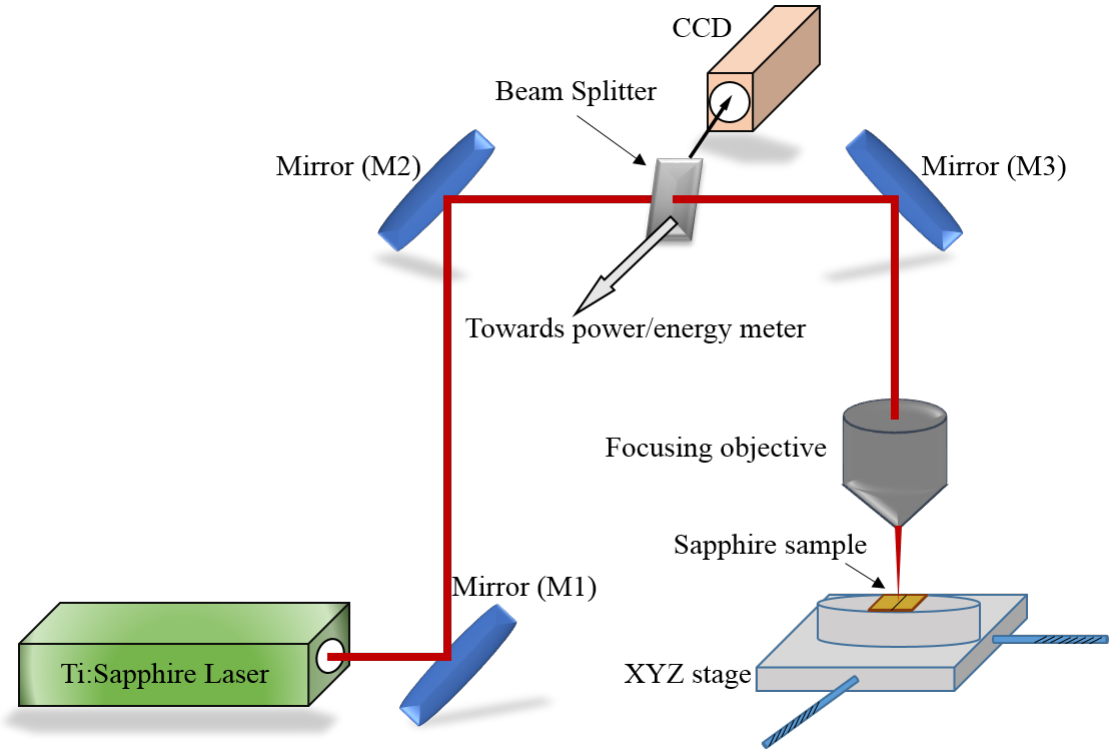

Fig. 3.11 Experimental setup

3.3.1 Experimental Setup

In this study a 350 μm sapphire wafer was used for all our investigations. The Ti:Sapphire (Spectra Physics/ Tsunami) laser system used here produces 140 fs pulses with 1kHz repetition frequency at a wavelength of 800nm. A $\times$100 microscope objective with NA of 0.55 for 800nm is used to achieve tightly focused beam with focal spot = 0.74 μm respectively of otherwise 3 mm collimated beam. To scan the sample across in three spatial directions (x,y,z) (fig. 3.11) according to our requirements, a high precision stage, Aerotech (with tilt and rotation along with x,y,z control) is used. The movement of the stage is controlled by the custom build

computer program in Visual Basic/C♯. After dicing, the samples were imaged with optical microscope and TEM without any thinning or lapping.

To monitor the power/energy of the beam the laser beam steered by mirror M1 and M2, controlling the spatial position of the beam, is passed through the beam splitter (fig. 3.11). One output of the beam splitter is focused by the objective via mirror M3 and the second output which is about 1/10th portion of the original laser beam is fed to the detector/ power meter (fig. 3.11).

3.3.2 Results and Discussion

3.3.2.1 Pulse energy vs Depth of focus

As the aim of this study is to investigate stealth dicing with NIR fs pulse emission, for which sapphire has $> 80\%$ transmission, first a pulse energy mapping scheme augmented with systematic variation of depth of focus is developed. As depicted in figure 3.12, pulses with energies in the range of 1μJ to 30μJ are used to inflict damage with a horizontal separation of 10 μm between two spots along with the change of depth by 10 μm at with each spot from left to right. From the map, based on the damage inflicted at a certain energy along the depth of the sample

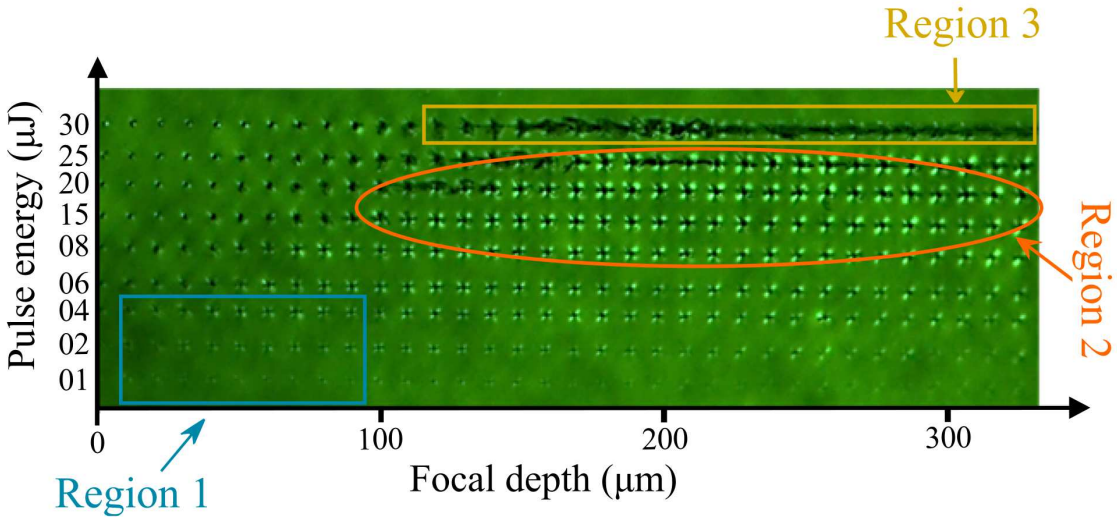

Fig. 3.12 Optical microscope image of the damage induced by fs pulses with different energy (increasing along the vertical axis) when focused at different depths (increasing along the horizontal axis) on and inside sapphire wafer. Each focal spot is exposed for 100 ms (limited by the shutter speed).

three regions are identified. These regions are (fig. 3.12(a)), region 1 with energy 1-2 μJ, region 2 with energy 6-25 μJ and region 3 with energy 30 μJ.

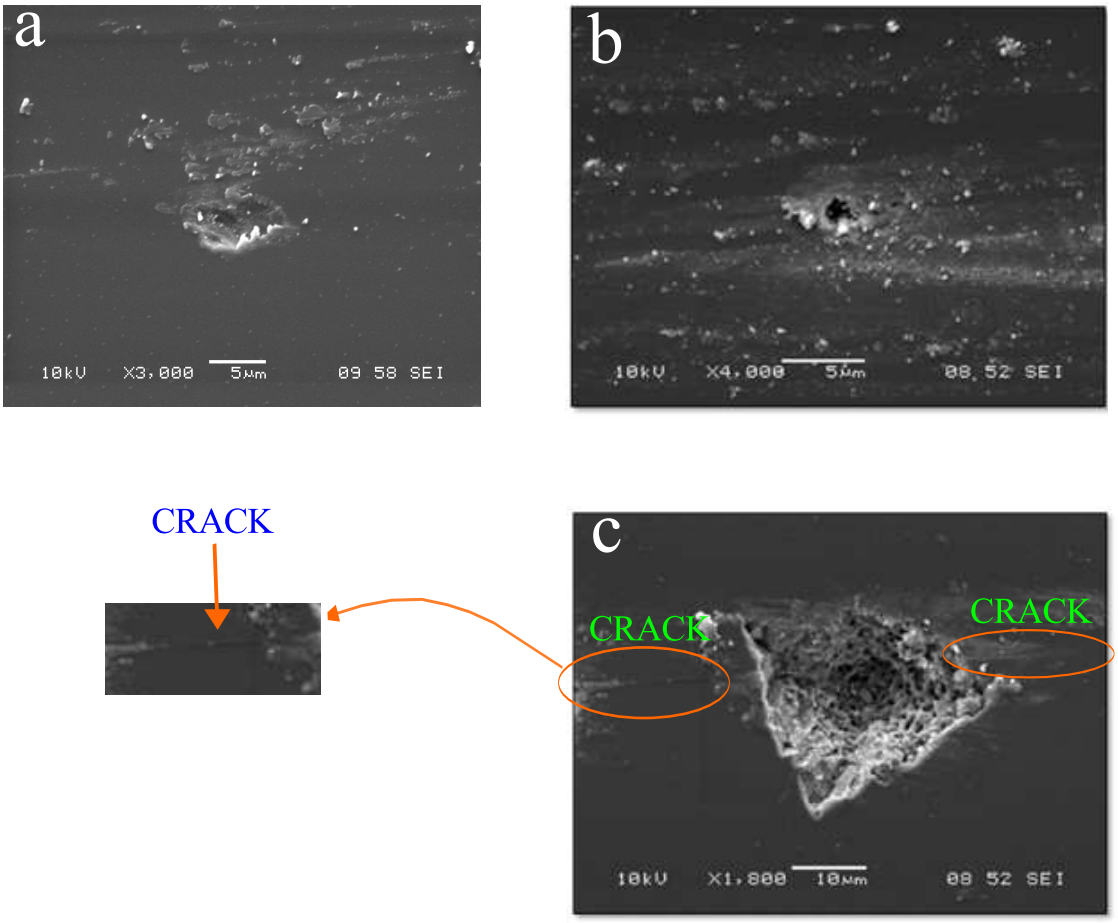

Fig. 3.13 SEM images of damage induced by the fs pulses with (a) energy = 2 μj and focal distance = 0 μm; (b) energy = 6 μj and focal distance = 25 μm; (c) energy = 25 μj and focal distance = 200 μm; Inset: shows the cracks produced by 25 μj pulses.

In region 1, the energy of the pulse was able to inflict superficial damage and as the depth is increased the damage seems to be reducing before disappearing completely. Figure 3.13(a) from the paper depicts the SEM image of a 2 μm deep crater with oval shape created by the damage done with a 2 μJ pulse on surface of the sample. The damage is similar to chipping of surface most likely due to a process similar to explosion. Moreover, oval shape indicates that the energy used is in close proximity of the threshold energy needed to make damage.

In region 2, with pulses of 6 μJ the damage induced has minimal chipping (see fig 3.13(b)) and a circular geometry on the surface of $\sim$ 2 μm in diameter along

with a depth of ~ 5 μm. Since the damage geometry is neat and has not propagated in arbitrary directions, as seen from the surface, it may be concluded that this energy is enough to evaporate the material from the epicentre. Next, at higher energy of 25 μJ in the same region a deeper and wider, ~ 15 μm and ~ 25 μm respectively, damage is inflicted. The shape of the crater made is closer to an equilateral triangular geometry. The induced damage is consistent with dielectric

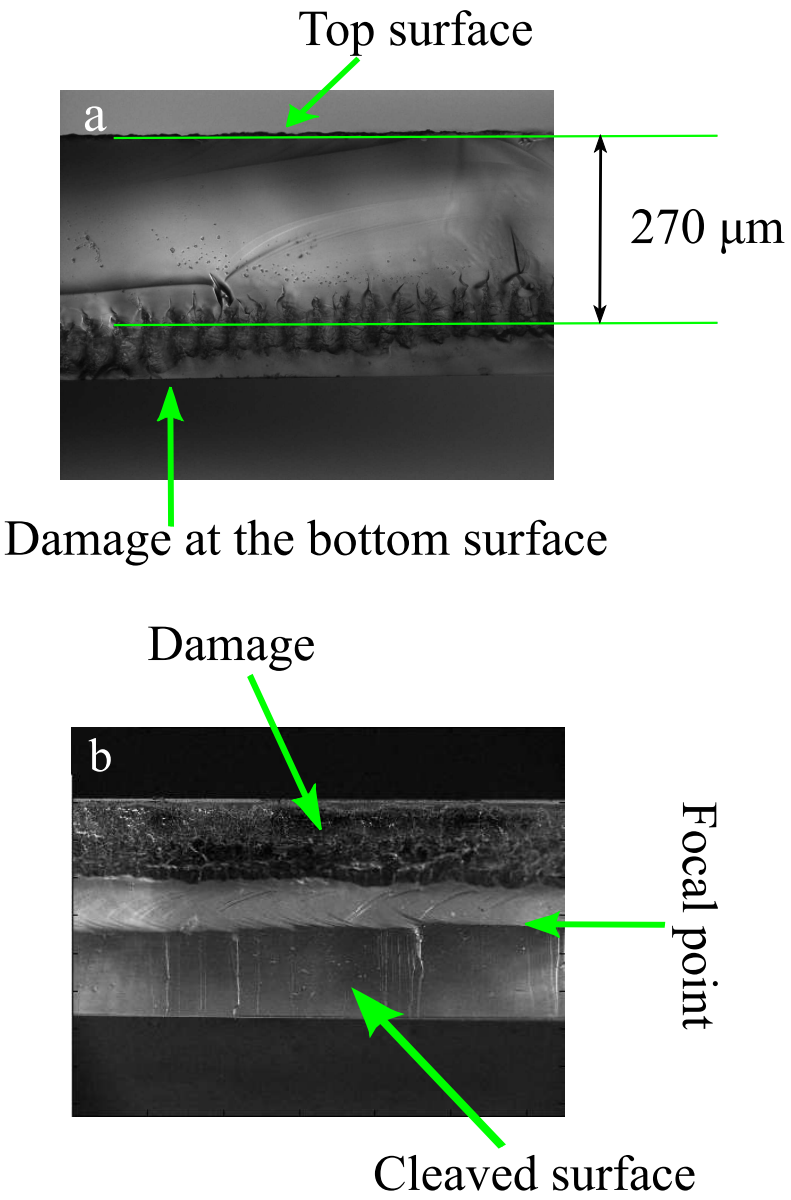

Fig. 3.14 (a) Cleaved surface of the wafer after stealth dicing with 25 μj pulses with varying focal depth; (b) Cleaved surface of the wafer after stealth dicing with 8 μj pulses at 170 μm of depth. In the case of 8 μj pulses cleaving is possible only after scanning the wafer for about 500 times.

breakdown or coulombic explosion due to multi-photon absorption. Also, from the pulse energy vs focal depth map from figure 3.12 it can be seen that at this energy damage or photo-modification can be done at all depths up to 300 μm. The kind and size of damage inflicted at higher energies in this region is appropriated for SD. In region 3, the pulse energy is too high as it damages the sample excessively.

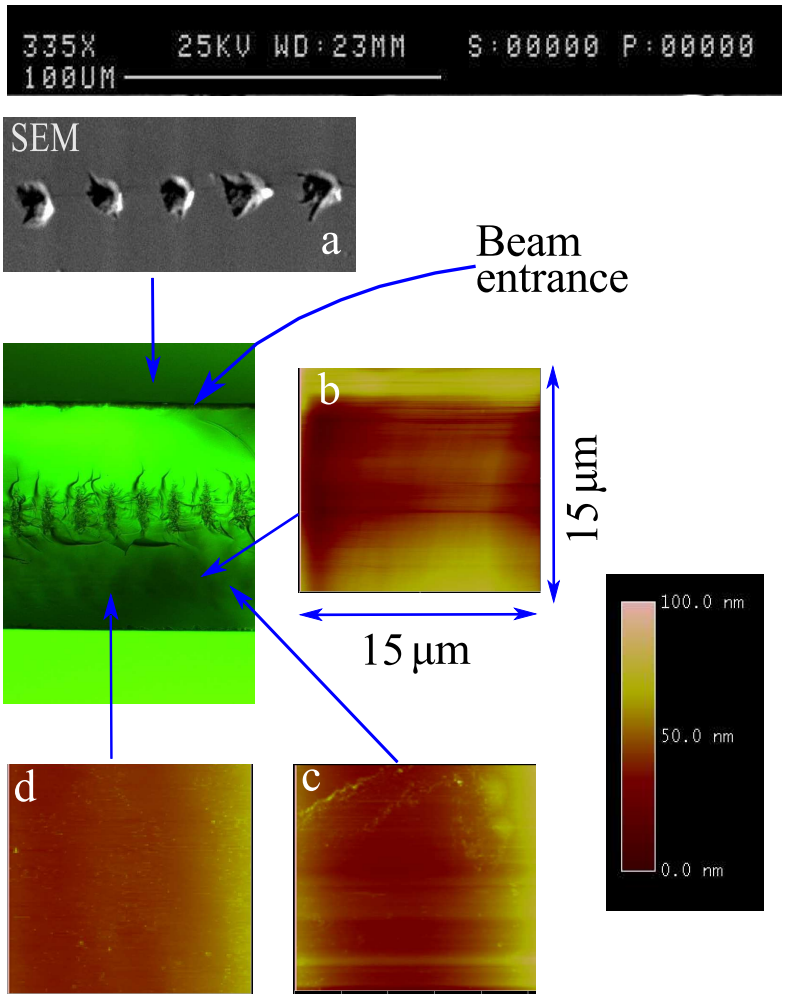

Fig. 3.15 Stealth dicing with 25 μj pulses (a)SEM image of the shots separated by 50μm in diastance (b) AFM images of the surface of the cleaved wafer after dicing.

3.3.2.2 Stealth Dicing

After identifying region 2 (in fig 3.12) as the most appropriate, stealth dicing using 25 μJ and 8 μJ pulse energy is performed. Optical microscopic images for both the energies is shown in figure 3.14 a and b respectively. Using a $\times$100 objective 25 μJ pulses were focused at the depth of 270 - 330 μm. The sample is exposed at

each location for 100 ms (limited by the mechanical shutter speed) with a distance of 50 μm. The bottom side, i.e. side opposite to the beam entry, of the sample gets damaged for depths $>$ 270 μm. However for depth of $\sim$ 270 μm the remaining 80 μm below the damage appears clean. Atomic force microscopy is then used to inspect the quality of the surface as shown in figure 3.15. The cleaved area below the focal point of the damage has a roughness of about 20-50 nm (fig 3.15 b, c and d). Towards the top of the sample (i.e. above the focal point of damaged area towards the beam entry side) ripples in $\sim$ 30 μm height and 10-30μm width are observed which might be advantageous in improving the LEE of LEDs due to roughening of the side walls thus reducing total-internal reflection.

For 8 μJ pulses the laser is focused at a depth of 170 μm, although damage is induced due to dielectric breakdown the damaged area is relatively small to break the sample with 50 μm separation between two focusing locations. To break the sample, as shown in fig 8b, using 8 μJ pulses the sample is scanned 500 times while decreasing depth by 1 μm with every scan. Furthermore, the sample is to be broken mechanically with a cleaver and the surface on the both sides (top and bottom) of the focal point are not clean.

3.3.3 Summary

In this chapter dicing of sapphire using an 800 nm fs pulses by *Stealth dicing* is demonstrated. Using 140 fs pulses of 25 μJ of energy 350 μm thick sample is cleaved by generating a single row of defects. The cleaved surfaces above (beam entering side) and below (opposite to beam entrance) the focal point of the laser exhibit different features. The bottom surface has a maximum roughness of 50 nm without damage, acceptable for blue and violet laser diode facets. On the other hand, ripples of 30 μm width on the top side are expected to improve LEE of LEDs by reducing the high total internal reflection at the air-sapphire interface. Moreover, this technology also has a potential to substantially reduce the dicing time with high repetition rate lasers and appropriate beam steering systems.

References

[1] E. F. Schubert and J. K. Kim (New York, N.Y.), "Solid-state light sources getting smart.," *Science*, vol. 308, no. 5726, pp. 1274, 2005.

[2] M. Crawford, "LEDs for Solid-State Lighting: Performance Challenges and Recent Advances.," *IEEE J. Sel. Top. Quantum Electron.*, vol. 15, no. 4, pp. 1028–1040, 2009.

[3] Cree Inc, "Cree First to Break 300 Lumens-Per-Watt Barrier," http://www.cree.com/News-and-Events/Cree-News/Press-Releases/2014/March/300LPW-LED-barrier (2014).

[4] E. F. Schubert, *Light-Emitting Diodes* (Cambridge University Press, Cambridge, 2006), 2nd ed.

[5] J. Y. Tsao, M. H. Crawford, M. E. Coltrin, A. J. Fischer, D. D. Koleske, G. S. Subramania, G. T. Wang, J. J. Wierer, and R. F. Karlicek, "Toward Smart and Ultra-efficient Solid-State Lighting.," *Adv. Opt. Mater.*, vol. 2, no. 9, pp. 809–836, 2014.

[6] S. Nizamoglu, T. Ozel, E. Sari, and H. V. Demir, "White light generation using CdSe/ZnS core–shell nanocrystals hybridized with InGaN/GaN light emitting diodes.," *Nanotechnology*, vol. 18, no. 6, pp. 065709, 2007.

[7] S. Chang, L. Wu, Y. Su, C. Kuo, W. Lai, Y. Hsu, J. Sheu, J. Chen, and J. Tsai, "Si and Zn co-doped InGaN-GaN white light-emitting diodes.," *IEEE Trans. on Electron Devices*, vol. 50, no. 2, pp. 519, 2003.

[8] B. Damilano, N. Grandjean, C. Pernot, and J. Massies, "Monolithic White Light Emitting Diodes Based on InGaN/GaN Multiple-Quantum Wells.," *Jpn. J. Appl. Phys.*, vol. 40, no. 9A/B(Part 2), pp. L918 – L920, 2001.

[9] M. Yamada, Y. Narukawa, and T. Mukai, "Phosphor Free High-Luminous-Efficiency White Light-Emitting Diodes Composed of InGaN Multi-Quantum Well.," *Jpn. J. Appl. Phys.*, vol. 41, no. 3A(Part 2), pp. L246 – L248, 2002.

[10] Chih-Feng Lu, Chi-Feng Huang, Yung-Sheng Chen, Wen-Yu Shiao, Cheng-Yen Chen, Yen-Cheng Lu, and Chih-Chung Yang, "Phosphor-Free Monolithic White-Light LED.," *IEEE J. Sel. Top. Quantum Electron.*, vol. 15, no. 4, pp. 1210 – 1217, 2009.

[11] A. F. Tsatsulnikov, W. V. Lundin, A. V. Sakharov, E. E. Zavarin, S. O. Usov, A. E. Nikolaev, V. S. Sizov, A. L. Zakgeim, M. N. Mizerov, N. A. Cherkashin, and M. Hytch, "Effect of stimulated phase separation on properties of blue, green and monolithic white LEDs.," *Phys. status solidi (c)*, vol. 9, no. 3-4, pp. 774 – 777, 2012.

[12] M. Funato, K. Hayashi, M. Ueda, Y. Kawakami, Y. Narukawa, and T. Mukai, "Emission color tunable light-emitting diodes composed of InGaN multifacet quantum wells.," *Appl. Phys. Lett.*, vol. 93, no. 2, pp. 19 – 22, 2008.

[13] H. P. T. Nguyen, S. Zhang, K. Cui, X. Han, S. Fathololoumi, M. Couillard, G. A. Botton, and Z. Mi, "p-Type Modulation Doped InGaN/GaN Dot-in-a-Wire White-Light-Emitting Diodes Monolithically Grown on Si(111).," *Nano Letters*, vol. 11, no. 5, pp. 1919 – 1924, 2011.

[14] H. Li, P. Li, J. Kang, Z. Li, Z. Li, J. Li, X. Yi, and G. Wang, "Phosphor-Free, Color-Tunable Monolithic InGaN Light-Emitting Diodes.," *Appl. Phys. Express.*, vol. 6, no. 10, pp. 102103, 2013.

[15] C.-K. Tan and N. Tansu, "Nanostructured lasers: Electrons and holes get closer.," *Nature Nanotechnology*, vol. 10, no. 2, pp. 107 – 109, 2015.

[16] B. Damilano, P. Demolon, J. Brault, T. Huault, F. Natali, and J. Massies, "Blue-green and white color tuning of monolithic light emitting diodes.," *J. Appl. Phys.*, vol. 108, no. 7, pp. 073115, 2010.

[17] I. E. Titkov, A. Yadav, V. L. Zerova, M. Zulonas, A. F. Tsatsulnikov, W. V. Lundin, A. V. Sakharov, and E. U. Rafailov, "Internal quantum efficiency and tunable colour temperature in monolithic white InGaN/GaN LED," in "SPIE OPTO," , J.-I. Chyi, Y. Nanishi, H. Morkoç, J. Piprek, E. Yoon, and H. Fujioka, eds. (International Society for Optics and Photonics, 2014), p. 89862A.

[18] S. Y. Karpov, N. A. Cherkashin, W. V. Lundin, A. E. Nikolaev, A. V. Sakharov, M. A. Sinitsin, S. O. Usov, E. E. Zavarin, and A. F. Tsatsulnikov, "Multi-color monolithic III-nitride light-emitting diodes: Factors controlling emission spectra and efficiency.," *Phys. status solidi (a)*, vol. 213, no. 1, pp. 19 – 29, 2016.

[19] A. F. Tsatsulnikov, W. V. Lundin, A. V. Sakharov, E. E. Zavarin, S. O. Usov, A. E. Nikolaev, N. V. Kryzhanovskaya, M. A. Synitsin, V. S. Sizov, A. L. Zakgeim, and M. N. Mizerov, "A monolithic white LED with an active region based on InGaN QWs separated by short-period InGaN/GaN superlattices.," *Semiconductors*, vol. 44, no. 6, pp. 808 – 811, 2010.

[20] W. Lundin, A. Nikolaev, A. Sakharov, E. Zavarin, G. Valkovskiy, M. Yagovkina, S. Usov, N. Kryzhanovskaya, V. Sizov, P. Brunkov, A. Zakgeim, A. Cherniakov, N. Cherkashin, M. Hytch, E. Yakovlev, D. Bazarevskiy, M. Rozhavskaya, and A. Tsatsulnikov, "Single quantum well deep-green LEDs with buried

InGaN/GaN short-period superlattice.," *J. Crys. Growth*, vol. 315, no. 1, pp. 267 – 271, 2011.

[21] A. E. Chernyakov, K. A. Bulashevich, S. Y. Karpov, and A. L. Zakgeim, "Experimental and theoretical study of electrical, thermal, and optical characteristics of InGaN/GaN high-power flip-chip LEDs.," *Phys. status solidi (a)*, vol. 210, no. 3, pp. 466 – 469, 2013.

[22] D. Zhu, J. Xu, N. A. Noemaun, K. J. Kim, E. F. Schubert, M. H. Crawford, D. D. Koleske, "The origin of the high diode-ideality factors in GaInN/GaN multiple quantum well light-emitting diodes.," *Appl. Phys. Lett.*, vol. 94, no. 8, pp. 081113, 2009.

[23] J. M. Shah, Y.-L. Li, Th. Gessmann, and E. F. Schubert, "Experimental analysis and theoretical model for anomalously high ideality factors (n»2.0) in AlGaN/GaN p-n junction diodes.," *J. Appl. Phys.*, vol. 94, no. 4, pp. 2627, 2003.

[24] K. C. Phillips, H. H. Gandhi,E. Mazur and S. K. Sundaram, "Ultrafast laser processing of materials: a review.," *Adv. Opt. Photon.*, vol. 7, no. 4, pp. 684 – 712, 2015.

[25] S. Juodkazis, K. Nishimura, S. Tanaka, H. Misawa, E. G. Gamaly, B. Luther-Davies, L. Hallo, P. Nicolai, v. T. Tikhonchuk, "Laser-Induced Microexplosion Confined in the Bulk of a Sapphire Crystal: Evidence of Multimegabar Pressures.," *Physical Review Letters*, vol. 96, no. 16, pp. 166101, 2006.

[26] S. Juodkazis, and H. Misawa, "Laser processing of sapphire by strongly focused femtosecond pulses.," *Applied Physics A*, vol. 93, no. 4, pp. 857–861, 2008.

Chapter 4

Phosphor-covered Di-chromatic White LED

I.E Titkov, **A. Yadav**, S. Yu. Karpov, A. V. Sakharov, A. F. Tsatsulnikov, T. Slight, A. Gorodetsky and E. U. Rafailov, "Superior colour rendering with a phosphor-converted blue-cyan monolithic light-emitting diode," Lasers & Photonics Review, vol. 10, no. 6, pp. 1031-1038, 2016.

In this chapter, a novel hybrid approach, comprising of dual wavelength LED and two phosphors, to generate warm white light is presented. Using this approach a warm white light at CCT of 3400K with an utmost colour rendering with R_a of 98.6 is demonstrated. Moreover, the colour characteristics can be tuned with operating current by adjusting the amplitude of blue and cyan bands of emission from the epi-structure.

4.1 Introduction

One of the key challenges for LED based lighting solutions to replace the existing indoor lighting sources is to offer a white light source with utmost colour rendition i.e. CRI $\sim$ 100. To achieve this different approaches can been used. A CRI of 67 has been demonstrated in chapter 3 using di-chromatic monolithic approach. Although such CRI values might be acceptable for certain applications like street lighting, better CRI values are needed for critical applications like galleries, museums, hospitals, and exhibitions [1, 2]. Figure 4.1 depicts an example of colour perception using Munsell colour pallets under light sources with different CRI's. Source with CRI of 99 better differentiate the colours thus an emphasis on a LED source with ultimate colour rendition along with maximum efficacy. Towards achieving high CRI a novel hybrid approach involving two phosphors is investigated.

The most common and popular approach for white light generation is of yellow phosphor (YAG:Ce3+) coated blue LED. These devices have achieved LER of $>$ 250 lm/W [3], however in general their CRI $<$ 75 [4–6]. The low CRI is attribute to missing red component in their emission spectrum which also keeps CCT $\geq$ 6000K [4–6]. A theoretical study suggest CRI can be improved up to $\sim$96-98 by optimising the emission spectra with use of multiple, broad band phosphors while maintaining luminous efficacy of radiation between 234-285 lm/W [7]. Based on the discussed approach Fukui et al. [8] demonstrated a white light source with a CRI of 99.1 and luminous efficacy of 59 lm/W with a near UV (405 nm) source. They used a multi-layered approach by stacking layer of red, green and blue phosphors to suppress cascade excitation, i.e. the overlapping of excitation spectra of one phosphor with the photoluminescence spectra of the other one.

Nevertheless, use of UV LEDs as a pump source requires three phosphors to obtain a quasi-uniform spectral emission and it is important that the number of phosphors used are kept at a minimum. Firstly because of increase in losses due to Stoke's shift with each added phosphor. Second, to suppress cascade excitation. Furthermore, the difference in degradation time of each type of phosphor and temperature dependence of quantum efficiencies of phosphors suggests minimizing

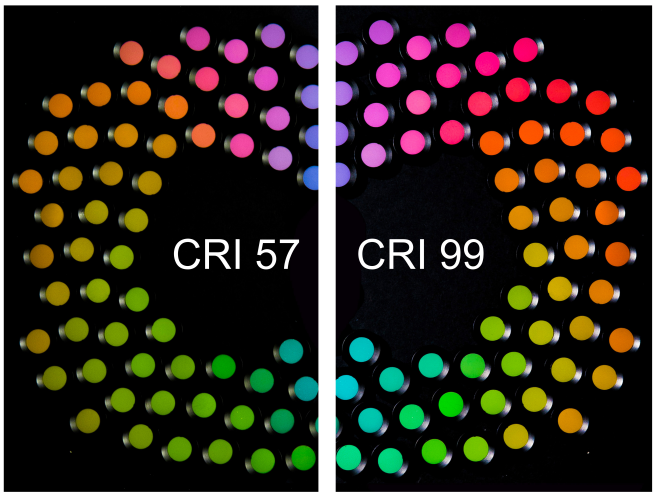

Fig. 4.1 Munsell colour samples perceived when illuminated by a source with CRI = 57 (a regular office lamp), and CRI = 99 (halogen lamp).

the number of phosphors used. Moreover, using blue LED as a pump source would improve the luminous efficacy since unlike UV the emission spectra of the LED is within the photopic eye sensitivity spectrum along with the benefit of higher quantum efficiency. Thus, more research is needed to produce an excellent colour rendering source by minimising the use of phosphors and improved efficacy [1].

Towards this, a recent theoretical study suggests an intermediate approach of a phosphor (YAG:Ce^{3+}) covered di-chromatic LED to further improve CRI from 78 with blue ($\lambda = 475$ nm) LED to 91 with dual wavelength ($\lambda_1 = 475$ nm, $\lambda_2 = 490$ nm) LED [9]. This approach has been tested experimentally by Stauss et al. [10] with an improvement in CRI to 76 from 67 while not sacrificing on efficiency. In this chapter the approach is further exploited with use of only two phosphors (red and green) and dichromatic blue-cyan LED for better light quality parameters.

4.2 Device structure and Experiment

The monolithic di-chromatic epi-structures (Fig.4.2.(a)) studied in this work were grown, in AIX2000HT MOCVD reactor, and fabricated at Ioffe institute (St. Petersburg, Russia). C-pane sapphire with micro-cones is used as the growth substrate. The micro-cones were introduced to improve light extraction efficiency (LEE) [11]. To improve carrier injection into the multiple quantum wells a graded short period superlattice (SPSL) [12] of 24 nm thickness with alternate repetitions of InGaN and GaN, each 1 nm thick, is grown on top of n-GaN. The structural quality of the QWs grown on top of the graded SPSL has also been shown to improve this improving the efficiency of MQW LEDs with higher In content [13]. There after 2 QWs, separated by a 8nm GaN layer, were grown on top of SPSL. First a 3 nm blue QW emitting in the spectral range of 430-435 nm followed by a 3 nm cyan QW in the range of 460-475 nm were deposited. Further a semi-transparent gold ohmic contacts in a grid format were deposited on the top of the mesa. (Fig.4.2(b)). The wafers were then processed as epi-up structures with mesa size of 240 $\times$ 320 μm^2 by CSTG, Glasgow. The as grown and processed LEDs were mounted on star shaped aluminium plates to improve heat transfer from the device.

The monolithic devices are then used to pump a mixture of phosphors emitting in red and green spectral range. The 1 mm thick phosphor sheets (PS) are commercially available from Phosphortech Corporation. PS, RF3000K-96, used in this experiment was designed to provide a warm white emission when pumped with 450 nm with a CCT of 3000K and a maximum CRI of 96. These sheets contained a patented composition of Nitride and YAG phosphors [14].

For this experiment the PS are cut into a cylindrical shape to act as remote phosphor cover (Fig.4.2(c)). The choice of shape is determined considering the wide angular emission from the surface emitting LEDs and symmetry along with feasibility and simplicity. Dimensions (Height$\times$Diameter) of the cylinder used in the experiment is 20 $\times$ 10 mm. The LED is placed at the bottom centre of the cylinder such that it is almost equidistant from the walls of the cylinder and thus

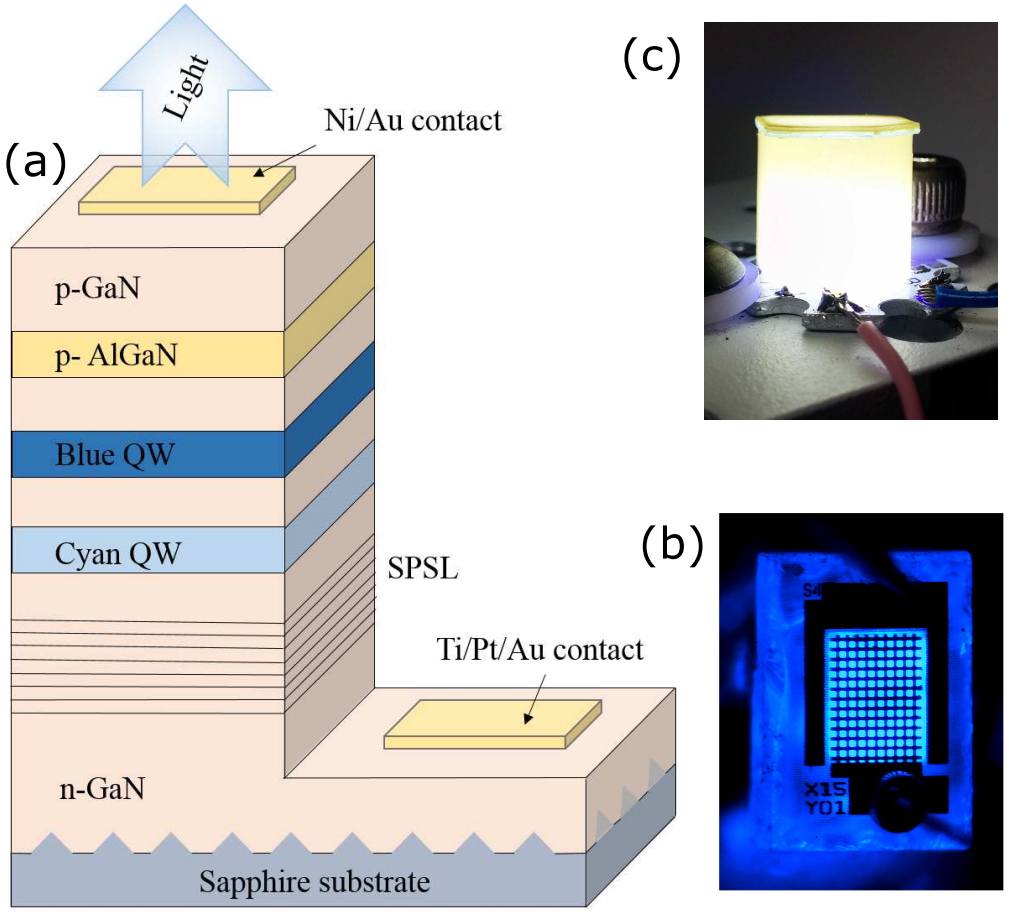

Fig. 4.2 (a) Schematic for the layer structure of the monolithic blue-cyan LED, (b) monolithic blue-cyan LED under CW operation, a grid of gold ohmic contact is clearly visible, and (c) cylindrical shape remote phosphor covering the blue-cyan LED under CW operation.

allowing uniform pumping along an imaginary circular surface placed horizontally at any given height.

The optical characteristics of both the monolithic blue-cyan device and the phosphor covered device were measured under CW regime. An integration sphere (Diameter = 10 inches) from Labsphere Co, Ltd and a CDS-600 spectrometer was used to record the values for radiant flux, peak emission wavelength, full bandwidth width at half maximum (FWHM) and the spectrum. Further the recorded data was processed using LightMtrx software The LED was driven in CW regime with a programmable current source Keithley-2400.

4.3 Results

In this section, the efficiency and optical characteristics of the monolithic blue-cyan (MBC) LED (Fig.4.2b) and phosphor-converted MBC (pc-MBC) (Fig.4.2c) are presented. First, efficiency and spectral behaviour of MBC LED is determined as a natural progression and to reflect on the characteristics of pc-MBC.

4.3.1 Monolithic Blue-Cyan LED

4.3.1.1 Efficiency of MBC LED

At first the external quantum efficiency (EQE) of the MBC LEDs under CW regime is determined from the experimental data with $\text{EQE}_{max} = 9.3\%$ and is presented in Fig.4.3a. To determine the maximum IQE and LEE for the di-chromatic LED the procedure based on ABC model as described in section 5.3 is used. The ratio $\text{EQE}_{max}/\text{EQE}$, as described in step 5 of section 5.3, is plotted as a function of $p^{1/2} + p^{-1/2}$ to determine the quality factor Q. The experimental points when approximated by straight line, see fig.4.3b, Q = 3.4 is determined. Next, using the relations 4.1 and 4.2 $\text{IQE}_{max} = 63\%$ and LEE = 14.8% is evaluated.

$$IQE_{max} = \frac{Q}{Q+2} \tag{4.1}$$

$$LEE = \frac{EQE_{max}}{IQE_{max}} \tag{4.2}$$

As shown in figure 4.3a, the experimental EQE data as a function of normalised optical power (p) can be fitted reasonably well with the theoretical EQE curve

$$EQE = LEE \times \frac{Q}{(Q + p^{1/2} + p^{-1/2})} \tag{4.3}$$

for p values less than ~ 10 i.e. for currents less than ~ 30 mA. For currents more

than $\sim$ 30 mA the deviation of theoretical curve is attributed to the growing cyan emission and is discussed in next section.

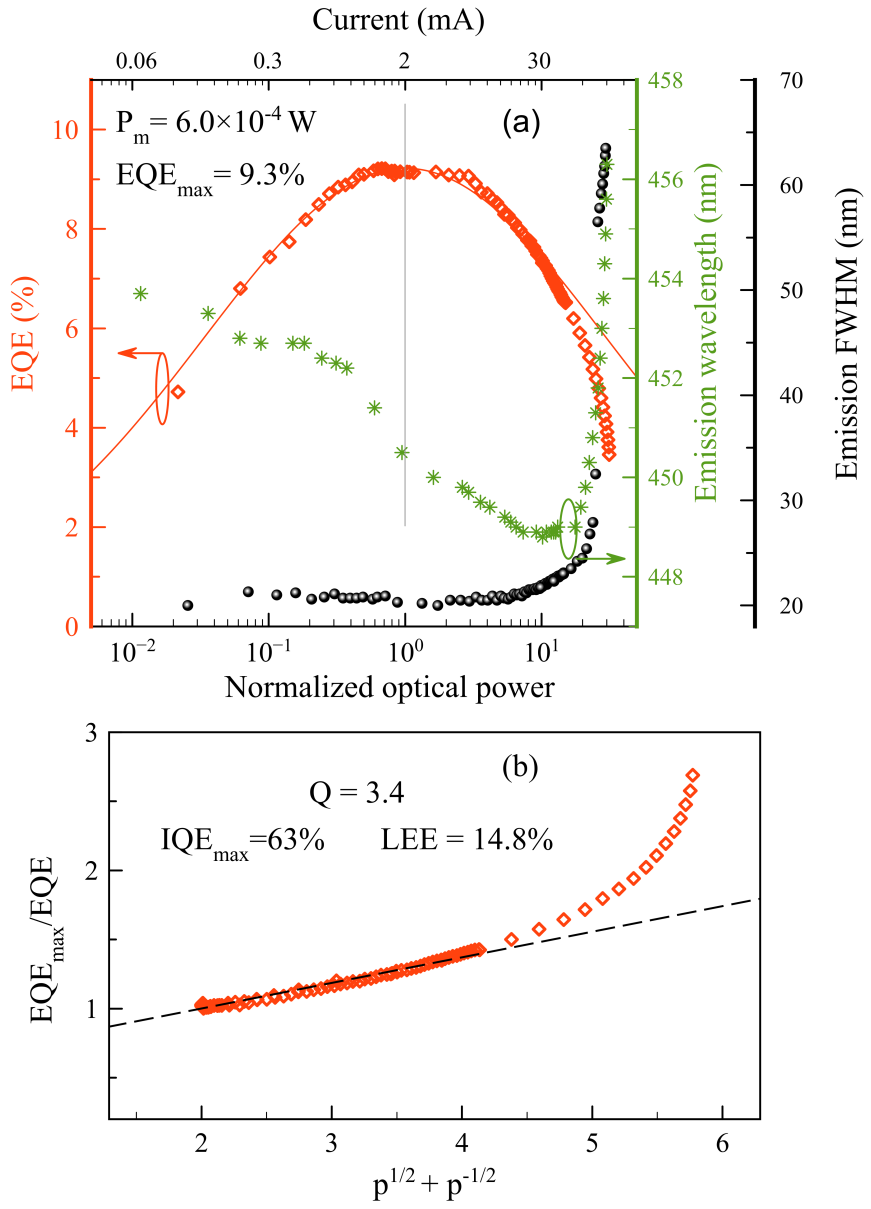

Fig. 4.3 (a) External quantum efficiency, centroid wavelength, and spectral FWHM of monolithic blue-cyan LED as a function of normalized optical power (p) , and current (mA); orange line is the ABC-model theoretical fit for EQE (b) Fitting of data (orange squares) by the procedure based on ABC-model to calculate light extraction efficiency and internal quantum efficiency.

4.3.1.2 Spectral analysis

Th evolution of centroid wavelength (see section 2.4.3) and full width at half maximum (FWHM) with current and normalised optical power for the MBC LED is presented in fig. 4.3a. It can be seen from the figure that with increasing current the centroid wavelength shift to the higher emission energy i.e. a blue shift is observed with practically negligible change in the emission spectral width for currents less than $\sim$ 30 mA. This observation is attributed to the polarisation induced electric fields within the QW's [17]. With further increase of current (see 4.3a) the centroid emission wavelength starts to shift towards the lower energy side of the visible spectrum, i.e the onset of red shift, which becomes strong for currents greater than $\sim$ 70 mA. A pronounced increase in spectral width must also be noticed under these operating conditions.

Investigating the spectrum under these operating conditions, as seen in Fig.4.4a, a few observations are made.

a) For I $<$ 30 mA, the blue emission peak dominates with a blue shift of peak wavelength for both blue and cyan emissions.

b) For 30 mA $<$ I $<$ 130 mA, blue emission peak gradually saturates whereas the cyan emission is steadily increasing with negligible red shift of peak wavelength compared to at I $\sim$ 30 mA .

c) For I $>$ 130 mA, spectral power decrease in blue peak along with noticeable red shift of peak wavelength. On the other hand though the peak emission wavelength of cyan emission exhibits no red shift while the spectral power keeps increasing with current.

So, the simultaneous increase of spectral width and red shift of centroid wavelength are understood in terms on increased intensity of the cyan emission peak. Moreover, since the peak emission wavelength for both emission peaks exhibits negligible red shift, device self-heating can be neglected as the probable cause for efficiency decrease in fig.4.3a. Thus it can be concluded that cyan QW, being in the close proximity of the "green gap" region, has lower efficiency and thus increased cyan intensity with current for I $>$ 30 mA leads to the discrepancy between experimental and predicted EQE.

4.3.2 Characteristics of pc-LED

To achieve white light emission from the MBC LED it was covered with a phosphor mixture as described in section 4.2. The spectral evolution of such a pc-LED as a function of current is depicted in figure 4.4b. Figure 4.5 presents the spectra of the RF3000K-96 phosphor mixture when pumped with 450 nm blue LED as provided by the vendor. Comparing the emission spectrum of MBC LED (fig.4.4a),

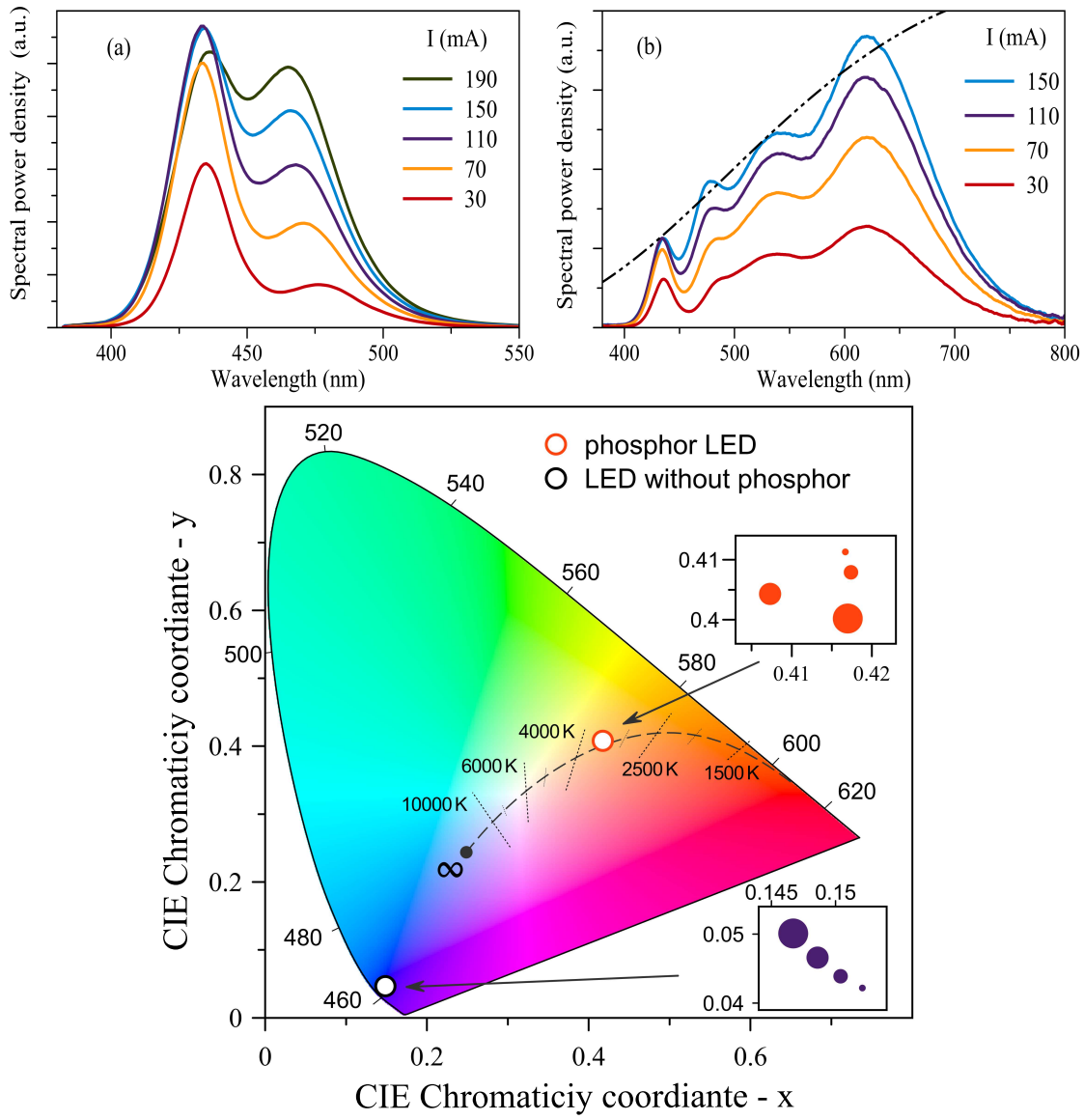

Fig. 4.4 (a) Emission spectrum for monolithic blue-cyan LED; (b) emission spectrum for pc-LED; black-body radiation spectrum at 3400K shown as the dashed line and (c) chromaticity coordinates corresponding to the spectrum depicted in (a) and (b); Top inset - coordinates for pc-LED; Bottom inset - coordinates for blue-cyan LED.

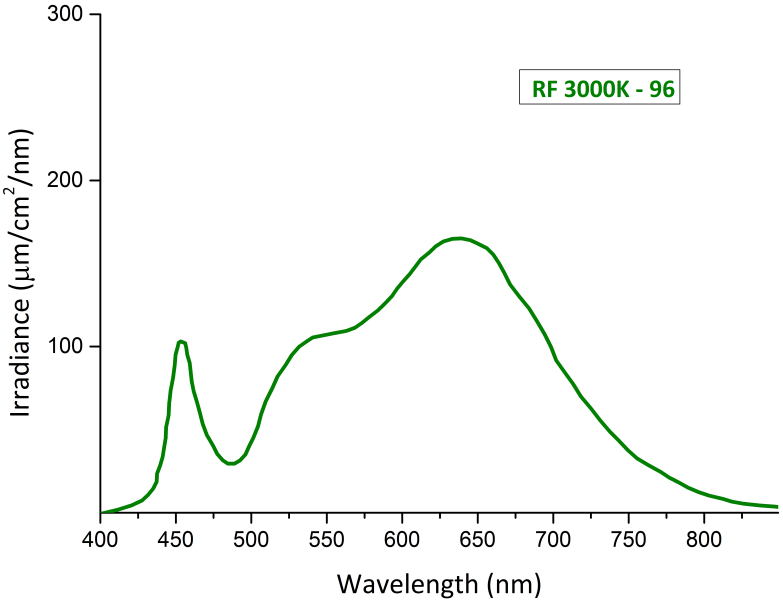

Fig. 4.5 Emission spectrum of the RF 3000K 96 phosphor sheet when pumped with 450 nm [14].

pc-LED (fig.4.4b) and figure 4.5 it can be seen that the blue emission from the MBC LED gets strongly absorbed by the phosphor mixture with increasing current even though the blue emission is around $\sim$ 435 nm instead of 450 nm intended for the phosphor used thus indicating that the pump wavelength used is in close proximity of the peak of the excitation spectra of the phosphor mixtures. On the other hand the cyan emission (see fig.4.4b) peak gets stronger with current thus not absorbed as strongly as the blue emission. The observed selective absorption allows the total emission from the pc-LED to cover almost whole of the visible emission spectrum and is advantageous for achieving utmost colour rendition from such devices. Figure 4.4b also depicts a truncated black-body radiation spectrum at colour temperature of 3400 K and the pc-LED emission spectra for similar CCT (for 70 mA $<$ I $<$ 190 mA). It is evident, and as observed, that the emission spectrum of pc-LED must have a prominent cyan emission peak with spectral magnitude greater than the blue peak to achieve such colour temperatures.

Next, the evolution of colour parameters, CCT, CRI and the chromaticity coordinates of the pc-LED as a function of current are depicted in Fig. 4.6. A variation oc CCT from $\sim$3500 K to $\sim$3300 K in the current range of 1 mA to 200 mA is quiet stable. Figure 4.6c depicts a reasonably stable evolution of chromaticity

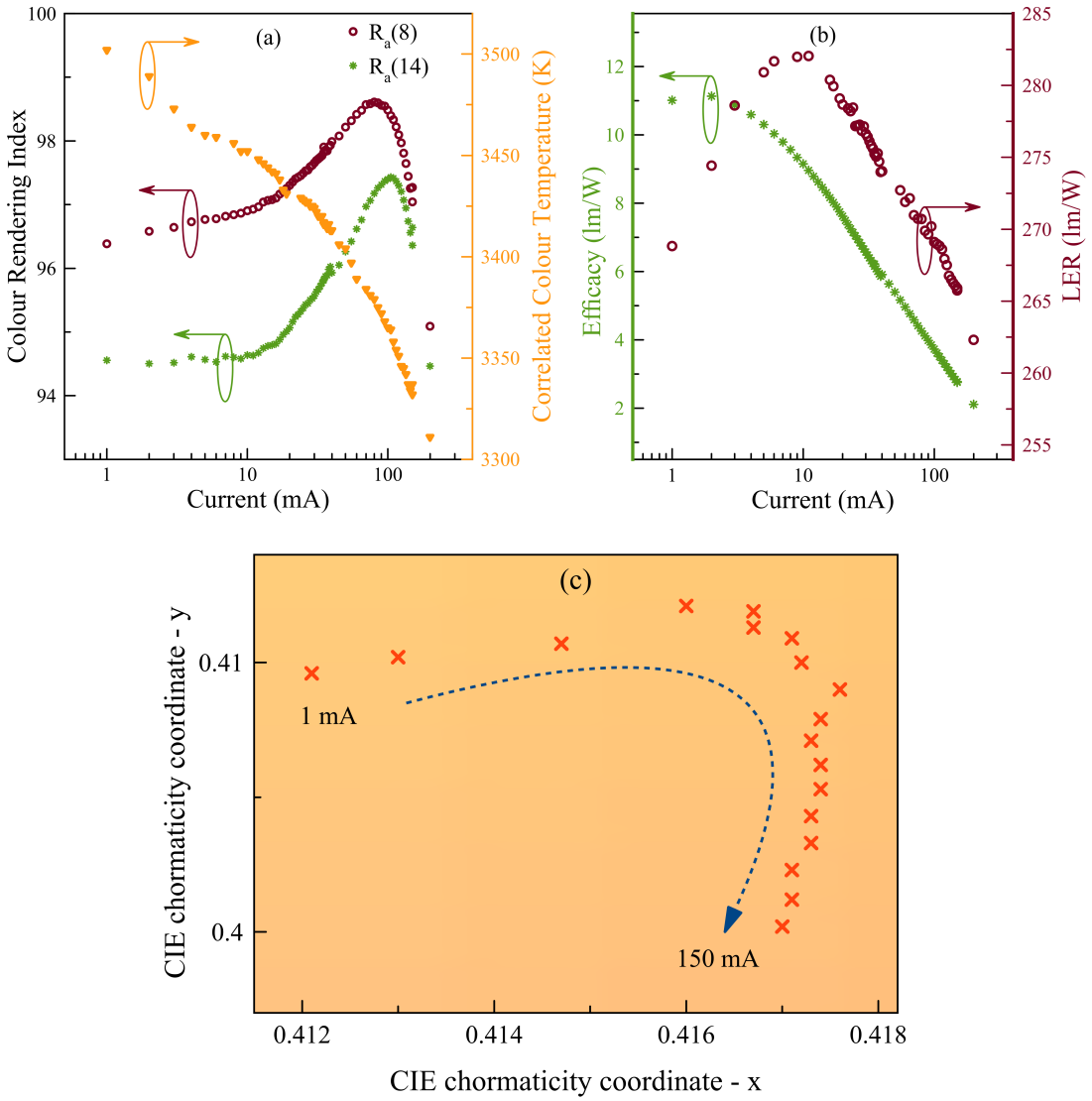

Fig. 4.6 (a) CRI and CCT determined for standard 8 Munsell samples [$R_a(8)$] and 14 (8 standard + 6 extended) Munsell samples [$R_a(14)$]; (b) Luminous Efficacy (LE) and Luminous Efficacy of Radiation (LER) for the pc-LED; (c) x, y CIE 1931 chromaticity coordinates as evolving with injection current.

coordinates with increasing current in the range of 30-150 mA. Furthermore, the luminous efficacy of radiation (LER) for the device varies in the range of 282-262 lm/W with a maximum value of 282 lm/W at 10 mA. The LER values are within the expected range of truncated solar spectrum[16].

The colour rendering index is determined with the basic eight ($R_a(8)$), and extended ($R_a(14)$) Munsell reference colour samples. Evolution of CRI, both $R_a(8)$ and $R_a(14)$, with current is depicted in fig.4.6(a). Both $R_a(8)$ and $R_a(14)$ bear

qualitative resemblance as a function of current. The general CRI $R_a(8)$ is around $\sim$ 96 at low currents, which is as claimed by the vendor, due to predominantly blue emission under these operating currents. From figure 4.6(a) it can be seen that both $R_a(8)$ and $R_a(14)$ increases with current which corresponds well with the increasing cyan emission. A maximum $R_a(8) = 98.6$ is achieved at 80 mA. Further increase in current leads to steep decrease in $R_a(8)$. Spectral broadening and red-shift in the MBC spectrum are also observed for similar current values. This indicates that colour rendition for such devices is tuneable with current. Next, the changes in partial CRI's are observed and compared for three regions of operating current as shown in fig. 4.7.

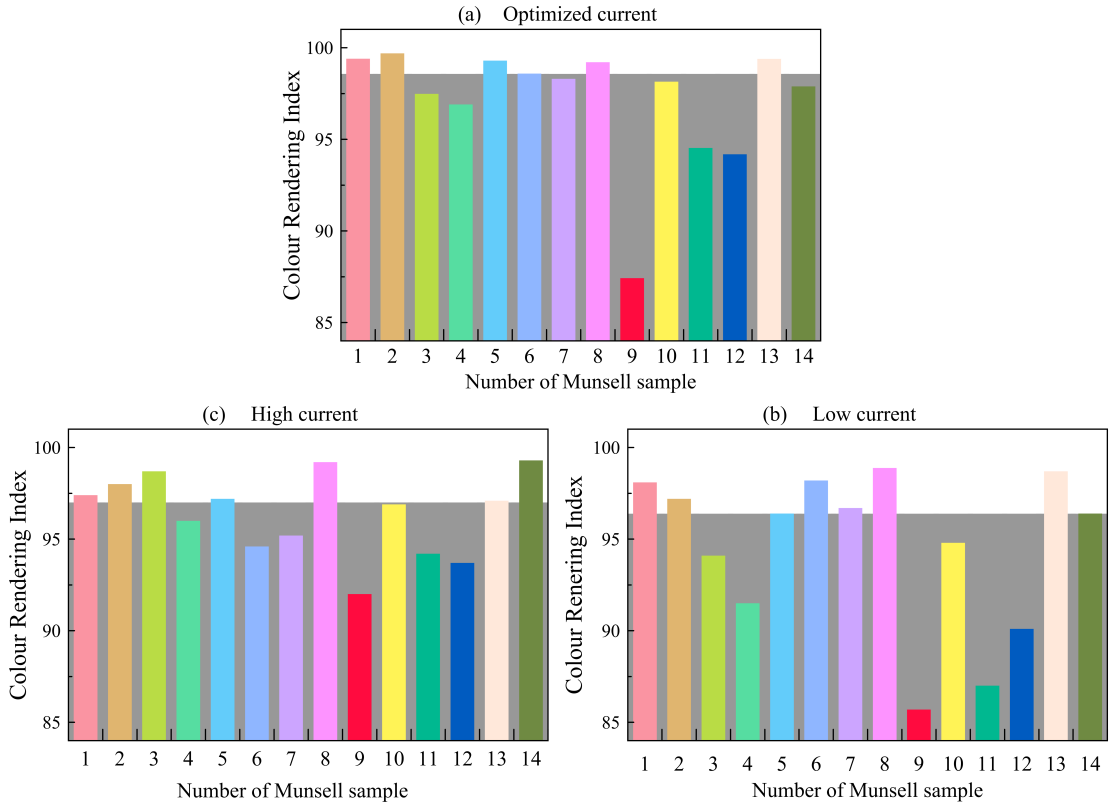

Fig. 4.7 Partial CRI's for the 14 Munsell colour samples at (a) optimal (80 mA), (b) low (1 mA) and (c) high (150 mA) current for the pc-LED. The dark grey background in each figure indicates the average CRI $R_a(8)$.

At optimal current (Fig.4.7a), i.e. $\sim$ 80mA in this case, the all partial CRI's have improved to more than 94 in comparison to their values at low current (Fig.4.7b) operation, i.e. less than $\sim$ 20-30 mA, except R_9 which is < 88. R_9 shows very little

improvement compared to improvements shown by R_3, R_4, R_{11} and R_{12} under these operating conditions. At high currents (Fig.4.7c), i.e. $\geq$ 150 mA, while the spectral shift of the MBC LED and growing cyan emission leads to a drop in most partial CRI's, as compared to their values for optimal current, R_8 shows little change and R_{14} grows along with R_9. However, the growing R_9 and R_{14} are dominated with dropping R_1 and R_5-R_7 thus leading to a lower CRI of 97.

4.3.3 Discussion

A maximum CRI of 98.6 is obtained at 80 mA and the corresponding luminous efficacy at this current is 4 lm/W. The maximum luminous efficacy achieved with the epi-up structure is 11 lm/W at an operating current of 1-2 mA. These values are quite low for practical applications and this is attributed primarily to low LEE of 14.8%. Since LEE is strongly affected by total internal reflection (TIR), free carrier absorption, and reflection at the contact electrodes, optimal chip designs such as nanocorrugated substrate to reduce TIR, carefully designed contact electrodes to reduce absorption at contacts, use of silicone lens and others; which presumably be enacted in commercial state-of-the-art high power LED designs from OSRAM, can substantially improve the LEE. Along with improvements towards reducing TIR and contact electrode absorption, the LEE of di-chromatic LED may also be limited, to a certain extent, due to free carrier absorption in QW's with higher In composition due to In segregation effects and at the interface of different layers in the AR. Though explicit studies to investigate LEE for the blue-cyan device has not been carried out, it is understood that the above discussed factors contribute towards low LEE for this device along with the losses due to phosphor. Better chip designs along with silicone lens can possibly improve the efficacy to acceptable values of $\sim$ 50 lm/W for such di-chromatic pc-LEDs. Also, any further improvement in efficacy would depend on IQE improvement. Nevertheless, since the peak efficacy (and maximum EQE) and efficacy related to highest CRI occur at different currents improvement can be made by adjusting the electrical properties of spacer in between the two (blue and cyan) QW's[18] such that maximum CRI corresponds to maximum efficacy(or EQE).

On the other hand, from the colour characteristics of pc-LED it can be seen that of all the partial CRI's improvement in R_9 is the way forward to achieve ultimate colour rendering source. The lower R_9 is because of lower than required spectral content in the wavelength range of $\sim$ 650-700 nm. This can be improved by (a) using a red phosphor with broader emission band or, (b) adding another, i.e third phosphor with emission centred around 700 nm with a very narrow spectral width. In both the cases, it is expected that the luminous efficacy will be affected negatively because a part of the red phosphor spectrum beyond photopic eye sensitivity spectrum will not be accounted for and is practically lost for efficacy calculations. Hence it is important that emission spectrum width and the peak wavelength of the red phosphor, to improve R_9, is carefully chosen taking into account its affects on efficacy.

4.4 Conclusion

A hybrid approach to generate warm white, CCT $\sim$ 3400 K, light using a novel hybrid approach with an outstanding CRI ($R_a(8)$) of 98.6 is demonstrated. To achieve such high colour rendition a di-chromatic LED emitting in the blue and cyan spectral range along with a green-red two phosphor mixture is used. The assembled pc-LED has a peak luminous efficacy of 11 lm/W, whereas the LEE and IQE for the monolithic blue-cyan device is 14.8% and 63% respectively. The efficacy can be improved with better chip design and silicone lens by improving LEE and IQE of MBC. For further improvements in CRI the partial CRI R_9 needs improvement, towards that two approaches involving careful optimisation of red phosphor have been discussed in section 4.3.3.

The given approach has a distinct advantage of employing only two phosphors with overlapping emission and excitation bands thus opening the possibility to achieve high CRI. Another advantage stems from the dual wavelength excitation LED with emission wavelengths which do not fall into the "green gap"region thus allowing for far better IQE.

References

[1] J. Y. Tsao, M. H. Crawford, M. E. Coltrin, A. J. Fischer, D. D. Koleske, G. S. Subramania, G. T. Wang, J. J. Wierer, and R. F. Karlicek, "Toward Smart and Ultra-efficient Solid-State Lighting.," *Adv. Opt. Mater.*, vol. 2, no. 9, pp. 809–836, 2014.

[2] M. Crawford, "LEDs for Solid-State Lighting: Performance Challenges and Recent Advances.," *IEEE J. Sel. Top. Quantum Electron.*, vol. 15, no. 4, pp. 1028–1040, 2009.

[3] Y. Narukawa, M. Ichikawa, D. Sanga, M. Sano, T. Miyachi, T. Mukai, "White light emitting diodes with super-high luminous efficacy.," *J. Phys. D: Appl. Phys.*, vol. 43, no. 35, pp. 354002, 2010.

[4] M. R. Krames, O. B. Shchekin, R. Mueller-Mach, G. O. Mueller, L. Zhou, G. Harbers, M. G. Craford, "Status and future of high-power light-emitting diodes for solid-state lighting.," *J. Disp. Techn.*, vol. 3, no. 2, pp. 160–175, 2007.

[5] A. A. Setlur, "Phosphors for LED-based solid-state lighting..," *Electrochemical Society Interface*, vol. 16, no. 4, pp. 32 – 36, 2009.

[6] S. Nakamura, "Present performance of InGaN-based blue/green/yellow LEDs.," in: Proc. SPIE 3002, Light-Emitting Diodes: Research, Manufacturing, and Applications, vol. 3002, pp. 26–35, (April 4) 1997.

[7] A. Žukauskas, R. Vaicekauskas, F. Ivanauskas, H. Vaitkevičius, and M. S. Shur, "Spectral optimization of phosphor-conversion light-emitting diodes for ultimate color rendering.," *Appl. Phys. Lett.*, vol. 93, no. 5, pp. 051115, 2008.

[8] T. Fukui, K. Kamon, J. Takeshita, H. Hayashi, T. Miyachi, Y. Uchida, S. Kurai, and T. Taguchi, "Superior Illuminant Characteristics of Color Rendering and Luminous Efficacy in Multilayered Phosphor Conversion White Light Sources Excited by Near-Ultraviolet Light-Emitting Diodes.," *Jpn. J. Appl. Phys.*, vol. 48, no. 11, pp. 112101, 2009.

[9] R. Mirhosseini, M. F. Schubert, S. Chhajed, J. Cho, J. K. Kim, and E. F. Schubert, "Improved color rendering and luminous efficacy in phosphor-converted white light-emitting diodes by use of dual-blue emitting active regions.," *Opt. Express*, vol. 17, no. 13, pp. 10806, 2009.

[10] P. Stauss, M. Mandl, P. Rode, A. Laubsch, A. Biebersdorf, R. Windisch, B. Galler, P. Drechsel, and U. Steegmüller, "Monolitically grown dual wavelength InGaN LEDs for improved CRI.," *Phys. status solidi (c)*, vol. 8, no. 7-8, pp. 2396–2398, 2011.

[11] M. Zulonas, T. J. Slight, I. E. Titkov, A. V. Sakharov, K. A. Fedorova, W. V.Lundin, A. E. Nikolaev, W. Meredith, A. F. Tsatsulnikov, and E. U. Rafailov, "Improvement of external quantum efficiency of blue and green InGaN LEDs using corrugated interface substrates.," in: European Conference on Lasers and Electro-Optics - European Quantum Electronics Conference, (Optical Society of America, 2015), paper CE_11_3, 2015.

[12] A. F. Tsatsulnikov, W. V. Lundin, A. V. Sakharov, E. E. Zavarin, S. O. Usov, A. E. Nikolaev, N. V. Kryzhanovskaya, V. S. Sizov, M. A. Synitsin, E. V. Yakovlev, A. E. Chernyakov, A. L. Zakgeim, N. A. Cherkashin, and M. Hytch, "InGaN/GaN short-period superlattices: synthesis, properties, applications.," *Phys. status solidi (c)*, vol. 8, no. 7-8, pp. 2308–2310, 2011.

[13] A. F. Tsatsulnikov, W. V. Lundin, A. V.Sakharov, E. E. Zavarin, S. O. Usov, A. E. Nikolaev, N. V. Kryzhanovskaya, M. A. Synitsin, V. S. Sizov, A. L. Zakgeim, and M. N. Mizerov, "A Monolithic White LED with an Active Region Based on InGaN QWs Separated by Short-Period InGaN/GaN Superlattices A.," *Semiconductors*, vol. 44, no. 6, pp. 808–811, 2010.

[14] *PhosphorTech Corporation*, PhosphorTech Datasheet, 2014.

[15] International Commission on Illumination, "Method of measuring and specifying color rendering properties of light sources.," Tech. rep.

[16] T. W. Murphy, "Maximum spectral luminous efficacy of white light.," *J. Appl. Phys.*, vol. 111, no. 10, pp. 104909, 2012.

[17] N. G. Young, R. M. Farrell, S. Oh, M. Cantore, F. Wu, S. Nakamura, S. P. DenBaars, C. Weisbuch, and J. S. Speck, "Polarization field screening in thick (0001) InGaN/GaN single quantum well light-emitting diodes.," *Appl. Phys. Lett.*, vol. 108, no. 6, pp. 1–6, 2016.

[18] S. Y. Karpov, N. A. Cherkashin, W. V. Lundin, A. E. Nikolaev, A. V. Sakharov, M. A. Sinitsin, S. O. Usov, E. E. Zavarin, and A. F. Tsatsulnikov, "Multicolor monolithic III-nitride light-emitting diodes: Factors controlling emission spectra and efficiency.," *Phys. status solidi (a)*, vol. 213, no. 1, pp. 19–29, 2016.

Chapter 5

High brightness Blue LEDs: Temperature dependant efficiency and spectral behaviour

I. E. Titkov, S. Yu. Karpov, **A. Yadav**, V. L. Zerova, M. Zulonas, et. al, "Temperature-Dependent Internal Quantum Efficiency of Blue High-Brightness Light-Emitting Diodes." IEEE Journal of Quantum Electronics, vol. 50, no. 11, pp. 911-920, 2014.

I. E. Titkov, **A. Yadav**, V. L. Zerova, M. Zulonas, E. U. Rafailov, et. al, "Novel evaluation procedure for internal and extraction efficiency of high-power blue LEDs," 2014 International Conference Laser Optics, St. Petersburg, 2014, pp. 1-1.

In this chapter, the LEE and IQE of state-of-the-art commercial blue LEDs is calculated from the experimentally determined EQE using a novel data processing procedure based on the ABC-model. It is demonstrated that the ABC-model is capable of fitting the EQE dependence on current in a very wide range and in the whole temperature range between 13 K and 440 K. Using this procedure, for the first time the temperature dependence of LEE in state-of-the-art commercial blue LEDs is estimated and the mechanisms responsible for such a dependence are qualitatively discussed. In turn, this enabled derivation of the temperature-dependent internal quantum efficiency (IQE) both at its maximum and at a practical operation current.

5.1 Introduction

InGaN-based blue LEDs are at the core of the present day phosphor covered white LEDs. These device have seen significant improvements in their quantum efficiencies over the years with improved chip designs, growth and fabrication technologies. While the IQE for such devices has improved to more than 80% [1] they still suffer from drop in efficiency with increased operating current i.e. the efficiency droop phenomenon. This presents as a fundamental impediment for InGaN based high-power devices designed to emit more optical power per unit area of the device since they operate under current/current densities different from the peak efficiencies.

Efficiency droop in InGaN LEDs has been studied rigorously and various mechanism contributing to it has been reported. Among those processes Auger recombination [2–4] is considered to be the major contributor as has been demonstrated experimentally [5–7]. On the other hand, carrier leakage outside the active region due to asymmetric p-n junction [8, 9] and/or polarization effects [10, 11], saturated radiative recombination [12], poor hole injection [13], and defect assisted tunnelling are among the suggested theories for efficiency droop. Nevertheless, a general consensus still evades the researchers. This however has not impeded the progress in the addressing the issue. Among the LEDs grown on c-plane sapphire engineering of QW and EBL has been done to reduce or overcome carrier leakage [14–19], polarisation effects [10, 20–22] and QW carrier density [23, 24]. Nevertheless, understanding the processes involved in efficiency droop is critical for further improvements to EQE of InGaN based EQE.

External quantum efficiency is inherently a product of internal quantum efficiency (η_{int}) and light extraction efficiency (η_{ext}) (assuming negligible carrier leakage) and provides information on radiative and non-radiative recombination processes. Thus, separate evaluation of IQE and LEE would be useful to determine a correlation between device structure and recombination processes. IQE and LEE are most commonly determined theoretically by FDTD modelling [25] in case of LEE and temperature dependent variable excitation photoluminescence (PL) [26, 27] and temperature dependent electroluminescence (TDEL) [28, 34] for IQE. While FDTD

is resource hungry and time consuming, PL and TDEL are based on intuitive assumptions that temperature has no affect in LEE and at cryogenic temperatures non-radiative recombination can be ignored. In the latter case, this leads to nearly 100% IQE, which according to the data presented in [28, 34] indicating a peak value of IQE under certain range of current, seems improbable even at low temperatures and would require further experiments to confirm the assumption. The former assumption of LEE not being affected by temperature would be rendered incorrect taking into account that light absorption, whether within the die or in the contact layers due to free carriers, affects LEE due to thermally activated donors and acceptors.

Recently, more practical approaches requiring minimum or no computation based on ABC-model have been used to determine IQE [30–32]. In this chapter the efficiency evolution over the broad range of temperatures 13-440K is studied. To do so a step wise procedure [33] as described in section 5.3 based on ABC model is used.

5.2 Device structure and Experimental Setup

5.2.1 Samples

The III-nitride LEDs studied in this work were fabricated by Osram Opto Semiconductors. The InGaN based devices were grown on c-plane sapphire by metal organic chemical vapour deposition (MOCVD) method with peak emission wavelength of $\lambda = 450$ nm. First an undoped GaN layer is deposited on the sapphire substrate, which is then followed by n-type GaN. Silicon (Si) is used as the dopant material for the n-type conductivity. Next the MQW active region (AR) made up of alternate layers of undoped InGaN/GaN is grown on the n-GaN contact layer. This is followed by a Mg doped p-type AlGaN electron blocking layer (EBL) and a top p-GaN layer.

Further, to reduce photon absorption, contact electrodes/pads with high reflectivity were deposited/formed on the respective n- and p-GaN contact layers. The structures were then packaged in the Osram's proprietary Golden Dragon packages after being processed as state-of-the-art UX:3 chips. However, the packaging for these chips was adapted to not have any molding and a silicone lens. Though light extraction efficiency (LEE) of these devices drops in the absence of the any molding and lens, as compared to devices with silicone lens, absence of any media next to the chip surface is crucial to correctly measure temperature- and intensity-dependent electroluminescence (T-IDEL).

5.2.2 Experimental Setup

T-IDEL is used as the experimental technique for this study [34]. To determine the only efficiency parameter that can be obtained experimentally, EQE, electroluminesence (EL) of the blue LED was measured using CDS 600 spectrometer. The wide range of temperature variation ranging from 13 K to 440 K was achieved by, Janis CCS-450, a helium (He) based closed cycle cryostat. For all temperatures the LED was operated in the current range of 10^{-8}A to 0.8 A. Self-heating, as has been argued in the literature, along with other mechanism is detrimental for device efficiency and contributes strongly with increasing operation current. Pulsed current

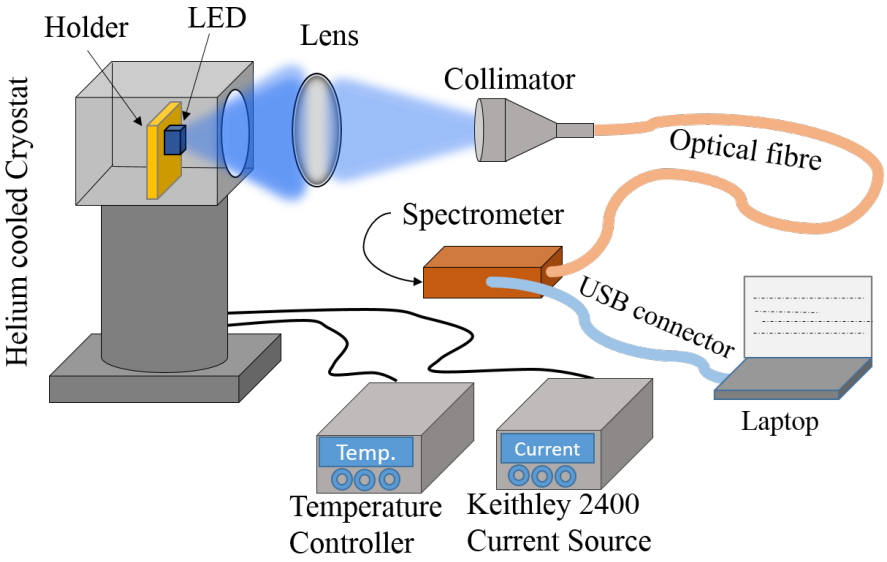

Fig. 5.1 Schematic of the T-IDEL experimental setup

with a duty cycle of 1% was employed to avoid self-heating of device for values of current $\geq$ 50 - 60 mA.

The radiant flux generated under the wide range of operation current was recorded first by reducing the exposure/integration time for the spectrometer from 5 seconds to 1 ms. Thereafter neutral-density (ND) filters from 1 to 4 were used to attenuate light intensity to record radiant flux with exposure time around 1-5 ms. For the absolute values of EQE, first measurements were made in an integrating sphere at room temperature (RT) and then in the cryostat. The normalisation factor calculated from these measurements was used to determine absolute EQE at temperatures other than RT. During the TDEL measurements to maintain a consistent optical alignment, which is of critical importance, at all temperatures it is initially established carefully at RT and is not changed thereafter. To account for the temperature dependant shift of the sample holder the cryostat is tuned at temperatures other than RT, thus maintaining a consistent optical alignment.

To establish the electrical quality of the chip, Keithly 4200, a semiconductor characterisation system was used to measure current-voltage (I-V) characteristics at all temperatures in the range of 13 K to 440 K.

5.3 IQE and LEE evaluation procedure based on the ABC model

In this section, a novel data processing procedure, as has been first proposed in [33] and developed by Dr. Sergey Karpov (STR Group, Russia), based on ABC model is detailed. The procedure relies on the fact that emitted power is proportional to BN^2 term in the model. A step-wise data processing account is presented in the section 5.3.1 below.

5.3.1 Step-wise process to evaluate IQE and LEE

The evaluate the values of IQE and LEE of a LED do the following -

Step 1) First determine the EQE (η_{ex}) of the device from the experimentally determined light-current characteristics. To do so the following relation is used

$$\eta_{ex} = \frac{qP_{out}}{I\hbar\omega} \tag{5.1}$$

where,P_{out} = emitted optical power,
q = charge of an electron,
$\hbar\omega$ = average photon energy over the emission spectral width, and
I = current

Step 2) Plot EQE as a function of emission power P_{out} and determine power P_{max} corresponding to the peak/max value of EQE (η_{ex}^{max}).

Step 3) Calculate normalised optical power, p = P_{out}/P_{max} and derive the EQE dependence on p i.e. $\eta_{ex}(p)$.

Following the procedure until step 3 allows to compare measured data to following analytical expressions -

$$p = \frac{P_{out}}{P_{max}} \tag{5.2}$$

$$Q = \frac{B}{(AC)^{1/2}} \tag{5.3}$$

$$\eta_{int} = \frac{Q}{Q + p^{1/2} + p^{-1/2}} \tag{5.4}$$

where, Q is the dimensionless independent parameter known as 'quality factor' after [35] and peak IQE can be determined solely by it using the relation

$$\eta_{int}^{max} = \frac{Q}{Q + 2} \tag{5.5}$$

where, A,B and C are Shockley-Read-Hall, Radiative and Auger recombination constants respectively. Using equation 5.4 and 5.5 a ratio between η_{ex}^{max} and $\eta_{ex}(p)$ can be determined as

$$\frac{\eta_{ex}^{max}}{\eta_{ex}(p)} = \eta_{int}^{max} + \frac{p^{1/2} + p^{-1/2}}{Q + 2} \tag{5.6}$$

providing a linear relation between $p^{1/2} + p^{-1/2}$ and $\eta_{ex}^{max}/\eta_{ex}(p)$.

Step 4) Plot the $\eta_{ex}^{max}/\eta_{ex}(p)$ ratio as a function of $p^{1/2} + p^{-1/2}$.

In such a plot the processed experimental data can be well fitted by a straight line if the $\eta_{ex}(p)$ dependence is symmetric. In the case of asymmetric dependence a low and high current branch appears and most reliable branch be used.

Step 5) Fitting the plot generated in step 4 with a straight line allows to determine Q factor as the slope of the line. Thereafter the peak IQE is determined using the relation 5.5. LEE can then be calculated using the standard relation $\eta_{ext} = \eta_{ex}^{max}/\eta_{int}^{max}$.

5.4 Results and Discussion

Experimentally obtained data pertaining to electrical and optical properties for the blue LEDs described in section 5.2 are presented and discussed here. This section also entails the results obtained after processing the current dependent EQE with the new procedure based on ABC model described in section 5.3 above.

5.4.1 Current Voltage characteristics

Current-voltage characteristics of the blue LED are shown in figure 5.2. The I-V characteristics of the LED at all temperatures is similar to a typical diode. Thus indicating good electrical quality of the p-n junction and the other layers of the chip.

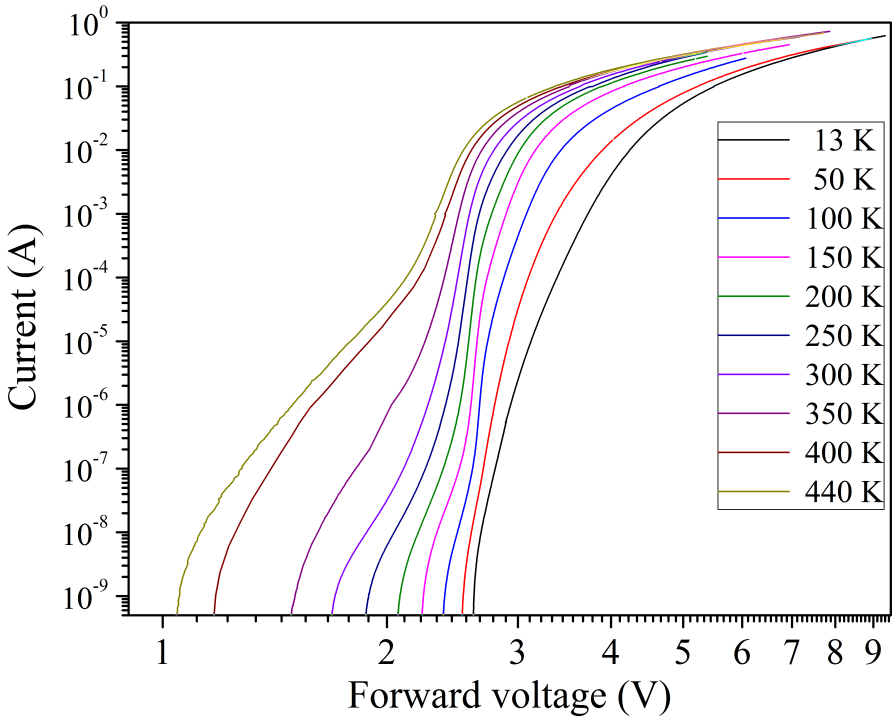

Fig. 5.2 Current-Voltage characteristics at various temperatures for the blue LED

For all temperatures the measured I-V curve can be analysed for low and high driving currents. Typically the section of the I-V plot with forward voltage less than $\sim$ 2.2 V is associated with low driving currents. While on the other hand for high currents the typical forward voltage is more than $\sim$ 2.7 V. Different mechanism

or processes can be attributed to these voltage levels. At low current injection the loss of carriers i.e. electrons and holes is predominant. The shallow and deep level impurities in the device material would create electronic states within the bandgap of the direct bandgap material. These sites could contribute to carriers loss by assisting the tunnelling of carriers. On the other hand, extended defects like V- defects, threading dislocations and micro-pipes introduced during the MOCVD growth of the devices efficiently assist in leakage of carriers at low currents. In any case these carriers do not recombine radiatively as can be confirmed from figure 5.5 by the absence of any peak at longer wavelengths. Apparently, these channels of carrier loss and are not considered by the ABC model. While, the Shockley-Read-Hall (SRH) recombination constant (A) can be adjusted to consider for trap-assisted tunnelling [36] it is not critical to implementing the procedure described in 5.3.1.

Figure 5.3 depicts the experimentally measured EQE as a function of current at various temperatures. It can be seen from figure 5.3 that for practically all temperatures the minimum current at which EQE could be measured is well above the low current ($> 10^{-8}$A, for temperature 13 K and 50 K) region of the I-V curves corresponding to tunnelling of carriers. For higher temperature the low and high current sections of the I-V curves merges together for current values, less than or equal to, the values of current for which EQE can be measured. This indicates that low current carrier loss is not affecting the EQE measurements and thus allowing us to process the EQE data with the above mentioned procedure.

On the other hand, carrier injection in the active region dominates at high current section of the I-V curves irrespective of operating temperature. For this part of the I-V curve the slope changes with temperature. This variation is accounted for by the current dependent p-n junction resistance and a diode series resistance. The LED series resistance is estimated across the complete temperature range from 13 K to 440 K by accounting for the series resistance in the adapted Shockley's diode equation. Fitting the experimental curves with the adapted diode current equations reveals a linearly decreasing series resistance from 7.1 Ω to 6.0 Ω with increasing temperature from 13 K to 440 K respectively. Furthermore, a very little change in

LED series resistance establishes the electrical stability of the ohmic contacts for both the n-type and p-type contact pads. It also indicates that carrier freezing affect is absent from the n- and p-type contact layers even at temperatures as low as 13 K.

5.4.2 Temperature dependence of the EQE

External quantum efficiency measured as a function of current at temperatures from 13 K to 440 K is shown in figure 5.3. EQE curves for all temperatures exhibit the characteristic dome like shape as reported in the literature for InGaN/GaN LEDs. For cryogenic temperatures from 13 K to 100 K, the top of the dome is approximately flat over a wide current range however the width of the dome decreases with increasing temperature. This contraction of width continues for all temperatures along with the decrease of maximum value of EQE.

The well known efficiency droop can be observed at all temperatures. It is crucial to note that even at high currents up to 800 mA, the temperature EQE curves don't intersect. This observation is quiet opposite to the previous results reported on blue LEDs [37], where EQE curves at lower temperatures intersect with

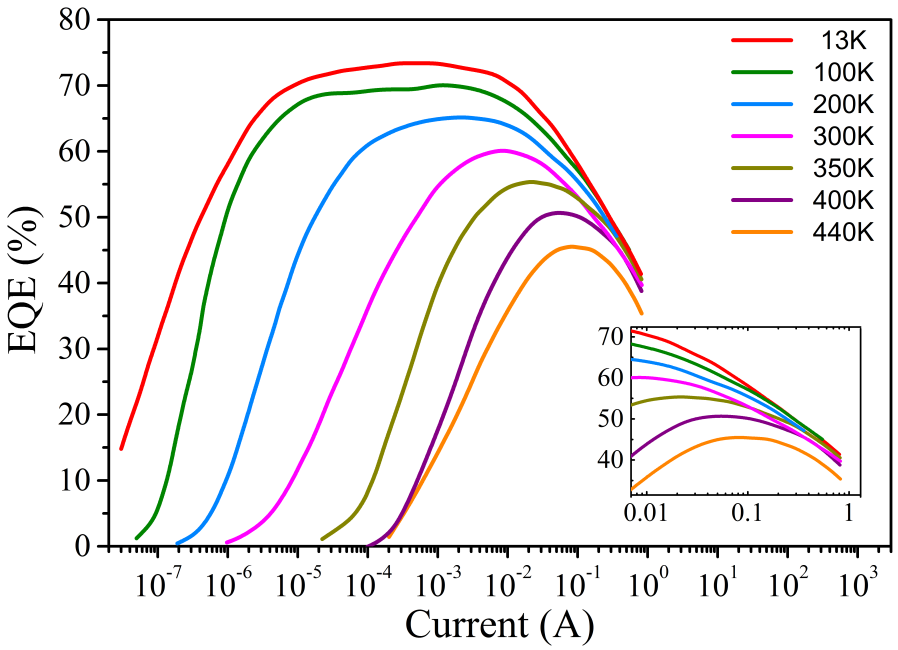

Fig. 5.3 EQE as a function of current at various temperatures (13 K to 440 K).

the high temperature curves. Unlike the results presented here in [37] the onset of droop shifts to lower currents with decreasing temperature thus the intersection of curves.

The maximum value of EQE along with the EQE value at the operating current of 350 mA for each temperature is shown in figure 5.4. The maximum value of EQE decreases with temperature from ∼74% at 13 K to ∼45% at 440 K. On the other hand the operating current EQE shows a very weak dependence on temperature as it is reduced only by ∼9% from 13 K to 440 K.

5.4.3 Spectral analysis

The EL spectra measured at 3 mA for the blue LED are presented in figure 5.5. A sharp peak around ∼ 452 nm is observed at all temperatures from 13 K to 300 K. This peak corresponds to the band to band excitonic emission from the QW's. Also, the presence of two phonon replicas, denoted as 1LO and 2LO where LO means longitudinal optical phonon, for temperatures ≤ 150 K is an indicator of good quality active region on the device .

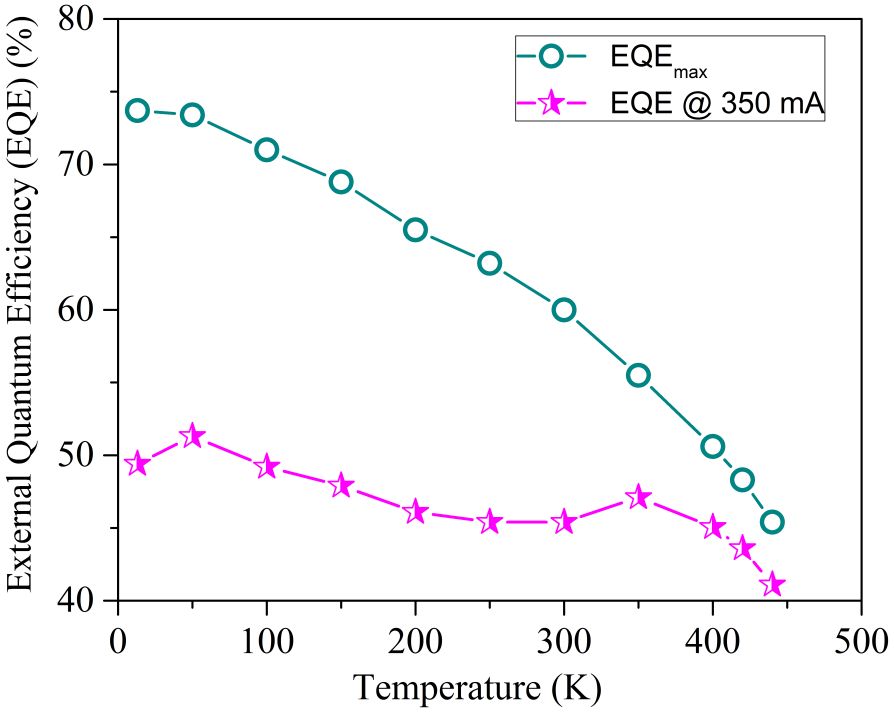

Fig. 5.4 EQE$_{max}$ and EQE at 350 mA at various temperatures (13 K to 440 K).

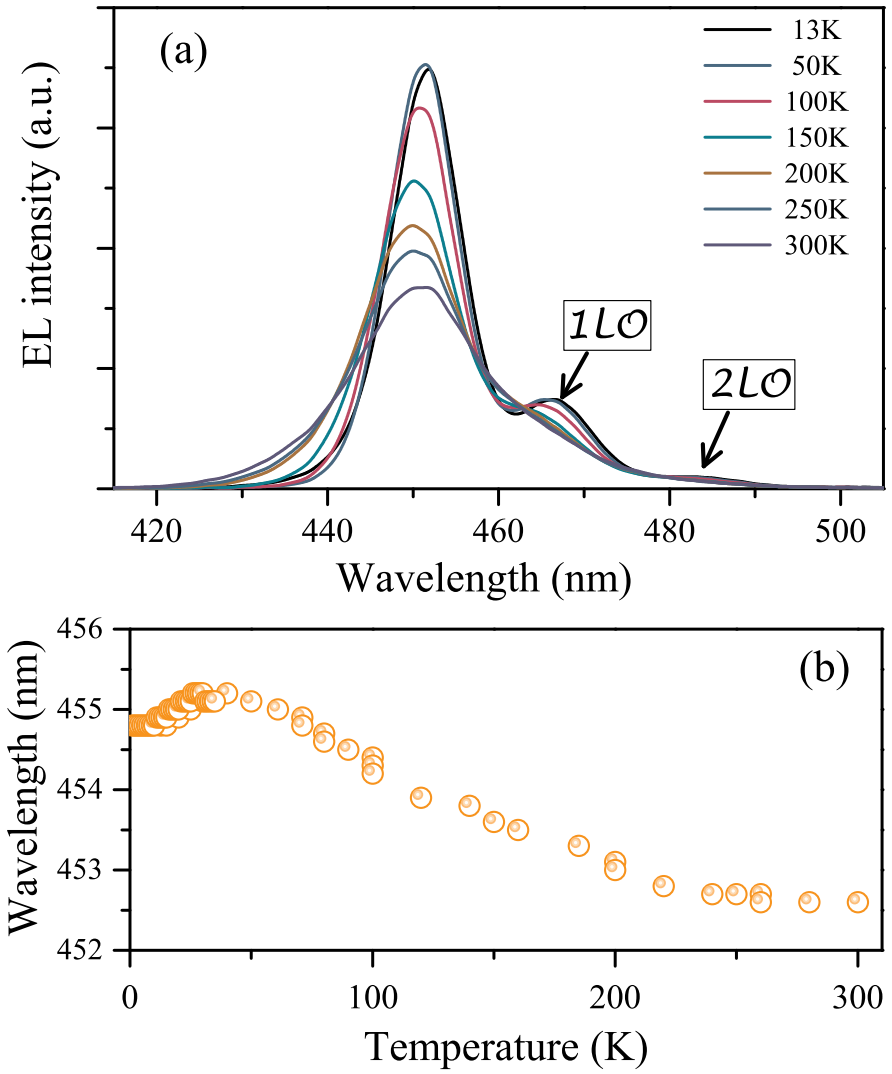

Fig. 5.5 (a)Emission spectrum at temperatures (13K to 300K) for blue LED and distinctly visible LO phonon (1^{st} and 2^{nd}) at temperatures $\leq$ 150 K, (b) S-shaped temperature dependence of dominant emission wavelength.

From figure 5.5 it is observed that at higher temperatures the EL spectra exhibit wings on the both side of the main emission peak around $\sim$ 452 nm. The high energy wings are attributed to carrier evolution in the energy bands of the active region with increasing temperature, whereas the long wavelength wings are mere merging of LO phonons replicas with the peak.

Under EL excitations with increasing temperature the dominant emission wavelength undergoes a redshift followed by a blueshift and then again gets redshifted. Thus exhibiting a S-shaped temperature dependence. Such a dependence can be explained by changing carrier dynamics due to carrier localisation and inhomo-

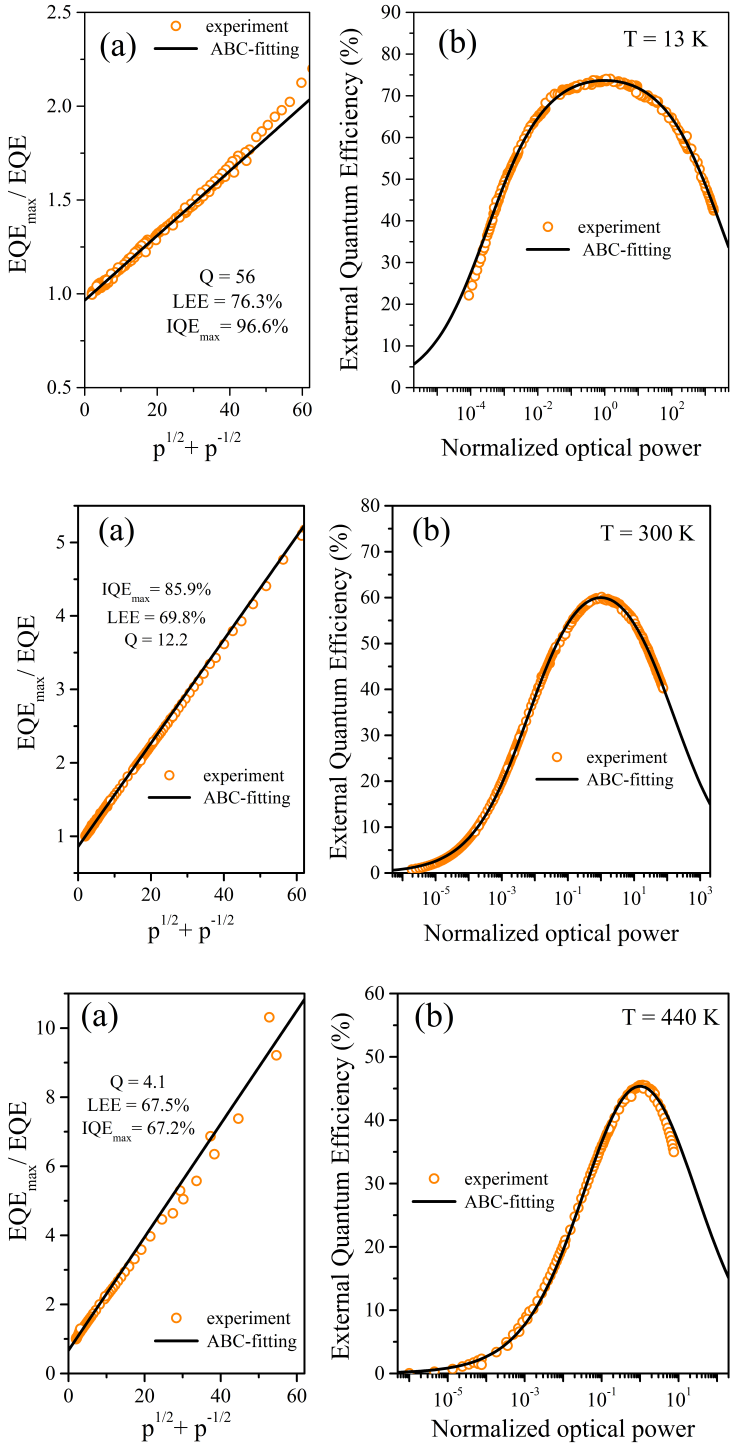

Fig. 5.6 Left column all (a)'s show EQEmax/EQE vs $p^{1/2} + p^{-1/2}$; right column all (b)'s show EQE vs normalised optical power (p) at three different temperatures. The black line in both column's represent the theoretical fitting with orange circles depicting the experimental data. The theoretical lines are obtained using the ABC-model described in section 5.3.1.

geneities in the InGaN/GaN QW structures [38]. A rather small shift of $\sim$ 3 nm over the temperature range of 13 K to 300 K is observed thus demonstrating a weak temperature dependence and stable emission behaviour.

5.4.4 LEE and IQE Evaluation

In this section, based on the procedure described initially in [33] and section 5.3.1 above, the LEE and IQE for the SQW blue LED is determined from the measured EL data. The experimental data at all temperatures is fitted in accordance with the procedure and the results at 13 K, 300 K and 440 K are presented in figure 5.6. The experimentally obtained ratio $\eta_{ex}^{max}/\eta_{ex}(p)$ is plotted as a function of $X = p^{1/2} + p^{-1/2}$ in figure 5.6(a)'s. A linear fit based on the ABC model best describes the evolution of the ratio $\eta_{ex}^{max}/\eta_{ex}(p)$ with X. It must be noted that the smaller values of X (i.e. close to the origin of the graph in figure 5.6(a)'s corresponds to the values close to maximum EQE for each temperature presented. On the other hand, the $\eta_{ex}^{max}/\eta_{ex}(p)$ ratio corresponding to the higher X values is associated with low or high, current or normalised optical power. The experimental data points are well accounted by the linear fit for the X values below 30 to 40. Thus it is expected that ABC-model shall fit the absolute experimental EQE as function of normalised optical power in whole range of interests. This is evident from figure 5.6(b)'s depicting the well fit experimental data by the theoretical curves, and deviation of the ratio $\eta_{ex}^{max}/\eta_{ex}(p)$ from theoretical linear fit (figure 5.6(a)'s) for values of X more than 30-40, which also corresponds to low or high, current or normalised optical power.

LEE obtained for all temperatures as calculated by the processing the experimental data according to the procedure described in 5.3.1 is in the range of 69.3%, for 13 K to 64.2%, for 440 K. This temperature dependence is shown in figure 5.7 along with the evolution of IQE with temperature. A maximum IQE of 96.6% at 13 K is calculated and is expectedly high, since thermal carrier loss is negligible at such temperatures, which then drops by $\sim$ 45% with increasing temperature to 60.8% at 440 K.

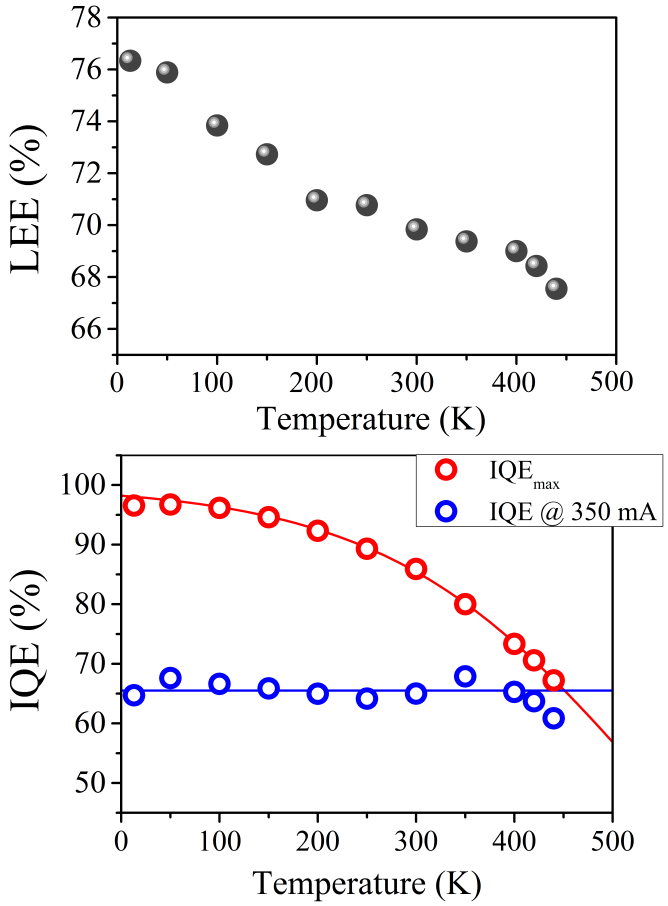

Fig. 5.7 Variation of maximum LEE (top), IQE_{max} and IQE at 350 mA (bottom). Blue line represents a constant 65% IQE and blue circles are the experimental points. Red line fitting the experimental IQE_{max} data points is approximated using known Q factors in the relation $\eta_{int}^{max} Q/(Q+2)$.

Furthermore, it is observed that IQE is practically temperature independent at 350 mA, typical operating current for high brightness LEDs, (see fig 5.7) for all temperatures below 420 K.

5.4.5 Mechanisms leading to temperature dependence of LEE

Temperature dependence of LEE, although weak, as observed in section 5.4.4 is addressed in this section. To account for such a temperature dependence, as shown figure 5.7, optical losses within the device along with their temperature behaviour has to be considered. The optical losses can be due to following three mechanisms:

(a) free-carrier absorption outside the active region by the contact layers,

(b) band-to-band absorption in the active region of the device, and

(c) reflection losses at metal electrodes on contact layers.

Free-carrier absorption (FCA) in GaN, forming the contact layers for the InGaN/GaN blue, LED shows variation with changing temperature and is reduced at lower temperatures. Considering higher donor concentration it can be assumed that electron concentration in the n-type contact layer does not exhibit temperature dependence of practical significance. On the contrary, in magnesium (Mg) doped p-type contact layer hole concentration depends strongly on temperature due to high activation energy of Mg. Furthermore, the mobilities of the carriers (holes and electrons likewise) decreases dramatically with decreasing temperature, mostly due reduced thermal activation energy. Taking into account that FCA cross-section has an inverse proportionality with carrier mobility, it is expected that FCA will be pronounced at higher temperatures as against the lower cryogenic temperatures, thus contributing to the loss of photons in turn helping to in reducing the LEE at higher temperatures.

Band-to-band absorption is the dominating processes of the absorption spectrum for direct bandgap materials. The temperature dependence of the band-to-band absorption process is characterised by the shrinking forbidden gap or the red shift of the emission spectrum. Studies made on InGaN QWs in [39] reports a shift of peak absorption band edge by ~ 32 meV towards higher energy at operating temperatures < 70 K, such a shift vanishes with increasing temperatures thus contributing the optical losses and hence reduced LEE.

Reflection losses due to partial reflection of light at the metal electrodes originate from the temperature dependence reflectance properties of the electrodes. A simple method based on Drude model to estimates reflectivity at the silver(Ag)/GaN interface predicts a decline in reflectivity by $\sim 5\%$ points to $\sim 94\%$ at 300 K from $\sim$ 99% at 20 K. Thus indicating increased optical losses with increasing temperatures that is in-line with the trend for the highly reflective metals with plasma frequency (ω_p) > frequency of light (ω).

5.5 Conclusion

In this chapter commercial high-brightness blue LED was studied under wide range of variable temperatures from 13 K to 440 K. The evolution of both electrical and optical properties under these temperatures are presented. Next, an ABC-model based stepwise procedure is used to estimate the IQE and LEE for a packaged device from the experimentally determined EQE.

The procedure applied fits ABC model remarkably well to the experimental data at all measured temperatures thus allowing to evaluate IQE and LEE in the whole range. The quality factor, Q assumes a constant value over the range of 13-440K indicating a rather weak temperature dependence of recombination constants on carrier concentration. Maximum EQE as determined from the experimental data decreases from $\sim$ 74% at 13 K to $\sim$ 45% at 440 K. However, for operating current of 350 mA EQE exhibits a weak dependence on temperature with a drop of only 9% over the whole range of temperatures. On the other hand IQE ($\sim$ 65%) at all temperatures for the operating current of 350 mA showed no dependence on temperature indicating a non-monotonic nature of Auger recombination constants with temperature. Also, maximum IQE dropped by $\sim$ 32% from $\sim$ 97% at 13 K to $\sim$ 65% at 440 K. Furthermore, LEE also decreases as expected with increasing temperature from 76% at 13 K to 68% at 440 K.

References

[1] T. Sano, T. Doi, S. A. Inada, T. Sugiyama, Y. Honda, H. Amano, and T. Yoshino, "High Internal Quantum Efficiency Blue-Green Light-Emitting Diode with Small Efficiency Droop Fabricated on Low Dislocation Density GaN Substrate.," *Jpn. J. Appl. Phys.* vol. 52, no. 8S, pp. 08JK09, 2013.

[2] Y. C. Shen, G. O. Muller, S. Watanabe, N. F. Gardner, A. Munkholm, and M. R. Krames, "Auger recombination in InGaN measured by photoluminescence.," *Appl. Phys. Lett.*, vol. 91, no. 14, pp. 141101, 2007.

[3] K. A. Bulashevich and S. Y. Karpov, "Is Auger recombination responsible for the efficiency rollover in III-nitride light-emitting diodes?.," *Phys. status solidi (c)*, vol. 5, no. 6, pp. 2066–2069, 2008.

[4] A. Laubsch, M. Sabathil, W. Bergbauer, M. Strassburg, H. Lugauer, M. Peter, S. Lutgen, N. Linder, K. Streubel, J. Hader, J. V. Moloney, B. Pasenow, and S. W. Koch, "On the origin of IQE-'droop' in InGaN LEDs.," *Phys. Status Solidi (c)*, vol. 6, no. S2, pp. S913–S916, 2009.

[5] J. Iveland, L. Martinelli, J. Peretti, J. S. Speck, and C. Weisbuch, "Direct Measurement of Auger Electrons Emitted from a Semiconductor Light-Emitting Diode under Electrical Injection: Identification of the Dominant Mechanism for Efficiency Droop.," *Phys. Rev. Lett.*, vol. 110, no. 17, pp. 177406, 2013.

[6] M. Binder, A. Nirschl, R. Zeisel, T. Hager, H. J. Lugauer, M. Sabathil, D. Bougeard, J. Wagner, and B. Galler, "Identification of nnp and npp Auger recombination as significant contributor to the efficiency droop in (GaIn)N quantum wells by visualization of hot carriers in photoluminescence.," *Appl. Phys. Lett.*, vol. 103, no. 7, pp. 071108, 2013.

[7] B. Galler, H. J. Lugauer, M. Binder, R. Hollweck, Y. Folwill, A. Nirschl, A. Gomez-Iglesias, B. Hahn, J. Wagner, and M. Sabathil, "Experimental Determination of the Dominant Type of Auger Recombination in InGaN Quantum Wells.," *Appl. Phys. Express*, vol. 6, no. 11, pp. 112101, 2013.

[8] D. S. Meyaard, Q. Shan, Q. Dai, J. Cho, E. F. Schubert, M. H. Kim, and C. Sone, "On the temperature dependence of electron leakage from the active region of GaInN/GaN light-emitting diodes.," *Appl. Phys. Lett.*, vol. 99, no. 4, pp. 041112, 2011.

[9] D. S. Meyaard, G. b. Lin, Q. Shan, J. Cho, E. Fred Schubert, H. Shim, M. h. Kim, and C. Sone, "Asymmetry of carrier transport leading to efficiency droop in GaInN based light-emitting diodes.," *Appl. Phys. Lett.*, vol. 99, no. 25, pp. 251115, 2011.

[10] M. H. Kim, M. F. Schubert, Q. Dai, J. K. Kim, E. F. Schubert, J. Piprek, and Y. Park, "Origin of efficiency droop in GaN-based light-emitting diodes.," *Appl. Phys. Lett.*, vol. 91, no. 18, pp. 183507, 2007.

[11] J. Xu, M. F. Schubert, A. N. Noemaun, D. Zhu, J. K. Kim, E. F. Schubert, M. H. Kim, H. J. Chung, S. Yoon, C. Sone, and Y. Park, "Reduction in efficiency droop, forward voltage, ideality factor, and wavelength shift in polarization-matched GaInN/GaInN multi-quantum-well light-emitting diodes.," *Appl. Phys. Lett.*, vol. 94, no. 1, pp. 011113, 2009.

[12] J. -I. Shim, H. Kim, D. -S. Shin, and H. -Y. Ryu, "An Explanation of Efficiency Droop in InGaN-based Light Emitting Diodes: Saturated Radiative Recombination Rate at Randomly Distributed In-Rich Active Areas.," *J. Korean Phys. Soc.*, vol. 58, no. 3, pp. 503, 2011.

[13] I. Rozhansky, and D. Zakheim, "Analysis of the causes of the decrease in the electroluminescence efficiency of AlGaInN light-emitting-diode heterostructures at high pumping density.," *Semiconductors*, vol. 40, no. 7, pp. 839–845, 2006.

[14] P. M. Tu, C. Y. Chang, S. C. Huang, C. H. Chiu, J. R. Chang, W. T. Chang, D. S. Wuu, H. W. Zan, C. C. Lin, H. C. Kuo, and C. P. Hsu, "Investigation of efficiency droop for InGaN-based UV light-emitting diodes with InAlGaN barrier.," *Appl. Phys. Lett.*, vol. 98, no. 21, pp. 211107, 2011.

[15] Y. K. Kuo, M. C. Tsai, S. H. Yen, T. C. Hsu, and Y. J. Shen, "Effect of P-type last barrier on efficiency droop of blue InGaN light-emitting diodes.," *IEEE J. Quantum Electron.*, vol. 46, no. 8, pp. 1214–1220, 2010.

[16] C. H. Wang, S. P. Chang, W. T. Chang, J. C. Li, Y. S. Lu, Z. Y. Li, H. C. Yang, H. C. Kuo, T. C. Lu, and S. C. Wang, "Efficiency droop alleviation in InGaN/GaN light-emitting diodes by graded-thickness multiple quantum wells.," *Appl. Phys. Lett.*, vol. 97, no. 18, pp. 181101, 2010.

[17] S. H. Han, D. Y. Lee, H. W. Shim, G. C. Kim, Y. S. Kim, S. T. Kim, S. J. Lee, C. Y. Cho, and S. J. Park, "Improvement of efficiency droop in InGaN/GaN multiple quantum well light-emitting diodes with trapezoidal wells.," *J. Phys. D. Appl. Phys.*, vol. 43, no. 35, pp. 354004, 2010.

[18] Y. Y. Zhang and G. R. Yao, "Performance enhancement of blue light-emitting diodes with AlGaN barriers and a special designed electron-blocking layer.," *J. Appl. Phys.*, vol. 110, no. 9, pp. 093104, 2011.

[19] S. H. Yen, M. C. Tsai, M. L. Tsai, Y. J. Shen, T. C. Hsu, and Y. K. Kuo, "Effect of N-Type AlGaN Layer on Carrier Transportation and Efficiency Droop of

Blue InGaN Light-Emitting Diodes.," *IEEE Photonics Technol. Lett.*, vol. 21, no. 14, pp. 975–977, 2009.

[20] J. Xu, M. F. Schubert, D. Zhu, J. Cho, E. F. Schubert, H. Shim, and C. Sone, "Effects of polarization-field tuning in GaInN light-emitting diodes.," *Appl. Phys. Lett.*, vol. 99, no. 4, pp. 041105, 2011.

[21] M. F. Schubert and E. F. Schubert, "Effect of heterointerface polarization charges and well width upon capture and dwell time for electrons and holes above GaInN/GaN quantum wells.," *Appl. Phys. Lett.*, vol. 96, no. 13, pp. 131102, 2010.

[22] Y. K. Kuo, J. Y. Chang, and M. C. Tsai, "Enhancement in hole-injection efficiency of blue InGaN light-emitting diodes from reduced polarization by some specific designs for the electron blocking layer.," *Opt. Lett.*, vol. 35, no. 19, pp. 3285, 2010.

[23] M. Maier, K. Köhler, M. Kunzer, W. Pletschen, and J. Wagner, "Reduced nonthermal rollover of wide-well GaInN light-emitting diodes.," *Appl. Phys. Lett.*, vol. 94, no. 4, pp. 041103, 2009.

[24] D. A. Zakheim, A. S. Pavluchenko, and D. A. Bauman, "Blue LEDs - way to overcome efficiency droop.," *Phys. Status Solidi (c) Curr. Top. Solid State Phys.*, vol. 8, no. 7-8, pp. 2340–2344, 2011.

[25] A. Zhmakin, "Enhancement of light extraction from light emitting diodes.," *Phys. Rep.*, vol. 498, no. 4-5, pp. 189–241, 2011.

[26] S. Watanabe, N. Yamada, M. Nagashima, Y. Ueki, C. Sasaki, Y. Yamada, T. Taguchi, K. Tadatomo, H. Okagawa, and H. Kudo, "Internal quantum efficiency of highly-efficient $In_xGa_{(1-x)}N$-based near-ultraviolet light-emitting diodes.," *Appl. Phys. Lett.*, vol. 83, no. 24, pp. 4906–4908, 2003.

[27] A. Hangleiter, D. Fuhrmann, M. Grewe, F. Hitzel, G. Klewer, S. Lahmann, C. Netzel, N. Riedel, and U. Rossow, "Towards understanding the emission efficiency of nitride quantum wells.," *Phys. status solidi (a)*, vol. 201, no. 12, pp. 2808–2813, 2004.

[28] G. Chen, M. Craven, A. Kim, A. Munkholm, S. Watanabe, M. Camras, W. Götz, and F. Steranka, "Performance of high-power III-nitride light emitting diodes.," *Phys. status solidi (a)*, vol. 205, no. 5, pp. 1086–1092, 2008.

[29] M. Peter, A. Laubsch, W. Bergbauer, T. Meyer, M. Sabathil, J. Baur, and B. Hahn, "New developments in green LEDs.," *Phys. status solidi (a)*, vol. 206, no. 6, pp. 1125–1129, 2009.

[30] H. Y. Ryu, H. S. Kim, and J. I. Shim, "Rate equation analysis of efficiency droop in InGaN light-emitting diodes.," *Appl. Phys. Lett.*, vol. 95, no. 8, pp. 081114, 2009.

[31] G. B. Lin, Q. Shan, A. J. Birkel, J. Cho, E. F. Schubert, M. H. Crawford, K. R. Westlake, and D. D. Koleske, "Method for determining the radiative efficiency of GaInN quantum wells based on the width of efficiency-versus-carrier-concentration curve.," *Appl. Phys. Lett.*, vol. 101, no. 24, pp. 241104, 2012.

[32] P. Kivisaari, L. Riuttanen, J. Oksanen, S. Suihkonen, M. Ali, H. Lipsanen, and J. Tulkki, "Electrical measurement of internal quantum efficiency and extraction efficiency of III-N light-emitting diodes.," *Appl. Phys. Lett.*, vol. 101, no. 2, pp. 021113, 2012.

[33] I. E. Titkov, S. Y. Karpov, A. Yadav, V. L. Zerova, M. Zulonas, B. Galler, M. Strassburg, I. Pietzonka, H. J. Lugauer, and E. U. Rafailov, "Temperature-Dependent Internal Quantum Efficiency of Blue High-Brightness Light-Emitting Diodes.," *IEEE J. Quantum Electron.*, vol. 50, no. 11, pp. 911–920, 2014.

[34] M, Peter, A. Laubsch, W. Bergbauer, T. Meyer, M. Sabathil, and J. Baur, "New developments in green LEDs.," *Phys. status solidi (a)*, vol. 206, no. 6, pp. 1125 – 1129, 2009. and Berthold Hahn

[35] K. A. Bulashevich, O. V. Khokhlev, I. Y. Evstratov, and S. Y. Karpov, "Simulation of light-emitting diodes for new physics understanding and device design.," in: *Proc. SPIE*, edited by K. P. Streubel, H. Jeon, L. W. Tu, and N. Linder, pp. 827819, 2012.

[36] K. Sakowski, L. Marcinkowski, S. Krukowski, S. Grzanka, and E. Litwin-Staszewska, "Simulation of trap-assisted tunneling effect on characteristics of gallium nitride diodes.," *J. Appl. Phys.*, vol. 111, no. 12, pp. 123115, 2012.

[37] K. Fujiwara, H. Jimi, and K. Kaneda, "Temperature-dependent droop of electroluminescence efficiency in blue (In,Ga)N quantum-well diodes.," *Phys. status solidi (c)*, vol. 6, no. S2, pp. S814–S817, 2009.

[38] O. Rubel, M. Galluppi, S. D. Baranovskii, K. Volz, L. Geelhaar, H. Riechert, P. Thomas and W. Stolz, "Quantitative description of disorder parameters in (GaIn)(NAs) quantum wells from the temperature-dependent photoluminescence spectroscopy.," *J. Appl. Phys.*, vol. 98, no. 6, pp. 063518, 2005.

[39] C. S. Kim, J. H. Kim, K. J. Yee, H. K. Kwon, H. S. Lee, J. S. Park, and K. J. Yee, "Temperature- and Bias-dependent Study of Photocurrent Spectroscopy in an InGaN Light-emitting Diode Operating near 400 nm.," *J. Korean Phys. Soc.*, vol. 57, no. 4, pp. 793, 2010.

Chapter 6

High current pulsed pumping of AlGaInP red LEDs: Efficiency and Optical properties

A. Yadav, I. E. Titkov, G. S. Sokolovskii, S. Yu. Karpov, V. V. Dudelev, K. K. Soboleva, M. Strassburg, I. Pietzonka, Hans-Juergen Lugauer, and E. U. Rafailov, "AlGaInP red-emitting light emitting diode under extremely high pulsed pumping," Proc. SPIE 9768, Light-Emitting Diodes: Materials, Devices, and Applications for Solid State Lighting XX, 97681K, March 8, 2016.

In this chapter behaviour of efficiency of high power 620 nm AlInGaP LEDs when operated under high current density up to 4.5 kA/cm^2 and varied pulse width from microsecond down to sub-nanosecond is studied. No efficiency decrease and negligible red shift of the emission wavelength is observed in the whole range of drive currents at nanosecond-range pulses with duty cycles well below 1%. Analysis of the pulse-duration dependence of the LED efficiency and emission spectrum suggests the active region overheating to be the major mechanism of the LED efficiency reduction at higher pumping, dominating over the electron overflow and Auger recombination. Furthermore, a low LEE as calculated using AB-model suggest light extraction to still be the bottleneck for lower overall efficiency.

6.1 Introduction

AlGaInP based LEDs emits in the 560 - 650 nm wavelength range of the visible spectrum where wavelengths are tuned by varying the Al content in the quaternary alloy as discussed previously. Light emitting diodes based on AlGaInP material system are used in many applications such as outdoor displays, traffic lights, keypads, signage, automotive lighting, horticulture and SSL [1]. For SSL,a multichip approach that combines AlGaInP based red LEDs and AlGaInN blue LEDs is a promising way forward towards high CRI white light generation especially with significant luminous efficacy improvements over the last decade for devices from either material system [2].

To further improve the optical and efficiency parameters of AlGaInP LEDs, a better understanding of processes leading to reduction in efficiency at high current is crucial. It is argued that possibly the mechanism behind decrease of efficiency at high currents is common to both AlGaInP and AlGaInN material systems due to the similarities in the behaviour of external quantum efficiency (EQE) with increasing current [3]. The decrease in external quantum efficiency at high currents for III-nitrides has been attributed to prominent mechanisms such as: Auger recombination [4, 5], carrier delocalisation [6], saturated radiative recombination [7], carrier leakage [8, 9] and dislocation-induced non-radiative recombination [10]. However, AlGaInP red LEDs are grown on lattice matched GaAs substrate thus dislocation assisted non-radiative recombination is not likely to be the dominant mechanism towards reduction in EQE at high current densities. Further, absence of strong piezoelectric fields for this material system and reduced composition fluctuations indicates that carrier leakage due to polarization and delocalization of carriers respectively, may contribute to, but are not the dominant mechanism for EQE decrease in red LEDs at high current densities. Whilst this line of thought depends heavily on studies done on a material system which is different from AlGaInP in a number of ways, more direct investigations on red LEDs in the literature offers a better insight on the mechanism and methods regarding efficiency decrease in red LEDs.

The escape of carriers to confining layers, that are grown from an indirect bandgap material, from the active region has been suggested as the mechanisms for efficiency decrease with increasing current and increased Al content to achieve emission closer to green wavelength region [3, 11, 12]. The literature also offers other possible explanations to efficiency decrease in red LEDs. While Shi et. al. [13] suggest two mechanism, defect recombination and saturated radiative recombination, dependent on driving current, for efficiency decrease it has also been strongly argued that carrier leakage is the dominant mechanism. Authors in [14, 15] suggest that asymmetricity of the p-n junction leads to electron (carrier) leakage for low operating currents. On the other hand carrier leakage due to insufficient barrier heights of the confinement layers between the QWs which is very similar to [3, 11, 12] has been convincingly argued in [16, 17]. Following the presented line of argument a similar effect of decrease in efficiency must be observed under increased density of high energy electrons device due to self-heating or increased carrier concentration in the active region QWs raising the quasi-fermi level. Furthermore, at higher temperatures due to decrease in radiative constant and non-radiative carrier lifetime efficiency of LED might decrease irrespective of carrier leakage. To identify and better understand the contributions of low barrier electron leakage and elevated active region temperature during operation in the case of red LEDs there is need for further experiments.

In this chapter red LEDs studied under CW and pulse regimes for current as high as up to 45 A are presented. To avoid the elevated operating temperatures of the active region an aluminium heat sink and duty cycles of $\leq 1\%$ were used. The spectral and power characterisation data from CW, 100 μs, sub-microsecond and sub-nanosecond pulse operation is used and presented to better understand the nature of decrease in efficiency of red LEDs.

6.2 Device structure and Experimental setup

6.2.1 Samples

In this experiment the investigated high power AlGaInP based red LEDs were grown, using metal-organic vapour phase epitaxy (MOVPE), on GaAs substrate. The active region of 1×1 mm^2 devices was composed of vertically stacked $(Al_xGa_{(1-x)})_{0.5}In_{0.5}P$ multiple quantum wells (MQWs). These MQWs were enclosed by the confining layers of $Al_xIn_{(1-x)}P$. Next an AlGaAs window layer is grown on top of p-confinement layer followed by a p-type GaAs top contact layer. To achieve emission around $\sim$ 620 nm Al composition in the MQW's is attuned to $\sim$ 12-16%. Thereafter the singulated devices were processed with OSRAM Thin film process and packaged with Golden Dragon casing.

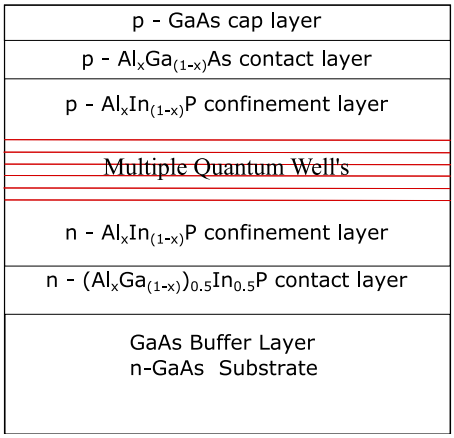

Fig. 6.1 Schematic for the MQW red LED layers.

6.2.2 Experimental details

The AlGaInP LEDs were studied under both continuous wave (CW) and pulsed regime. All room temperature measurement under both regimes were made using an integration sphere and CDS-600 spectrometer. The collected data was processed using LightMtrx software to obtain absolute values for radiant flux and thus EQE along with other peak emission wavelength, full bandwidth at half maximum (FWHM), centroid wavelength and spectral data. Keithly 2400 is used as the source for CW operation with a maximum current of 1 A. To operate the LED under

pulsed regime, 100 μs and sub-microsecond pulses, for current up to 2 A an Agilent 8114 A pulse generator was used and for currents 2 A - 23 A, IXYS Colorado PCX-7420 pulse laser diode driver with external trigger was used. Furthermore, to operate the LED under sub-microsecond regime (0.7ns) a custom built pulse generator producing peak currents up to 45 A was used. Also, a non-contact current probe, TCP0030 AC/D, was used to monitor and determine the actual current flowing through the device thus accounting for the non-linear impedance behaviour of the LED.

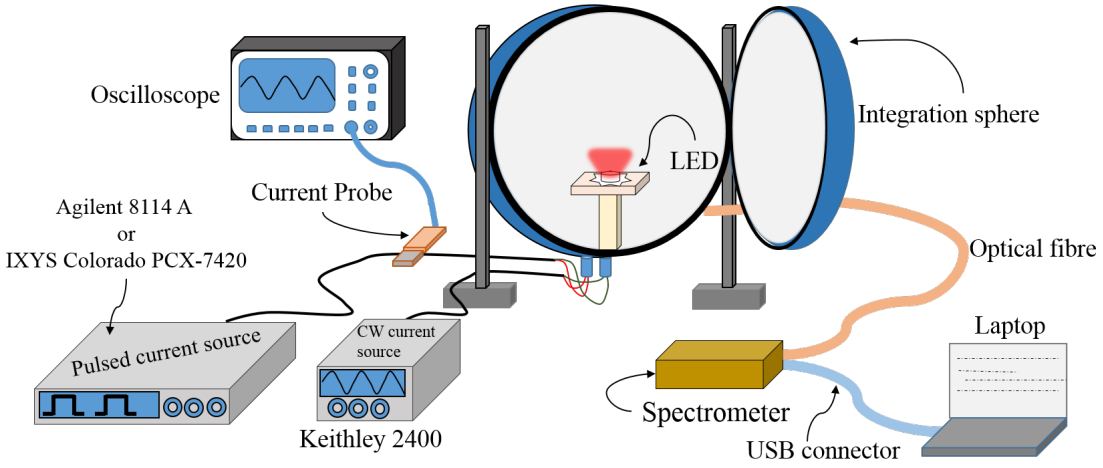

Fig. 6.2 Experimental Setup

The electroluminescence (EL) of the LED driven at high current under pulse regime was also recorded. Oscilloscopes and photo-detectors with appropriate bandwidth (BW) and rise time respectively, were used. For, 100 μs & sub-microsecond regime the EL response was recorded using a 1 GHz oscilloscope and 30 GHz photo-detector. On the other hand a 50 GHz oscilloscope with a 14ns rise time photo-detector was used to record EL response of the device when operated under sub-nanosecond regime. For all pulse regimes duty cycle of $\leq 1\%$ is employed to avoid inter pulse heating effect.

Lastly, to determine dependence of peak wavelength on temperature, under various regimes of operation, temperature dependent electroluminescence (TDEL) measurements were performed in CW regime. A closed cycle helium (He) based cryostat, Janis CCS450, was employed to achieve temperatures in the range of 13 - 450 K.

6.3 Results

The room temperature current-voltage (I-V) characteristics of the studied device is shown in figure 6.3. Fitting the given I-V with Shockley's diode equation yields an ideality factor of 1.3 and resistance of 1.15 Ohms in series. An ideality factor of less than 2 and a very low series resistance are indicative of better design of LED structure electrically.

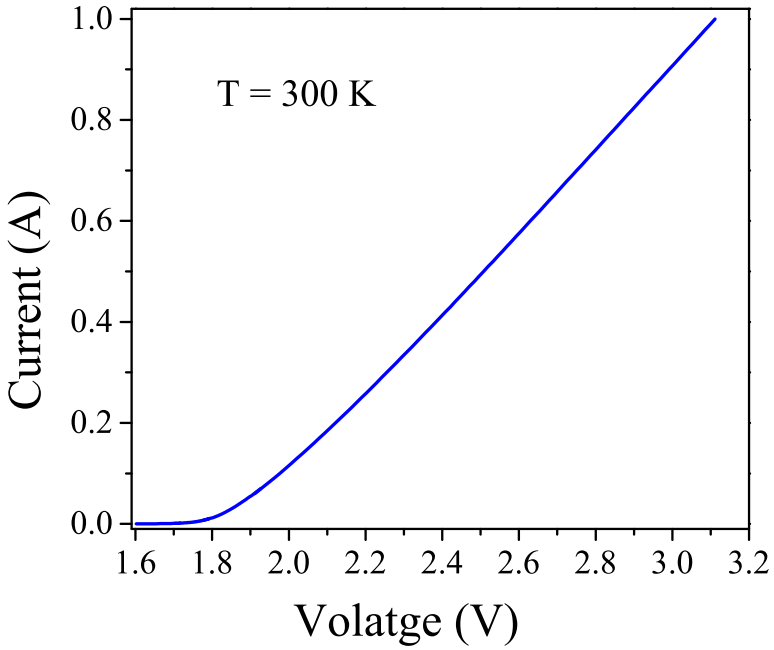

Fig. 6.3 Current-voltage characteristics of AlGaInP LED at room temperature

6.3.1 Spectral analysis

Spectral evolution as a function of current under 100 μs pulse regime, duty cycle = 1%, for currents range of 100 mA to 5 A is shown in Fig 6.4(a). A shift of emission peak towards longer wavelengths with increasing current is clearly noted. An increase of current from 100 mA to 5 A under these conditions leads to a red shift [18] of $\sim$ 6 nm as shown in fig.6.4(b). Under CW operation in the current range of 10 mA to 100 mA a similar red shift of $\sim$ 6-8 nm can be observed (see fig. 6.4(b)). This shift is indicative of elevated operating temperature of the device, i.e. self-heating.

Under 100 μs pulse operation, for currents up to 1 A, a very small red shift of $\sim$ 2 nm (fig. 6.4(b)) along with a spectral broadening of $\sim$ 2.5 nm (fig. 6.5(a)) was observed. Moreover, a red shift of about 6 nm along with $\sim$ 8.5 nm spectral broadening is observed upon increasing the driving current to up to 5 A. This dramatic increase in spectral width and red-shift is a strong indication of elevated junction temperature of device. This observation is supported by the observed increased slope of the short wavelength part of emission spectrum as discussed in [15]. Furthermore, the photo-detector response of LED as shown in figure 6.5(b) depicts the effect of increased operation current on the response of the LED emission during the pulse. The sharp decrease of emission during the pulse for currents $\geq$ 2A is evident and further supplements the observation of increased junction temperature with current.

The above observation warranted investigation under shorter pulses. The LED was next driven with sub-microsecond (200 - 600 ns), and sub-nanosecond (0.7ns) pulses in the high current range of up to 45 A. Fig 6.4(b) and 6.5(a) depicts the red shift based on evolution of peak wavelength, and spectral broadening as full width half maximum (FWHM) respectively for both regimes. A red shift of $\sim$ 4 nm and FWHM of $\sim$ 10 nm for sub-microsecond (200 - 600 ns) pulses is evident. Further suggesting increase in junction temperature.

However, a two slope character in red shift, slow change at low current and rapid change at high currents, is observed. Under low current of 10-30 mA start of red shift seems to practically have no correlation with applied pulse width except 0.7 ns pulses. The observed behaviour can be better explained by thermal shrinking of bandgap and constant Fermi level because of device capacitance being recharged. Contrary to these observations, see fig. 6.4(b), the current values for change in slope of red shift from slow to rapid are different for different pulses. It starts from the current values of $\sim$ 10 A for sub-microsecond pulses, much higher than $\sim$ 1 A for 100 μs pulses, suggesting current dependence of onset of red shift on pulse width.

Assuming $\sim$ 2nm (see Fig. 6.4(b)) of red shift to correspond to change in slope of red shift, a pulse duration (τ_p) dependent critical current (I_c) for the slope change can be plotted, as shown in fig 6.6. The experimental data is well fitted by $\tau_p^{-1/2}$

thus suggesting device self heating leading to rapid red shift. As for the red shift at low currents, it can be attributed to shrinking of bandgap due to non-equilibrium injection of carriers in the active region [19].

A similar observation regarding the different mechanism at low and high currents can be made from the evolution of spectral FWHM as a function of current. From Fig. 6.5(a) it can seen that irrespective of the applied pulse width the spectral width curves follow the same trajectory with the increase in carrier concentration

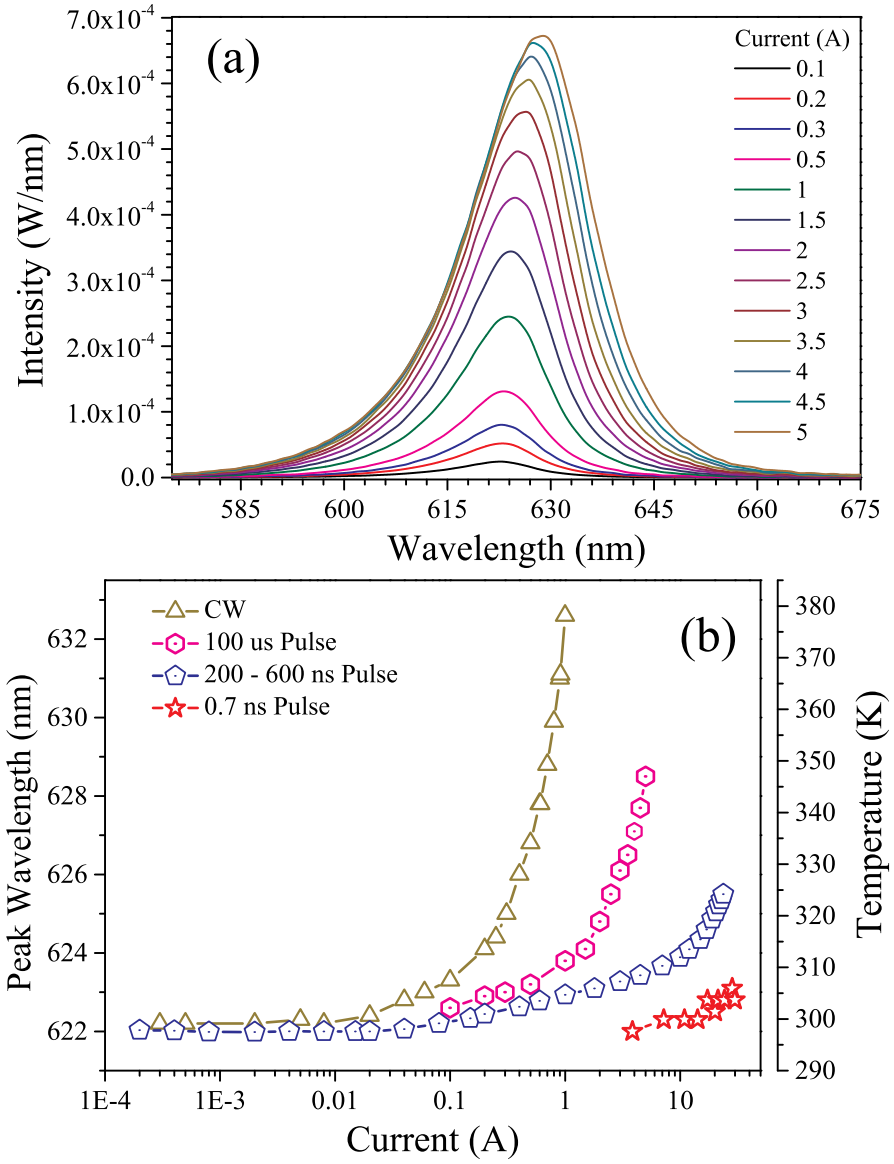

Fig. 6.4 (a) Emission spectrum of red LED under 100 μs pulses for current up to 5 A. (b) Peak wavelength vs current for CW and various pulse width (100 μs to sub-nanosecond (0.7ns)) along with corresponding change in junction temperature with changing peak emission wavelength.

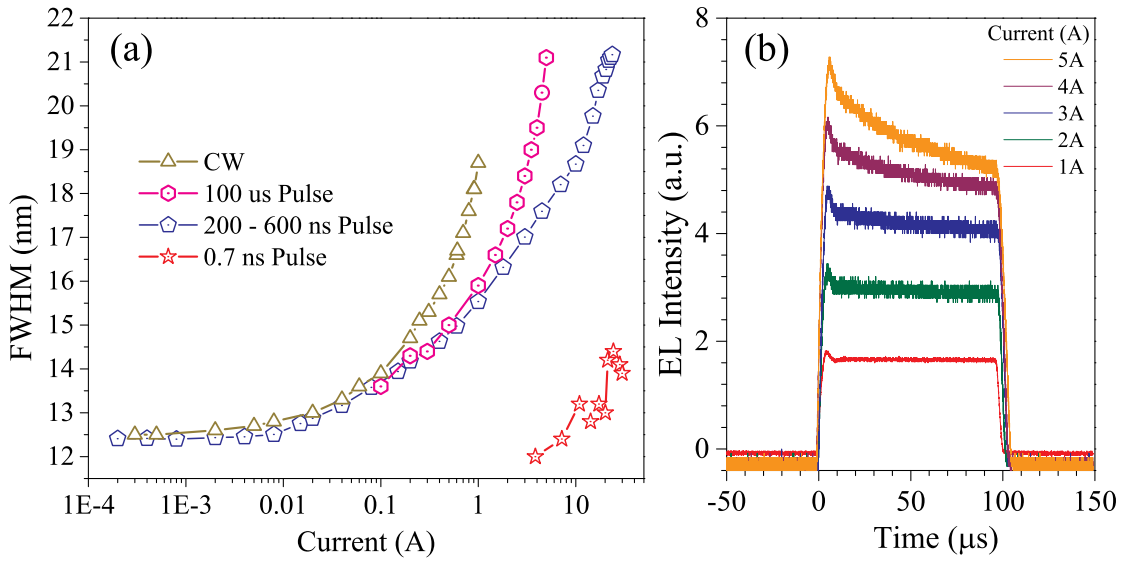

Fig. 6.5 (a) Evolution of FWHM as a function of current under CW and pulsed regime (100 μs to sub-nanosecond (0.7 ns)). (b) Observed change in EL intensity of the LED during 100 μs pulses for the peak current in the range of 1A - 5A.

with current until I_c is reached and enhanced broadening of spectrum is observed due to device self-heating.

On the other hand, for sub-nanosecond pulses ($\sim$ 0.7 ns) for currents up to 45 A with 0.1% duty cycle, the observed red shift is merely $\sim$ 1nm (fig 6.4(b)) indicative of negligible change in active region/junction temperature thus exceptionally low overheating even under high current pumping.

Next, to estimate temperature of self-heated active region, dependence of peak emission wavelength on temperature was studied under wide range of temperatures from 13 K to 450 K under CW regime. A linear coefficient of 7.5 K/nm for temperatures $\geq$ 150 K is found to best describe the dependence. This corresponds to 30 K increase junction temperature for 4nm of red shift observed up to 23 A of current under sub-microsecond regime, as shown in fig 6.4(b).

6.3.2 Efficiency under varying current and pulse width

EQE as a function of current under CW and sub-microsecond regime is shown in Fig. 6.7(a). EQE(I) increases gradually at lower currents for both regimes. Under CW regime of operation EQE reaches a maximum value $\sim$ 29% at $\sim$ 60 mA. Further increase in driving current is accompanied by decrease in EQE which

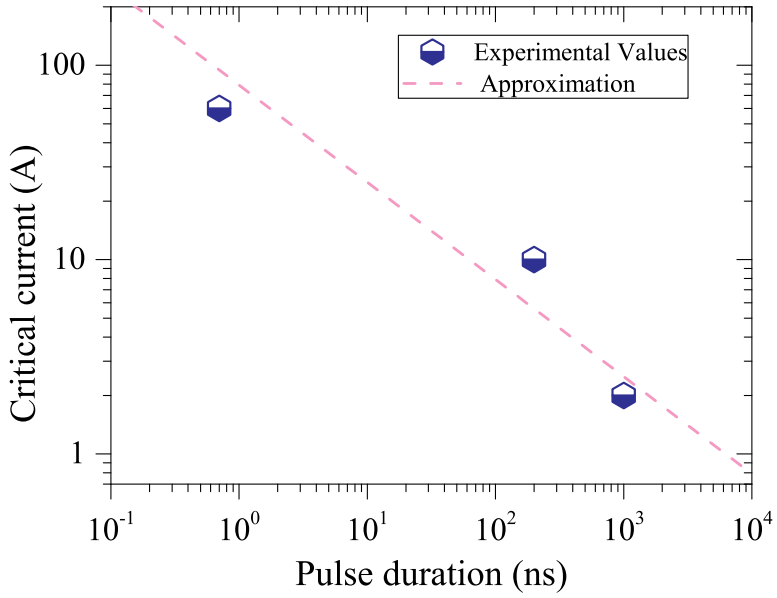

Fig. 6.6 Critical current (I_c) as a function of pulse duration corresponding to the change of slope in the red shift behaviour. Solid line is an approximation assuming $I_c \propto$ pulse duration.

reduces to about 15% of its maximum value at 700 mA. The rapid drop in EQE can be attributed to increased junction temperature at higher currents due to self-heating. On the other hand for sub-microsecond regime peak or maximum EQE is reached at $\sim$ 200-250 mA and a 15% of its maximum value is reached at $\sim$ 8-9 A. Thus a shift in onset of EQE decrease is observed under pulsed regime.

To estimate IQE and LEE, under CW regime, from measured EQE(I) reduced ABC-model (refer to section 5.3 for details on ABC model) i.e.AB-model proposed in [20] [21] was used. The EQE(I) as predicted by AB-model is presented as dashed line in Fig. 6.7(a) and fits well at smaller current values under the assumption of absence of electron leakage and isothermal condition of operation. Maximum IQE value as obtained using the model was 90% at $\sim$ 10-30 mA of CW current. This value correlates well with previous reports. On the other hand, a relatively low value of maximum EQE of $\sim$ 29% was attributed to the absence of silicone lens leading to a comparatively low LEE = 32.3% as would be expected.

Fig.6.7(b) illustrates optical power at 50% IQE_{max} ($P_{0.5}$), as calculated using the AB-model [20], as a function of current along with apparent LEE (which is related to LEE).The deviation of both these quantities from the constant values

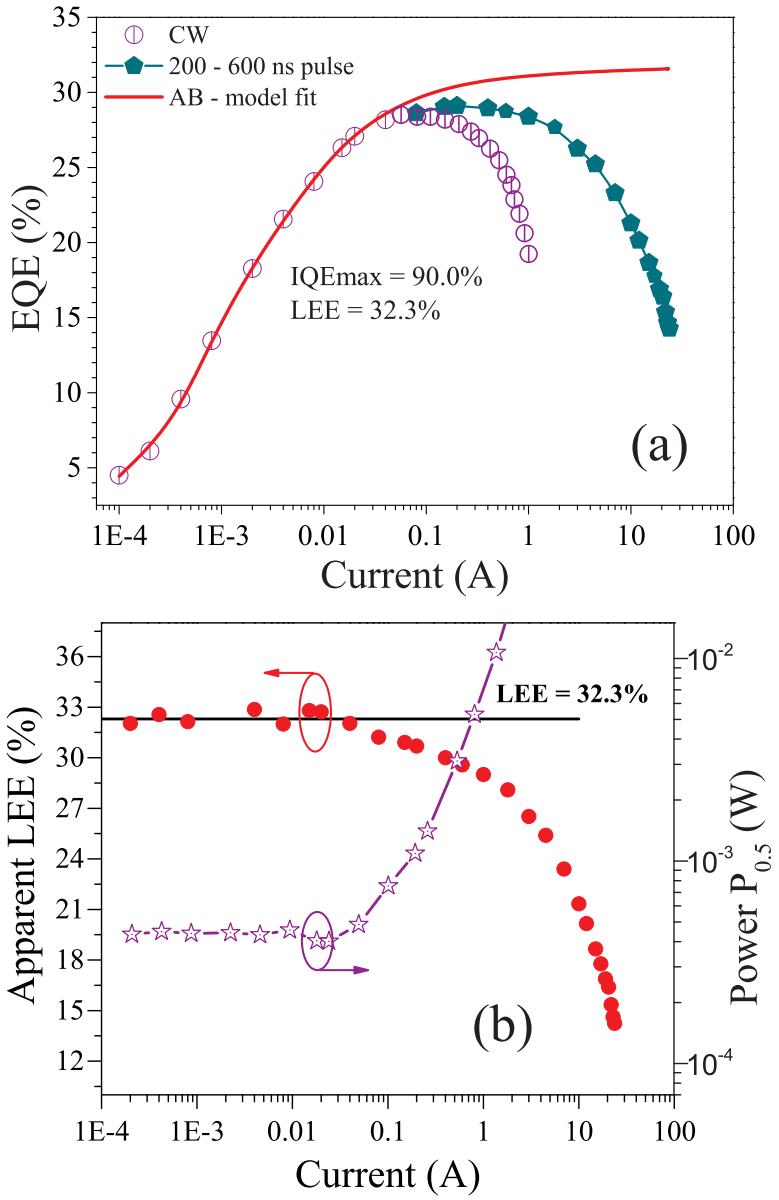

Fig. 6.7 (a) EQE vs current for CW and nanosecond pulse regime of operation; the solid red line represents the theoretical fit obtained with AB-model, (b) evolution of apparent LEE and $P_{0.5}$ with current where both parameters were extracted using experimental EQE data; the solid black line in (b) represents a constant LEE of 32.3%

of 32.3% (LEE) and 0.45 mW ($P_{0.5}$) with increasing currents signifies reduction in IQE as a result of electron leakage or self-heating or both.

Next, a deviation of experimental EQE(I) with respect to theoretical curve as predicted by AB-model can be seen from Fig.6.7(a). The observed deviation at first leads to EQE saturation followed by a sharp decrease. Saturation of EQE(I)

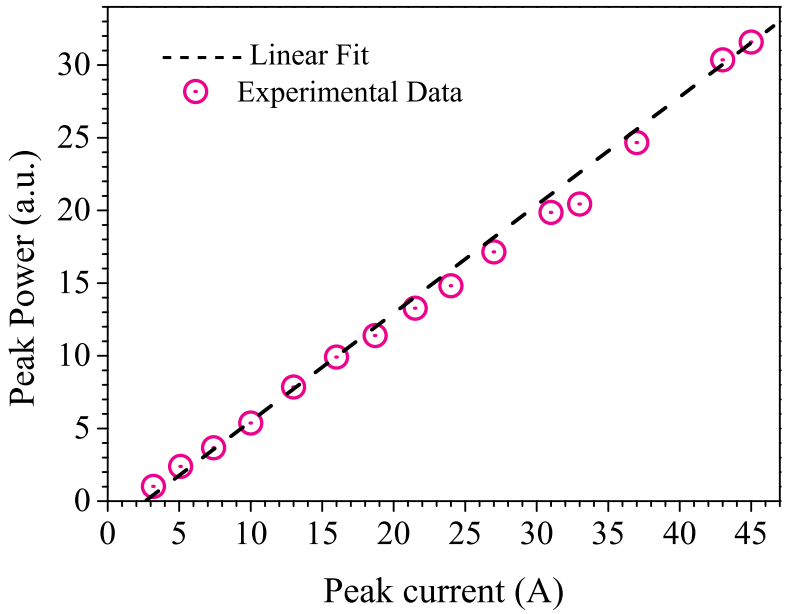

Fig. 6.8 Peak power of the LED under sub-nanosecond (0.7 ns) regime for peak currents up to current 45 A. A good approximation of experimental data (circles) with a linear fit (dashed black line) is obtained.

connotes a proportional relation between driving and leakage current. The onset of sharp EQE(I) drop, under CW regime corresponds remarkably to the critical current related to change of slope of peak wavelength red shift and roughly under 200-600ns pulse regime. This leads to the conclusion that carrier injection leads to EQE saturation first and a sharp decrease in EQE(I) is due to self-heating.

To exclude self-heating effects, 0.7 ns pulses with a repetition rate of 10kHz were applied to the LED for currents up to 45 A and its photoresponse was studied. The evolution of experimental maximum of the photoresponse w.r.t to the peak valued of the applied current, as shown in 6.8, is well fitted with a linear function (dashed blue line). The observed linear relation suggests that under sub-nanosecond pulses the EQE does not decrease with increasing current. However, this observation must be treated carefully since the optical response time duration for LEDs, as suggested by the authors in [21], is much longer than the applied 0.7 ns pulses. Under such operating conditions usual method of EQE determination must be reconsidered accounting for the longer duration of optical response w.r.t current pulse along with development of suitable comparison method for efficiency comparison under sub-nanosecond and CW regimes.

6.4 Conclusion

In this chapter spectral and power characteristics of high power AlInGaP red LEDs were studied under high current CW and pulsed regimes from 100 μs to sub-nanoseconds pulses. The effectiveness of such characterisation to analyse physical mechanisms contributing towards efficiency decrease in AlInGaP LEDs is demonstrated. Critical current (I_c) corresponding to the change in slope in the dual slope character of the red shift in peak emission wavelength with increasing current is determined.

A correlation between I_c along with current corresponding to the start of red shift,i.e. I_o and saturation and/or decrease of EQE with current allows to distinguish between various mechanisms involved during device operation. Depending on the strength of applied current (I) w.r.t. I_c and/or I_o three regions of operation have been identified.

Region A) $I < I_c$: in this case experimentally determined EQE exactly follows the theoretical efficiency values as predicted by the AB model, i.e. reduced ABC model. Thus neither self-heating nor increased carrier concentration influence device operation.

Region B) $I_o < I < I_c$: in this case thermally induced bandgap shirking results in a weak red shift of peak emission wavelength. On the other hand, increased carrier concentration induces leakage on electrons in the p-side of LED leading to saturation of EQE(I).

Region C) $I > I_c$: under such operating conditions a sharp decrease in EQE(I) accompanied with enhanced spectral broadening and strong red shift (corresponding to steeper slope in the dual slope character) was observed predominantly due to self-heating of device.

It has also been observed that the onset of sharp EQE decrease due to device self-heating can be shifted to higher currents without incurring noticeable losses in emission efficiency by operating under pulsed regime, i.e I_c is shifted to higher values. An increase of two orders of magnitude in I_c under sub-microsecond regime when compared to CW regime was observed. Sub-nanosecond pulse may preclude

device self-heating completely even at high currents up to 45 A. However, a better approach accounting for different durations of optical response and current pulse for sub-nanosecond pulses needs to be developed.

On the other hand, a LEE of 32.3% indicates that unlike III-nitride devices with LEE $\sim$ 90% [22] light extraction remains as the most significant factor limiting the overall emission efficiency. Nevertheless the need for improvement of LEE from $\sim$ 32% to $\sim$ 90% is far greater than losses in IQE due to electron leakage.

References

[1] J. Y. Tsao, M. H. Crawford, M. E. Coltrin, A. J. Fischer, D. D. Koleske, G. S. Subramania, G. T. Wang, J. J. Wierer, and R. F. Karlicek, "Toward Smart and Ultra-efficient Solid-State Lighting," *Adv. Opt. Mater.*, vol. 2, no. 9, pp. 809–836, 2014.

[2] M. Crawford, "LEDs for Solid-State Lighting: Performance Challenges and Recent Advances," *IEEE J. Sel. Top. Quantum Electron.*, vol. 15, no. 4, pp. 1028–1040, 2009.

[3] J. Cho, E. F. Schubert, and J. K. Kim, "Efficiency droop in light-emitting diodes: Challenges and countermeasures," *Laser Photon. Rev.*, vol. 7, no. 3, pp. 408–421, 2013.

[4] Y. C. Shen, G. O. Mueller, S. Watanabe, N. F. Gardner, A. Munkholm, M. R. Krames, "Auger recombination in InGaN measured by photoluminescence," *Appl. Phys. Lett.*, vol. 91,no. 14, pp. 141101, 2007.

[5] K. T. Delaney, P. Rinke, C. G. Van de Walle, "Auger recombination in InGaN measured by photoluminescence," *Appl. Phys. Lett.*, vol. 94, no. 19, pp. 191109, 2009.

[6] T. Mukai, M. Yamada, S. Nakamura, "Characteristics of InGaN-Based UV/Blue/Green/Amber/Red Light-Emitting Diodes," *Jpn. J. Appl. Phys.*, vol. 38, part 1, no. 7A, pp. 3976–3981, 1999.

[7] S. Jong-In, K. Hyungsung, S. Dong-Soo, Y. Han-Youl, "An Explanation of Efficiency Droop in InGaN-based Light Emitting Diodes: Saturated Radiative Recombination Rate at Randomly Distributed In-Rich Active Areas," *J. Korean Phys. Soc.*, vol. 58, no. 3, pp. 503, 2011.

[8] D. S. Meyaard, Q. Shan, Q. Dai, J. Cho, E. F. Schubert, M.-H. Kim, C. Sone, "On the temperature dependence of electron leakage from the active region of GaInN/GaN light-emitting diodes," *Appl. Phys. Lett.*, vol. 99, no. 4, pp. 041112, 2011.

[9] J. Xu, M. F. Schubert, A. N. Noemaun, D. Zhu, J. K. Kim, E. F. Schubert, M. H. Kim, H. J. Chung, S. Yoon, et al., "Reduction in efficiency droop, forward voltage, ideality factor, and wavelength shift in polarization-matched GaInN/GaInN multi-quantum-well light-emitting diodes," *Appl. Phys. Lett.*, vol. 94,no. 1, pp. 011113, 2009.

[10] N. I. Bochkareva, V. V. Voronenkov, R. I. Gorbunov, A. S. Zubrilov, Y. S. Lelikov, P. E. Latyshev, Y. T. Rebane, A. I. Tsyuk, Y. G. Shreter, "Defect-related tunneling mechanism of efficiency droop in III-nitride light-emitting diodes," *Appl. Phys. Lett.*, vol. 96, no. 13, pp. 133502, 2010.

[11] D. Patel, J. M. Pikal, C. S. Menoni, K. J. Thomas, F. A. Kish, and M. R. Hueschen, "Effect of indirect minima carrier population on the output characteristics of AlGaInP light-emitting diodes," *Appl. Phys. Lett.*, vol. 75, no. 20, pp. 3201, 1999.

[12] P. Altieri, A. Jaeger, R. Windisch, N. Linder, P. Stauss, R. Oberschmid, and K. Streubel, "Internal quantum efficiency of high-brightness AlGaInP light-emitting devices," *J. Appl. Phys.*, vol. 98, no. 8, pp. 086101, 2005.

[13] J.-W. Shi, F.-M. Kuo, C.-W. Lin, W. Chen, L.-J. Yan, and J.-K. Sheu, "Investigation of the Efficiency-Droop Mechanism in Vertical Red Light-Emitting Diodes Using a Dynamic Measurement Technique," *IEEE Photonics Technol. Lett.*, vol. 23, no. 21, pp. 1585–1587, 2011.

[14] C.-F. Huang, Y.-F. Su, C.-B. Lin, and K.-N. Chiang, "Research on efficiency droop mechanism and improvement in AlGaInP Ultra-High-Brightness LEDs using the transient measurement method," *Solid. State. Electron.*, vol. 93, pp. 15–20, 2014.

[15] J.-I. Shim, D.-I. Han, H. Kim, D.-S. Shin, G.-B. Lin, D. S. Meyaard, Q. Shan, J. Cho, E. F. Schubert, H. Shim, and C. Sone, "Efficiency droop in AlGaInP and GaInN light-emitting diodes," *Appl. Phys. Lett.*, vol. 100, no. 11, pp. 111106, 2012.

[16] R. Windisch, P. Altieri, R. Butendeich, S. Illek, P. Stauss, W. Stein, W. Wegleiter, R. Wirth, H. Zull, and K. Streubel, "InGaAlP thin film LEDs with high luminous efficiency," *Proc. SPIE*, vol. 5366, pp. 43–52 2004.

[17] P. Royo, R. P. Stanley, M. Ilegems, K. Streubel, and K. H. Gulden, "Experimental determination of the internal quantum efficiency of AlGaInP microcavity light-emitting diodes," *J. Appl. Phys.*, vol. 91, no. 5, pp. 2563 2002.

[18] P. Manninen and P. Orreveteläinen, "On spectral and thermal behaviors of AlGaInP light-emitting diodes under pulse-width modulation," *Appl. Phys. Lett.*, vol. 91, no. 18, pp. 17–20, 2007.

[19] P. A. Wolff, "Theory of the Band Structure of Very Degenerate Semiconductors," *Phys. Rev. Lett.*, vol. 126, no. 2, pp. 405–412, 1962.

[20] A. Yadav, I. E. Titkov, G. S. Sokolovskii, S. Y. Karpov, V. V. Dudelev, K. K. Soboleva, M. Strassburg, I. Pietzonka, H.-j. Lugauer, and E. U. Rafailov, "AlGaInP red-emitting light emitting diode under extremely high pulsed pumping," in *SPIE OPTO,* , H. Jeon, L.-W. Tu, M. R. Krames, and M. Strassburg, eds., pp. 97681K, 2016.

[21] A. Yadav, I. E. Titkov, G. S. Sokolovskii, S. Y. Karpov, V. V. Dudelev, K. K. Soboleva, M. Strassburg, I. Pietzonka, H.-j. Lugauer, and E. U. Rafailov, "Temperature effects on optical properties and efficiency of red AlGaInP-based light emitting diodes under high current pulse pumping," *Optica*, (under review).

[22] S. Y. Karpov, "Light-emitting diodes for solid-state lighting: searching room for improvements," in *Proc. SPIE - Light. Diodes Mater. Devices, Appl. Solid State Light. XX. SPIE San Fr.*, , H. Jeon, L.-W. Tu, M. R. Krames, and M. Strassburg, eds., pp. 97680C, 2016.

Chapter 7

Conclusion

In this thesis, white LEDs with improved colour rendering and correlated colour temperature in two configurations a) monolithic and b) phosphor covered InGaN/GaN based LED are presented. Evaluation of IQE and LEE along with their dependence on temperature for $\sim$ 440 nm blue LED is discussed. AlGaInP red LED is studied under pulsed current injection regime to understand the nature of decrease of efficiency at high currents.

In chapter 3, InGaN/GaN MQW di-chromatic monolithic white LED with vertically stacked two blue QW's emitting at $\sim$ 450 nm and one green QW emitting $\sim$ 550 nm are demonstrated under CW and pulse regimes of operation. Under CW regime a CRI of 67 is achieved, the highest value demonstrated till date to the best of my knowledge for such devices i.e. phosphor free, monolithic di-chromatic MQW LED emitting in blue and green spectral region. Tuning of CCT from cool white ($\sim$ 13000 K) to warm white ($\sim$ 2700 K) light with current modulation is also shown. With another LED from the same wafer it is also demonstrated that almost constant luminous flux can be maintained at a constant current and duty cycle while varying the pulse width by two orders of magnitude from 0.1 μs to 100 μs.

Next, in the same chapter singulation of LED with 800 nm fs laser by stealth dicing is demonstrated. An energy vs depth map with pulse energies from 1 μJ to 30 μJ is prepared to find the most suitable energy range needed to inflict enough damage for separation in a single sweep. With 25 μJ pulses of 140 fs width the 350 μm thick sample is cleaved by generating a single row of defects due to dielectric

breakdown or coulomb explosion. From the focal point of the laser in side the sapphire sample the cleaved surfaces towards the beam entering side and away from beam entering side exhibit different features. Both sides are devoid of any propagating cracks. The bottom surface has a maximum roughness of 50 nm, tolerable for blue and violet laser diode facets. On the other hand towards the top ripples of 30 μm in width with $\sim$ 15 μm height are observed. These features could help improve LEE in the case of LEDs by compensating for total internal reflection due to refractive index difference. Moreover, this technology also has a potential to substantially reduce the dicing time with high repetition rate lasers and appropriate beam steering systems.

In chapter 4, a warm white light source at a CCT of about 3400 K, and an outstanding CRI ($R_a(8)$) of 98.6 is demonstrated. A novel hybrid approach based on a blue-cyan emitting di-chromatic LED along with a green-red two-phosphor mixture is used to achieve such high colour rendition. The peak luminous efficacy of 11 lm/W is exhibited by the pc-LED. The monolithic blue-cyan device demonstrated LEE of 14.8% and IQE of 63%. The efficacy can be improved with better chip design and silicone lens by improving LEE and IQE of MBC. For further improvements in CRI the partial CRI R_9 needs improvement, towards that two approaches involving careful optimisation of red phosphor have been discussed in section 4.3.3. The given approach has a two fold advantage a) use of only two phosphors to achieve high CRI and, b) di-chromatic emission with cyan spectral supplementing the spectral coverage needed for CRI improvements while not falling into the "green gap" region thus allowing for far better IQE.

In this chapter 5, evolution of electrical and optical properties of commercial blue LED in the temperature range of 13 K to 440 K is presented. The experimental data shows a good agreement with the theoretical curves predicted by the ABC-model. The IQE and LEE of the device is estimated using the procedure described in section 5.3. Peak IQE varied from $\sim$ 97% at 13K to $\sim$ 65% at 440K. On the other hand IQE ($\sim$ 65%) at all temperatures for the operating current of 350 mA showed no dependence on temperature indicating a non-monotonic nature of Auger recombination constants with temperature. This also suggests that carrier

delocalisation can be the probable caused of efficiency droop at higher currents due to increased junction temperature. Furthermore, LEE also decreases as expected with increasing temperature from 76% at 13 K to 68% at 440 K due to optical losses incurred by free carrier absorption, band-to-band absorption and reflection losses.

In chapter 6, high power AlInGaP red LEDs are studied under high current CW and pulsed regimes from 100 μs to sub-nanoseconds pulses. Red shift of peak emission wavelength as a function of current exhibited a dual slope character. A critical current (I_c) corresponding to the change in slope in the dual slope character of the red shift in peak emission wavelength with increasing current is determined. A correlation between I_c along with current corresponding to the start of red shift, i.e. I_0 and saturation and/or decrease of EQE with current allows distinguishing between various mechanisms during device operation. For applied current less than I_0 the experimental and theoretical (as predicted by the AB model, i.e. reduced ABC model) EQE curves agree indicating self-heating and excess carrier concentration not affecting device operation. For applied current values between I_0 and I_c a weak red shift in peak wavelength is observed attributed to thermally induced bandgap shirking. Also, increased carrier concentration induces leakage on electrons in the p-side of LED leading to saturation of EQE(I). Next, for applied current exceeding critical current a strong red shift in peak wavelength i.e. steeper slope in the dual slope character, increased spectral broadening along with stark efficiency decrease is observed that is attributed mostly to self-heating of device. The onset of this efficiency decrease can be shifted to higher current values by operating in pulse regime. Sub-nanosecond pulse may preclude device self-heating completely even at high currents up to 45 A.

Appendix A

List of Publications

Peer-reviewed publications

1. **A.Yadav**, S. A. Kolpakov, N. T. Gordon, H. Kbashi, E. U. Rafailov, and K. Zhou, "Stealth dicing of sapphire with NIR femto-second laser," Applied Physics A, vol. 123, no. 5, pp. 369, 2017.

2. I.E Titkov, **A. Yadav**, S. Yu. Karpov, A. V. Sakharov, A. F. Tsatsulnikov, T. Slight, A. Gorodetsky and E. U. Rafailov, "Superior colour rendering with a phosphor-converted blue-cyan monolithic light-emitting diode," Lasers & Photonics Review, vol. 10, no. 6, pp. 1031-1038, 2016.

3. I. E. Titkov, S. Yu. Karpov, **A. Yadav**, V. L. Zerova, M. Zulonas, B. Galler, M. Strassburg, I. Pietzonka, Hans-Juergen Lugauer, E. U. Rafailov, "Temperature-Dependent Internal Quantum Efficiency of Blue High-Brightness Light-Emitting Diodes." IEEE Journal of Quantum Electronics 50(11): 911-920, 2014.

4. **A. Yadav**, I. E. Titkov, G. S. Sokolovskii, S. Yu. Karpov, V. V. Dudelev, K. K. Soboleva, M. Strassburg, I. Pietzonka, Hans-Juergen Lugauer, and E. U. Rafailov, "Temperature effects on optical properties and efficiency of red AlGaInP-based light emitting diodes under high current pulse pumping," Submitted to Lasers & Photonics Review.

5. T.J. Slight, **A. Yadav**, O. Odedina, W. Meredith, K. E. Docherty, E. U. Rafailov, A. E. Kelly, "InGaN/GaN Laser Diodes with High Order Notched Gratings," Submitted to Photonics Technology Letters, April 2017.

Publications Under preparation

1. **A. Yadav**, I. E. Titkov, A. V. Sakharov, W. V. Lundin, A. Nikolaev, G. S. Sokolovskii, A. F. Tsatsulnikov, and E. U. Rafailov, "Di-chromatic InGaN based color tunable monolithic LED with highest color rendering index".

2. I. E. Titkov, D. Mamedov, **A. Yadav**, S. Yu. Karpov, E. U. Rafailov, Hans-Juergen Lugauer, "Efficiency of true green light-emitting diodes: non-uniformity and temperature effects".

Conferences

1. **A. Yadav**, I. E. Titkov, G. S. Sokolovskii, S. Yu. Karpov, V. V. Dudelev, K. K. Soboleva, M. Strassburg, I. Pietzonka, Hans-Juergen Lugauer, and E. U. Rafailov, "AlGaInP red-emitting light emitting diode under extremely high pulsed pumping," Feb 2016 Light-emitting diodes: materials, devices, and applications for solid state lighting XX. SPIE, 7 p. 9768-52. (SPIE proceedings; vol. 9768), Feb 2016.

2. M. Zulonas, I.E. Titkov, **A. Yadav**, K.A. Fedorova, A.F. Tsatsulnikov, W.V. Lundin, A.V. Sakharov, T. Slight, W. Meredith, and E.U. Rafailov, "Correlation between p-GaN growth environment with electrical and optical properties of blue LEDs," Feb 2016 Light-emitting diodes: materials, devices, and applications for solid state lighting XX. SPIE, 8 p. 9768-21. (SPIE proceedings; vol. 9768), Feb 2016.

3. **A. Yadav**, I. E. Titkov, A. V. Sakharov, W. V. Lundin, A. Nikolaev, G. S. Sokolovskii, A. F. Tsatsulnikov, and E. U. Rafailov, "High colour rendering dichromatic monolithic light emitting diode with tuneable colour temperature," in 2015 European Conference on Lasers and Electro-Optics - European Quantum Electronics Conference, (Optical Society of America, June 2015), paper CE_11_2.

4. I. E. Titkov, **A. Yadav**, V. L. Zerova, M. Zulonas, E. U. Rafailov, S. Yu. Karpov, M. Strassburg, I. Pietzonka, Hans-Juergen Lugauer, and B. Galler, "Novel evaluation procedure for internal and extraction efficiency of high-power blue LEDs" Laser Optics, 2014 International Conference, St. Petersburg, 2014, pp. 1-1.

5. **A. Yadav**, M. Zulonas, I.E. Titkov, V.L. Zerova, K. A. Fedorova, A. F. Tsatsulnikov, W. V. Lundin, A. V. Sakharov, G. S. Sokolovskii, and E. U. Rafailov, "Colour management of InGaN/GaN based monolithic two-wavelength LEDs," 28th Semiconductor and Integrated Optoelectronics Conference (SIOE 2014), Cardiff, March 2014.

6. I. E. Titkov, **A. Yadav**, V. L. Zerova, M. Zulonas, A. F. Tsatsulnikov, W. V. Lundin, A. V. Sakharov, E. U. Rafailov, "Internal quantum efficiency and tunable colour temperature in monolithic white InGaN/GaN LED," Proc. SPIE 8986, Gallium Nitride Materials and Devices IX, 89862A (March 8, 2014).

Posters

1. S. A. Kolpakov, N. T. Gordon, **A. Yadav**, H. Kbashi, I. E. Titkov, E. U. Rafailov, K. Zhou, "Dicing of a sapphire wafer using femtosecond pulses at a wavelength of 800 nm" CLEO®/Europe-EQEC 2015, paper CM_P_15.

Other Contributions

1. • Oral Presentation: "High CRI LEDs: Monolithic blue-green and phosphor covered monolithic blue-cyan InGaN LEDs", NEWLED Workshop, October 2015, Rome, Italy.